Copyright

by

Imtiaz Ahmed

2003

The Dissertation Committee for Imtiaz Ahmed Certifies that this is the approved version of the following dissertation:

Imaging the Lower Slope, Offshore Nicaragua and Costa Rica Using a New Residual Migration Velocity Analysis Technique in the Space-Offset Domain

Committee:

Paul L. Stoffa, Co-Supervisor

Kirk D. McIntosh, Co-Supervisor

Mrinal K. Sen

Clark R. Wilson

Robert H. Tatham

Imaging the Lower Slope, Offshore Nicaragua and Costa Rica Using a New Residual Migration Velocity Analysis Technique in the Space-Offset Domain

by

Imtiaz Ahmed, B.Sc., M.Sc.

Dissertation

Presented to the Faculty of the Graduate School of

The University of Texas at Austin

in Partial Fulfillment

of the Requirements

for the Degree of

DOCTOR OF PHILOSOPHY

The University of Texas at Austin

December, 2003

Dedication

To my parents

To my teachers

Acknowledgements

I would like to sincerely thank my supervisors, Dr. Paul L. Stoffa and Dr. Kirk D. McIntosh for their guidance, encouragement, help and fruitful discussions through out my graduate studies. I would like to thank Dr. Mrinal K. Sen. for his suggestions, help and enthusiasm in my work. I would like to thank Dr. Clark R. Wilson and Dr. Robert H. Tatham for serving as my committee members. I would also like to thank Dr. Tom Shipley and Dr. Nathan Bangs for their suggestions and help.

I would like to extend my thanks to my present and former colleagues at the Institute for Geophysics University of Texas at Austin: Dhananjay kumar, Chandan Kumar, Sylvia Nordfjord, Alejandro Escalona, Anubrati Mukherjee, Armando Sena, Saleh Al-Salani, Junru Jiao, Chengshu Wang, Abdulaziz Al-Aslani, Donna Cathro, Jean-Paul van Gestel, Xinxia Wu, Hongbo Lu, Hao Xun, Bob Burger, Laurie Duncan, Timothy Meckel, Robert Rogers, Ricardo Combellas, Veronica Castillo , Irina Filina, Martha Jaimes, Rishi Deb Bansal, Chris Rhea and April Kreller. With out them my stay at the Institute for Geophysics would have been incomplete. I also give special thanks to my friends

Lakshmi Nagajyothe Potluri, Anup Ramamurthy, Jyothy Atluri, Astrid Makowitz, Anuj Jain and Miki Suga for their wonderful company during my stay at Austin.

Special thanks are given to many staff at the Institute for their help; especially I thank Dr. Roustam Seifoullaev for his kind and patient help in developing the interactive graphical software. I also thank Mark Weiderspahn, Kevin Johnson, John Gerboc and Steffen Saustrup for their technical support, Susan Beaubien, Judy Sansom, Jan Everett, Eleanor Picard and Nancy Hard for their help. I would like to thank Miriam Pashby, Bill Woods and Phillip Guerrero from the Department of Geological Sciences for all their help.

I would like to thank all my teachers who have made me the person I am today. Especially I would like to thank Shabbir and Rajat, my high school teachers for leading me to study sciences. I would also like to thank Dr. Stephen P. Grand for his excellent teaching.

I would like to express my deepest thanks to my parents and my family for all their love and support and their positive influence in my life. I would also like to thank all my childhood friends for their continuous support.

I would also like to acknowledge NSF grant # OCE-9905355, ConocoPhillips and Ewing Worzell fellowship for financial support during my stay at the Institute.

Imaging the Lower Slope, Offshore Nicaragua and Costa Rica Using a New Residual Migration Velocity Analysis Technique in the Space-Offset Domain

Publication No._____

Imtiaz Ahmed, Ph.D.

The University of Texas at Austin, 2003

Supervisors: Paul L. Stoffa and Kirk D. McIntosh

There is a dramatic variation in geochemical sediment tracer signal along the Central American volcanic arc. Two contradicting theories, one supporting sediment accretion and the other subduction erosion, have been suggested as possible explanations for these variations. My goal in this dissertation is to use seismic images of the lower slope off Nicaragua and Costa Rica to study the influence of subducting plate structure on sediment dynamics. I am particularly interested in documenting the efficiency of sediment subduction, its along strike variation, and to see if it corresponds with the geochemical anomalies.

Although high quality seismic data was acquired offshore Nicaragua, it remained difficult to image the lower slope in detail with conventional processing techniques. Several characteristics of this geologic environment pose seismic imaging problems: the area is heavily faulted, adjacent reflection boundaries have

contrasting dips, and the velocity structure is complex. In this environment the common midpoint gathers do not represent a collection of true common subsurface reflection points. To get a clearer image, I needed to apply pre-stack depth migration (PSDM) techniques. An accurate velocity model is required to get a good PSDM image. Therefore one of the most important aspects of PSDM is velocity analysis.

Over the last few decades, residual migration velocity analysis (RMVA) has been an area of active research. Previous work on RMVA in the depth-offset domain required top down layer stripping migration in order to derive the interval velocities directly, hence making it very computationally intensive. Here I propose a new technique in which for each common image gather (CIG) we first create a table of offset-ray parameters-depth (*x*-*p*-*z*) using a local 1D assumption. Then I calculate the residual migration depth corrections in the *p*-*z* domain and finally map these depth corrections back to the *x*-*z* domain using the *x*-*p*-*z* table. Since I calculate the residual migration depth corrections in the *p*-*z* domain, the interval velocities are derived directly by top down residual migration. Hence I do not have to explicitly do the layer stripping migration followed by residual normal moveout to get the interval velocities.

The velocities generated by using the above RMVA technique produce interpretable depth images of the lower slope off Nicaragua and Costa Rica. From these images I interpret partial sediment accretion off Costa Rica and likely total sediment subduction off Nicaragua, and therefore provide a geophysical evidence for the observed geochemical disparity along this margin.

Table of Contents

List of Figures

Chapter 1: Introduction

1.1 OBJECTIVE AND ORGANIZATION

Around the world there are tremendous variations in the seismogenic character of convergent plate margins (Figure 1.1) and in the geochemical character of the associated volcanic arcs. This may be due to the wide range of upper and lower plate compositions, structure and thicknesses, and in variation of subduction parameters such as slab age, convergence rate and subduction angle. The arc chemistry and seismogenic patterns associated with the subduction system of Nicaragua and Costa Rica show variations in the strike direction comparable to those world wide (Carr et al., 1990; Ambraseys and Adams, 1996; Kanamori and Kikuchi, 1993; Protti et al., 1995, Morris et al., 2002). This situation allows us to investigate the nature of this variability along this margin with a single subducting plate and gradually changing subduction parameters. Specifically we can use MCS (Multi channel seismics) data to identify the processes of sediment accretion, subduction, or tectonic erosion that may bear on the arc chemistry.

The NW Costa Rica segment of the margin has been well studied. Shipley et al. (1992) suggested that oceanic sediments are accreted to the base of the upper plate in an underplating process. ODP Leg 170 drilling showed that frontal accretion has not been significant and the sediments of the incoming plate are subducted in their entirety near the toe of the prism (Kimura et al., 1997, Valentine et al., 1997) but was unable to test whether sediments are underplated.

von Huene et al. (1995) suggested that igneous activity associated with the Galapagos hotspot has given rise to three distinct segments of the Cocos plate subducting beneath Costa Rica: smooth, seamount dominated, and Cocos Ridge segments, from NW to SE. In contrast to Costa Rica, the Nicaragua margin has been poorly studied. Prior to our cruise (July, 2000), only one MCS (Multi Channel Seismic) profile (NIC-1) crossed the entire margin offshore Nicaragua (Ranero et al., 2000), and one OBH (Ocean Bottom Hydrophone) dip profile along the same transect has been recorded and analyzed (Walther et al., 2000). Walther et al. (2000) found that a major feature of the upper plate is an 80-km wide high velocity, high-density basement wedge that forms the front of the margin. They interpreted it as oceanic crust and mantle, possibly from an allochthonous terrain, which docked in Central America in Eocene-Oligocene time.

UTIG (University of Texas Institute for Geophysics) collected MCS data and wide-angle data offshore Nicaragua in a recent cruise (June 2000). My main aim is to provide good seismic reflection images of the lower slope of this margin offshore Nicaragua and Costa Rica, to help us to identify the processes of sediment accretion, subduction, or tectonic erosion that may bear on the arc chemistry and seismogenic properties. The lower slope region of convergent margins is geologically very complex. Figure 1.2 is a velocity depth model of a typical convergent margin, suggesting a large variation in lateral velocity. Seismic imaging of complex geological structures is still a very challenging problem. Reliable images of such structures, however, can be obtained by pre-stack depth

migration (Yilmaz, 1987, Claerbout, 1985), provided the velocity model used for migration is an adequate approximation of the real velocity distribution in the subsurface. Thus, the imaging problem is reduced to the problem of finding a correct velocity model.

Velocity models determination for complex structures has attracted considerable attention in the last decade. Indeed, classical velocity determination based on common midpoint (CMP) moveout analysis fails in areas of complex geology (Yilmaz, 1987, Claerbout, 1985): waves propagating through complex velocity fields and reflecting on structurally complicated interfaces do not yield hyperbolic moveout in CMP gathers. Moreover time domain data may not be interpretable at all because the interference of many events may destroy continuity. To overcome this difficulty, several authors (Yilmaz and Chambers, 1984; Yahya, 1989; Stork and Clayton, 1991; Liu and Bleistein, 1992, 1995; Tieman, 1995; Jiao et. al., 2002) proposed to perform velocity analysis via a detour through the pre-stack depth migrated domain. These methods are referred to as migration velocity analysis (MVA) methods.

In this dissertation I have developed a new interactive residual migration velocity analysis (RMVA) technique in the depth-offset domain, extending the ideas of RMVA in depth-plane wave domain of Jiao, 2002. I have used my RMVA technique to estimate the velocity depth model for pre-stack depth migration of the lower slope offshore Nicaragua and Costa Rica, and then used these interval velocity models to perform the pre-stack depth migrations, generating improved images of the lower slope.

In the remaining sections of this chapter, I include a brief description of the study area and discuss motivation for the study. Then in Chapter 2, I highlight the importance of pre-stack depth migration in structurally complex areas through examples. In chapter 3, I discuss the theory and application of the new residual migration velocity analysis technique in the depth- offset domain. In chapter 4, I apply the new RMVA method on the lower slope, offshore Nicaragua and Costa Rica dataset. Using these pre-stack depth images I discuss the implications for processes of sediment accretion, subduction, or tectonic erosion that may bear on the arc chemistry.

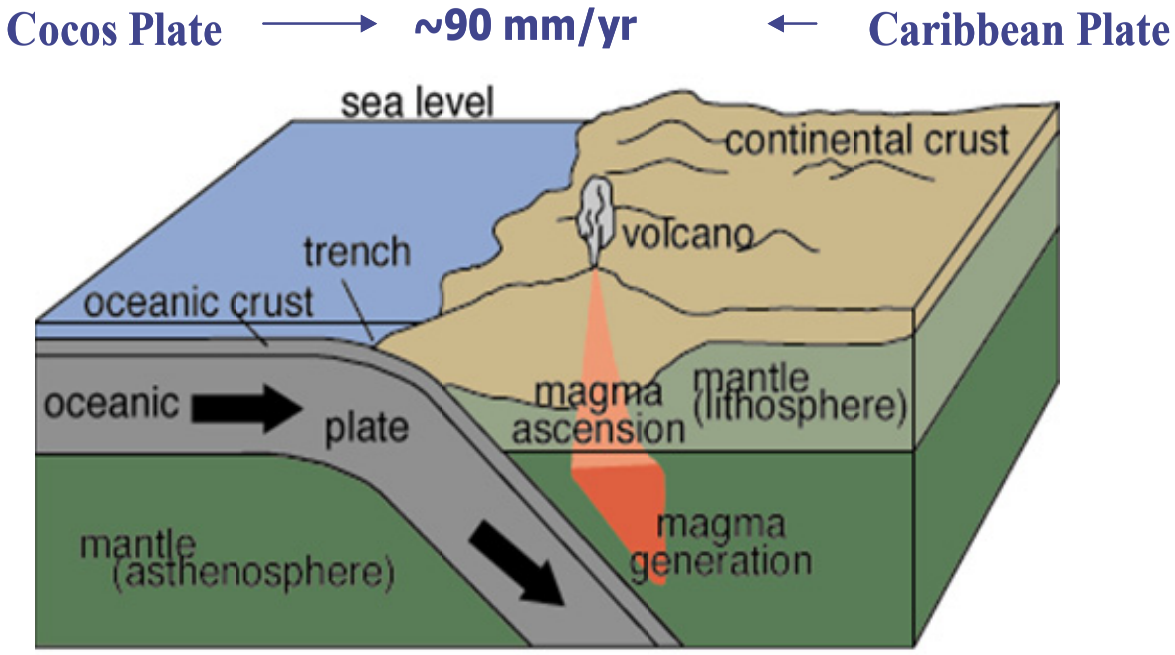

Figure 1.1. A cartoon showing a cross section of a subduction zone.

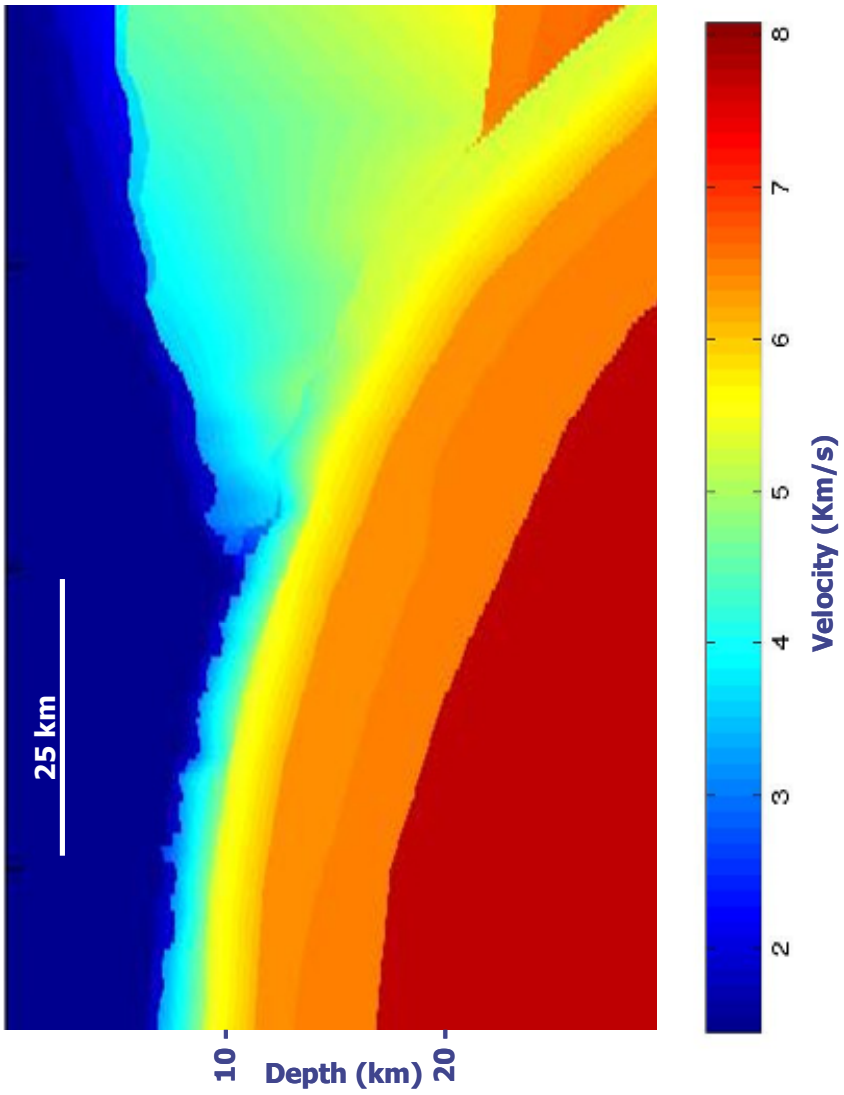

Figure 1.2. A typical interval velocity depth model of a subduction zone.

1.2 BRIEF DESCRIPTION OF THE STUDY AREA

Costa Rica and Nicaragua are neighboring countries in southern Central America (Figure 1.3) and make up part of the western edge of the Caribbean plate. The lithosphere of the Cocos plate subducts beneath the Caribbean plate along the Middle America Trench at relatively rapid rates varying from ~76 mm/yr in the north to ~91 mm/yr near the border with Panama (DeMets et al., 1994, 2001). The age of the plate at the trench is estimated at 20 to 25 Ma over much of the area (Hey, 1977, Barckhausen, 2001).

Associated with Cocos plate subduction, the Central American volcanic arc extends across the region to south central Costa Rica. The volcanic products of the arc have tremendous and systematic geochemical variation from Nicaragua to Costa Rica despite the common subducting plate providing a source of volcanics.

The character of the incoming plate subducting at convergent margins and the processes affecting it as it passes below the shallow forearc may play a major role in the magnitude of volcanism and the chemistry of lavas produced in the associated volcanic arc (Barckhausen et al., 2001). The Cocos plate subducting along the Nicaragua and Costa Rica portions of the Middle America Trench (MAT) have different origins and different igneous and structural modifications. For example, lithosphere of the southern Cocos plate was formed along the Galapagos spreading center while northern and western parts of the plate were created at the East Pacific Rise (EPR). The boundary between these lithospheric types falls offshore of the central Nicoya Peninsula trench segment (Barckhausen

et al. (2001). The crust in this area has been further modified by subsequent igneous activity associated with the Galapagos hotspot (Kimura et al., 1997). This has resulted in three distinct segments of the Cocos plate subducting beneath Costa Rica: smooth, seamount dominated, and Cocos Ridge segments, from NW to SE along the strike of the trench (von Huene et al., 1995).

Northwest of the smooth Nicoya segment, the morphologic character of the Cocos plate changes yet again. Here the seafloor (Figure 1.4) and basement surfaces are rough, the outer rise is well developed and the relief between the rise and trench increases. Figure 1.6 shows portions of three MCS profiles over the Cocos plate from offshore central Nicaragua to offshore from the central Nicoya Peninsula (locations in Figure 1.5). The Nicaraguan profile (NIC-80) has rough seafloor morphology due to intense faulting accompanied by large fault block rotation. There are fault scarps ~500-600 m high along this profile that exposes the igneous basement at the seafloor. The incoming sediment distribution is discontinuous due to large fault throws. In contrast, line CR-60 offshore from the central Nicoya Peninsula shows smaller listric faults developing above a relatively smoother oceanic crust. The sedimentary section here is uniform and continuous. Line NIC-10, located off souththernmost Nicaragua between the other two lines, reveals a section that appears to have structural character intermediate between the other sections in terms of fault development, structural relief, and sediment uniformity.

The three profiles in Figure 1.6 suggest that there is a continuum of structural variation in the Cocos plate from NIC-80 to CR-60. Following our

cruise in June 2000, we now have data that will enable characterization of the Cocos plate in this 250-km long segment. In addition to the MCS data, multibeam bathymetry data have been recorded by GEOMAR in a ~90x90 km region off central Nicaragua (von Huene, 2000). This bathymetry data set was supplemented on our cruise. This data set reveals seamounts on the subducting plate and shows that they are being faulted as the plate bends downward into the trench (Figure 1.4). The intense faulting documented by Line NIC-80 appears to continue throughout this surveyed region.

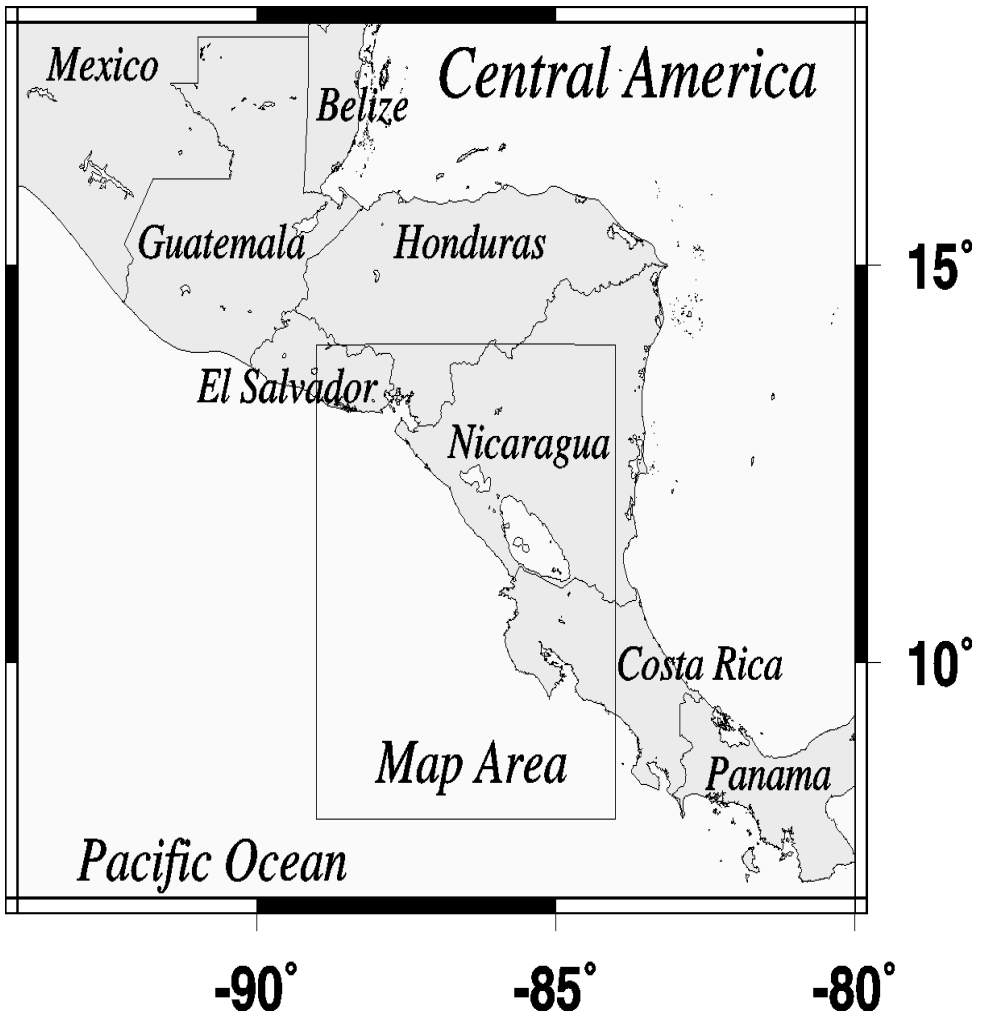

Figure 1.3. Map showing my study area. It is the Pacific side of the Central-America convergent margin (Offshore Nicaragua and Costa Rica).

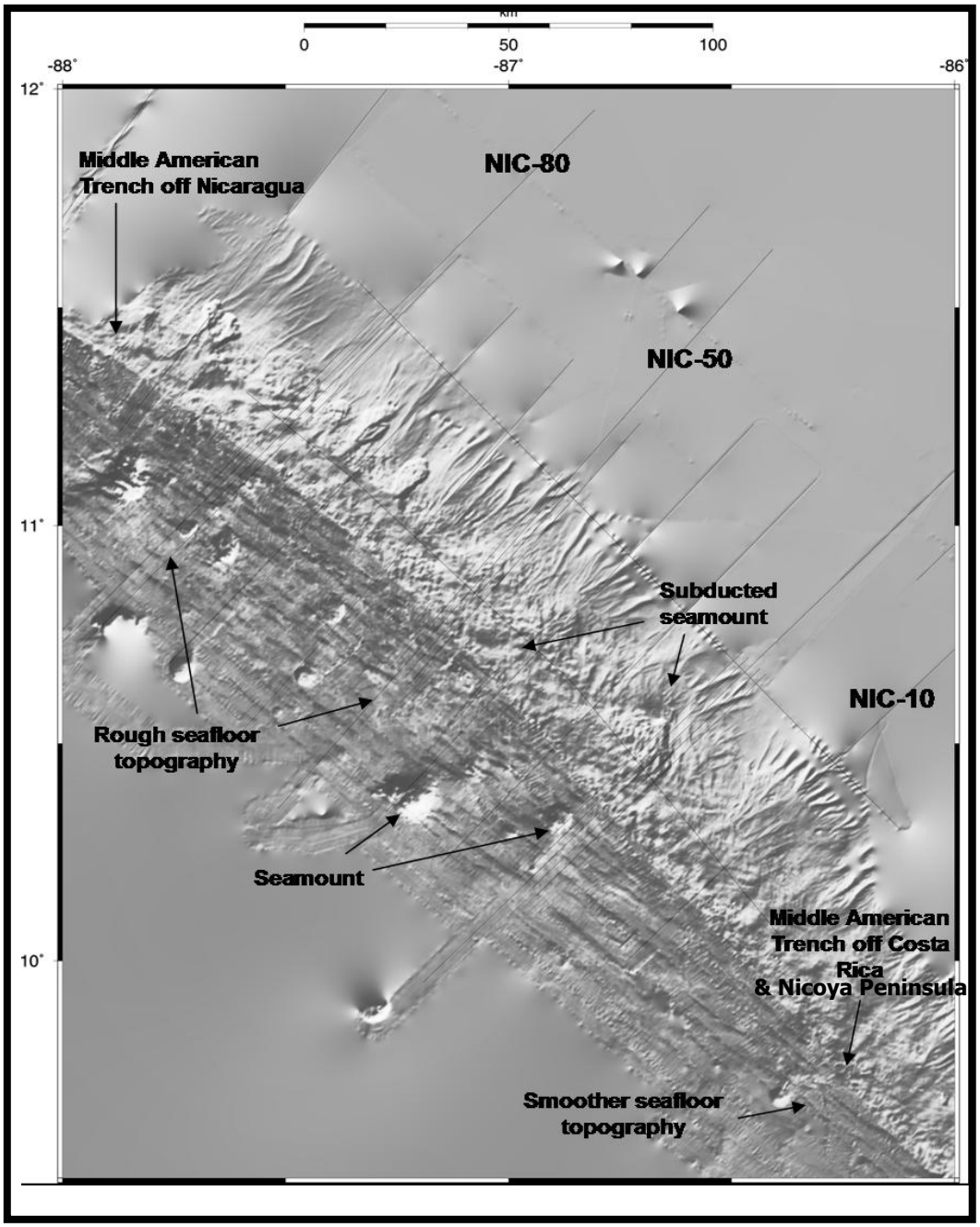

Figure 1.4. Illuminated perspective view of GEOMAR hydrosweep data set acquired off Central America. MCS lines shown for reference. Northwest of the smooth Nicoya segment, seafloor surfaces are rough.

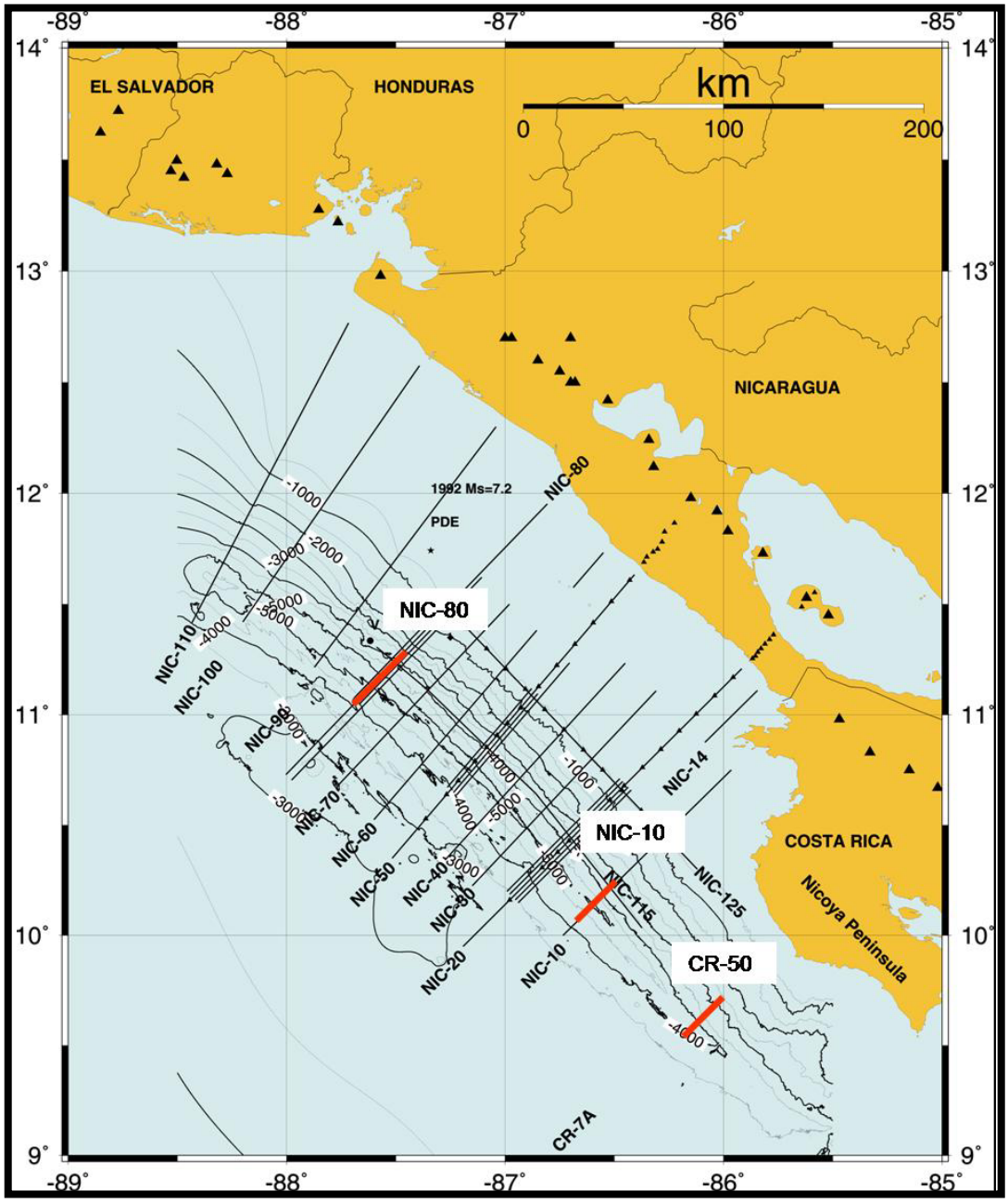

Figure 1.5. Map showing the study area with the 2D seismic profiles. The red lines are the location of the three seismic lines shown in Figure 1.6.

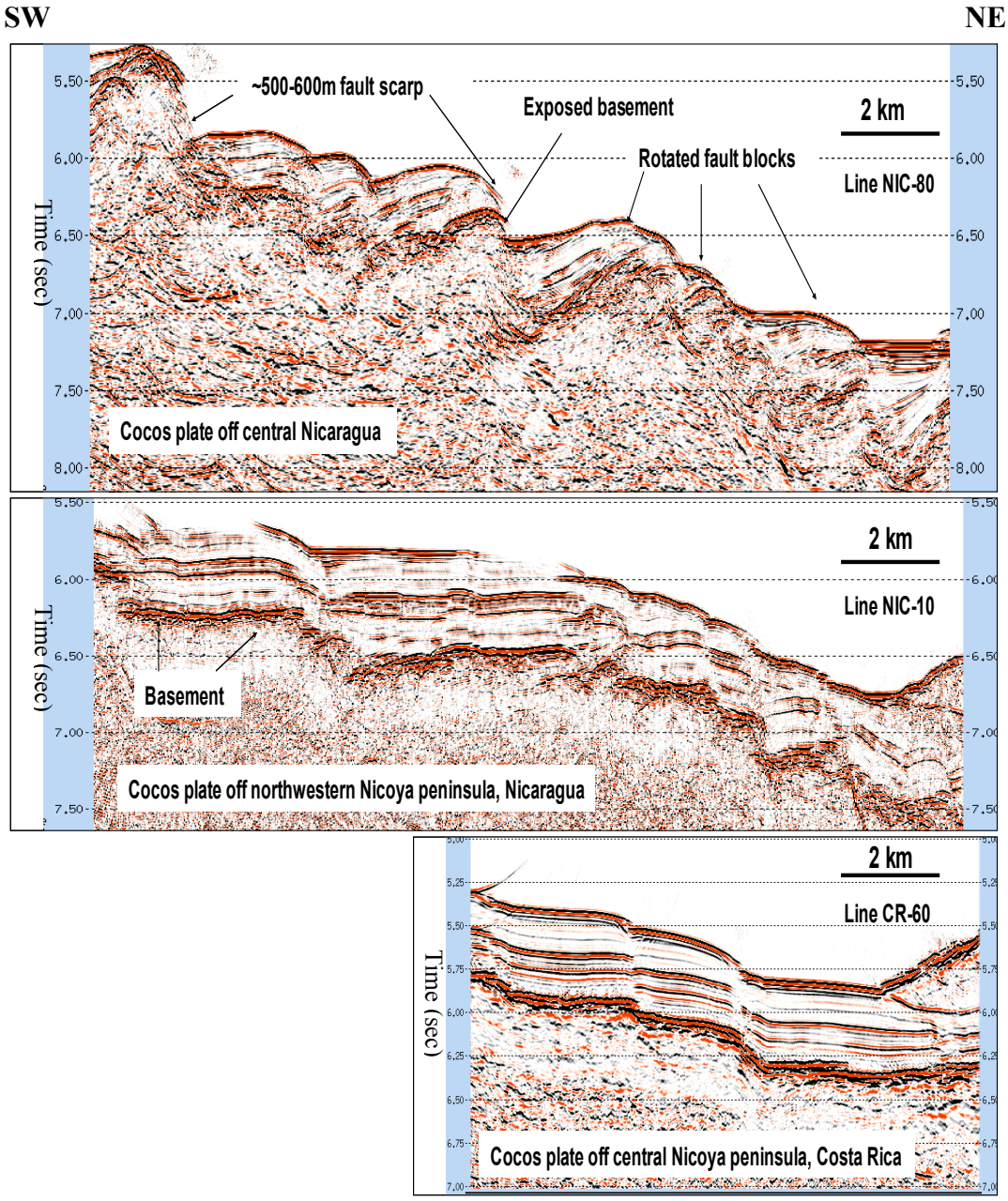

Figure 1.6. Comparison of the Cocos plate structure from segments subducting off central Nicaragua and off the northwestern and central Nicoya Peninsula. The profiles are plotted at the same scale. The three profiles suggest that there is a continuum of structural variation.

1.3 MOTIVATIONS OF WORK:

1.3.1 Geochemical

Nicaragua volcanics contain uniquely high concentrations of sediment/slab tracers (Carr et al., 1990, Morris et al., 1990, 2002). Beryllium 10 (^{10}Be), U/Th, and Ba/La in the Nicaragua volcanics are among the highest recorded globally. These geochemical tracers are typical of subduction zone lavas and are thought to originate in subducted sediment and/or slab-dehydration fluids, but nowhere are these characteristics better developed than in the Nicaragua volcanics. This observation, taken at face value, suggests there is a likelihood of complete sediment subduction at the trench off Nicaragua to give such high concentrations of element and isotope tracers in these sediments, and/or efficient transport of crustal material from the slab to the root zone of arc magmatism. A few hundred kilometers away along the same convergent margin, the Costa Rica volcanics have much smaller sediment signature (Figure 1.7), have little contribution from the uppermost hemipelagic sediments of the incoming plate, and a proportionally larger contribution from the basal carbonate section (Carr et al., 1990, Morris et al., 2002). Sediment/slab tracers also decrease from Nicaragua to the northwest, in the Guatemala volcanics.

The variation in the arc geochemistry of the single subducting system across its margin is quite an interesting phenomenon. Parameters such as convergence rate (~85 mm/yr), plate age (20-25 Ma), and slab dip (84-80^{o}) change only moderately and in a gradational rather than the abrupt manner of the

isotopes from Guatemala to Costa Rica (Carr, 1984; De Mets et al., 1994; Protti et al., 1995; von Huene et al., 2000; Barckhausen et al., 2001). Incoming sediments are lithologically and chemically similar along the length of the margin (Kimura et al., 1997; Patino et al., 2000). In particular ^{10}Be is immobile, insensitive to chemical variation in the mantle and is largely unaffected by involvement of continental crust (Morris et al., 1990). Given the above reasoning, sediment dynamics may play the most important part in explaining the geochemical disparity of the island arc volcanoes along this margin. One important reason may be that the rotated fault blocks on the Cocos plate off Nicaragua (Figure 1.6 and Figure 1.8), with exposed basements will present a superior mechanism to subduct sediment to depth. The MCS data set will help us in determining if this is actually the case, or whether other factors appear to be more important. Additional factors that we can investigate might include variation in vertical displacement of lower plate faults, variation in frontal accretion, or variation in underplating or subduction erosion.

Seismic images showing subducted sediments and accretionary processes are possible to obtain as shown in the Costa Rica data set (Figure 1.9; Shipley et al., 1986, 1992). I will seek to identify any indications of sediment accretion, subduction or tectonic erosion. We know (Morris et al., 1990) that even temporary sediment accretion, or storage, can significantly affect estimated geochemical fluxes of radiogenic tracers through this system, particularly ^{10}Be that is concentrated in the upper (younger) part of the sedimentary section.

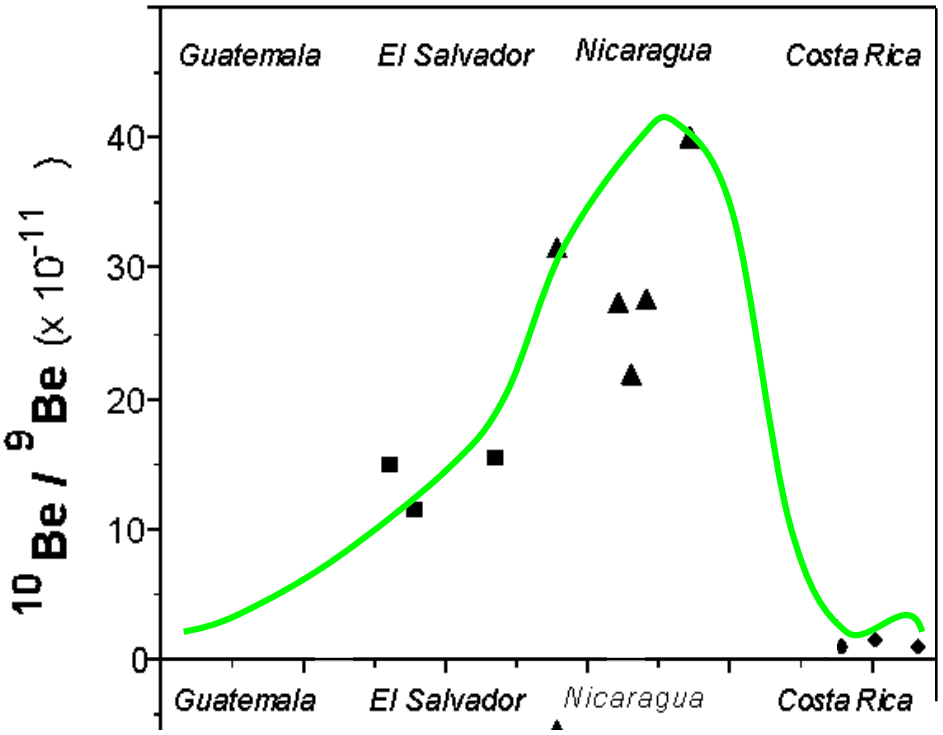

Figure 1.7. Regional variations in the $^{10}Be/^{9}Be$ isotope ratio of Central American arc volcanics. This subducted sediment tracer ratio peaks in Nicaraguan volcanics and decreases dramatically in Costa Rican volcanics.

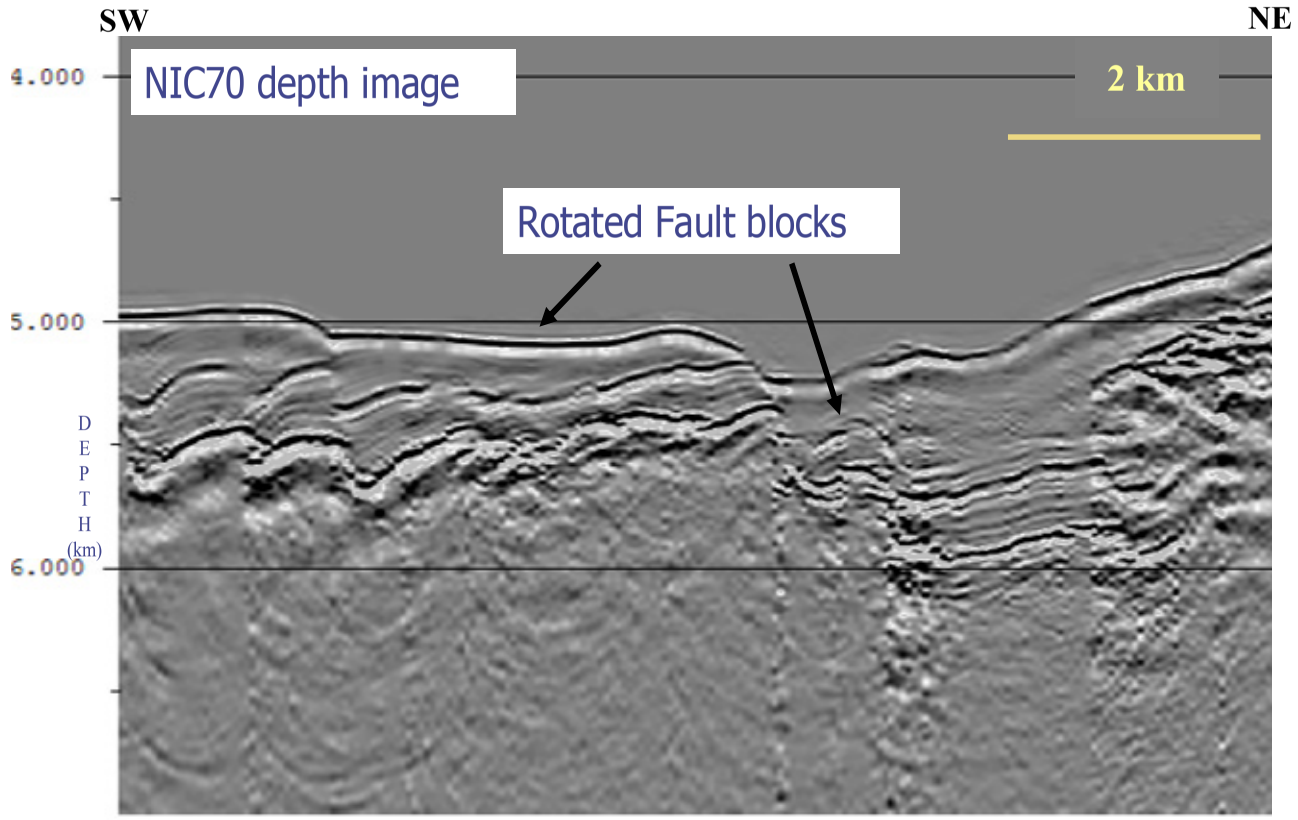

Figure 1.8. A depth image of a 2D MCS line offshore Nicaragua. The incoming plate has large extension faults. There are rotated fault blocks forming half graben like structures.

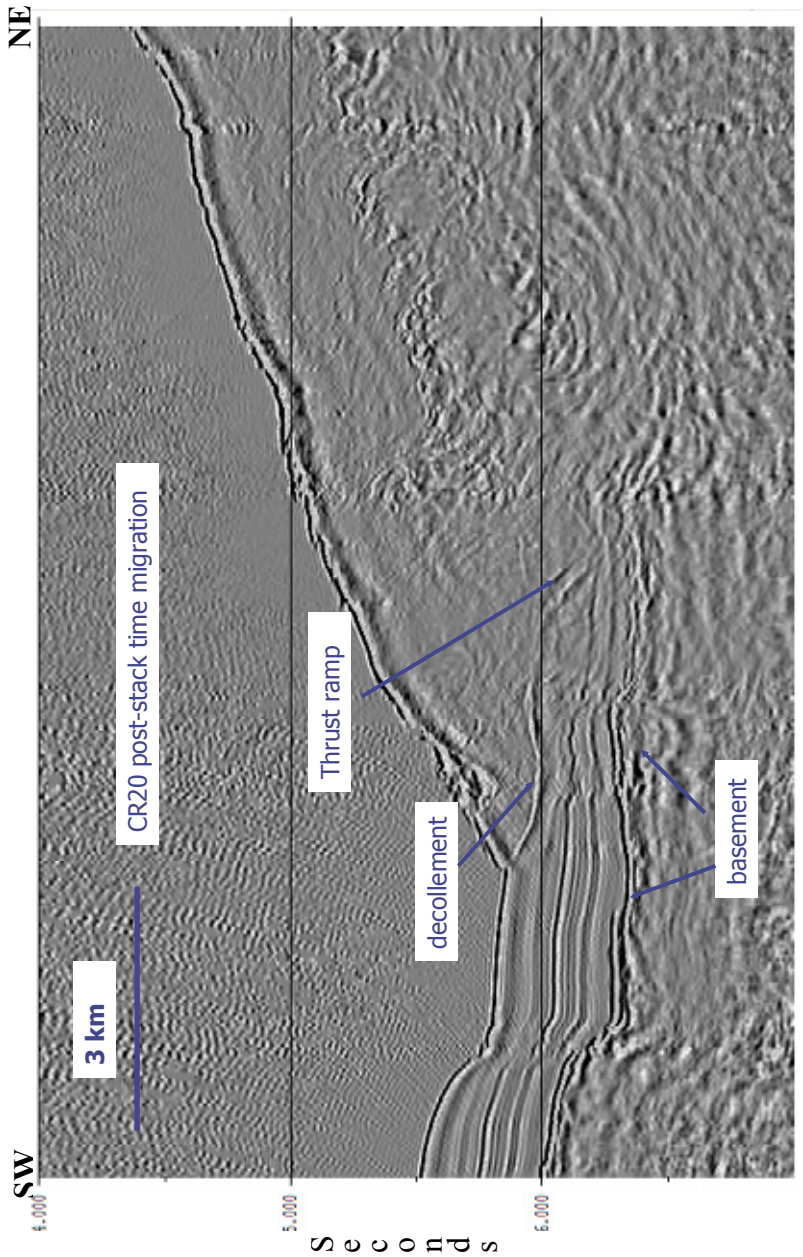

Figure 1.9. Seaward tip of plate boundary off Costa Rica. Seismic image showing subducted sediments and possible accretion processes.

1.3.2 Residual migration velocity Analysis

In residual migration velocity analysis (RMVA), velocity analysis is carried out after migration using the criterion that the results of migration with the correct velocity–depth model should reveal the same geologic structure on common image gathers (CIG). A CIG is the image of the same subsurface scatterer from different offset angles (Figure 1.10(a)). Therefore, the events on the CIG (Figure 1.10(b)) are aligned if we use the true velocity-depth model. Otherwise, if an incorrect velocity-depth model is used in the migration, the events on the CIG exhibit curvature and the energy focuses at nonzero time.

Figure 1.11(a) is a simple half space velocity-depth model. Figure 1.11(b) shows a CIG after migration with true velocity-depth model (Figure 1.11(a)). The event at 2 km depth is flat on this CIG. Figure 1.11(a) is a CIG generated with higher velocity (1.8 km/sec) used for migration. We see the event curve downwards. Figure 1.11(c) is a CIG generated with lower velocity (1.4 km/sec) used for migration. We see the event curve upwards. There are migration errors or residuals. This example demonstrates that migration using an incorrect trial velocity does not align the events on a CIG.

Previous works on residual migration velocity analysis in the depth-offset domain required top down layer stripping migration in order to derive the interval velocities directly, hence making it very computationally intensive. Recently, Jiao et. al. (2002) proposed residual migration velocity analysis in the plane-wave (τ-p) domain, which updates interval velocities directly in a top-down residual–difference correction for all layers after pre-stack depth migration instead of top-

down layer stripping migration followed by residual velocity analysis. This is less computer intensive and thus can be used for 3-D residual migration velocity analysis. Figure 1.12 (Jiao, 2002) shows a CIG (field data) before and after residual migration correction using Jiao's technique. The events on the CIG are certainly much flatter after the correction.

Most of the current reflection seismic analysis and migration algorithms, however, are applied in the depth-offset (*z*-*x*) domain. Therefore it is quite natural that we implement the residual migration velocity analysis in this domain. Thus our goal here is to extend the concepts described by Jiao, et. al. (2002) to the depth-offset domain. Since, we would expect mostly gradient velocities in the lower slope area; this RMVA technique is expected to give better and faster results, because it will update interval velocities directly in a top-down residual–difference correction for all layers after pre-stack depth migration.

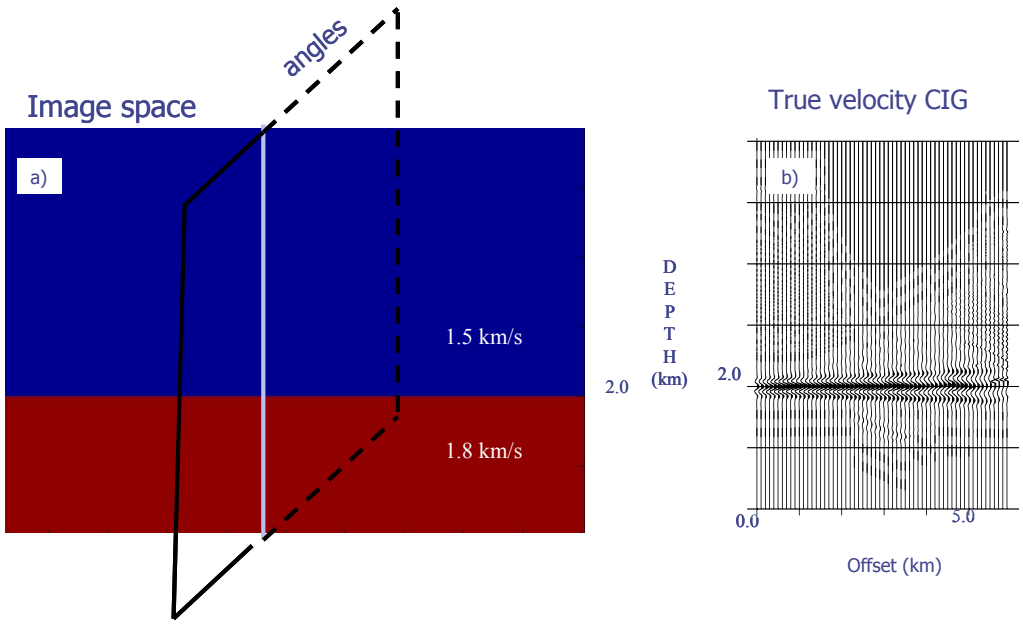

Figure 1.10 a) A cartoon explaining a CIG. The image of the white vertical line in the subsurface from different angles is a CIG (Figure 1.10(b)). Since they represent the image of the same position obtained at different angles the event is flat.

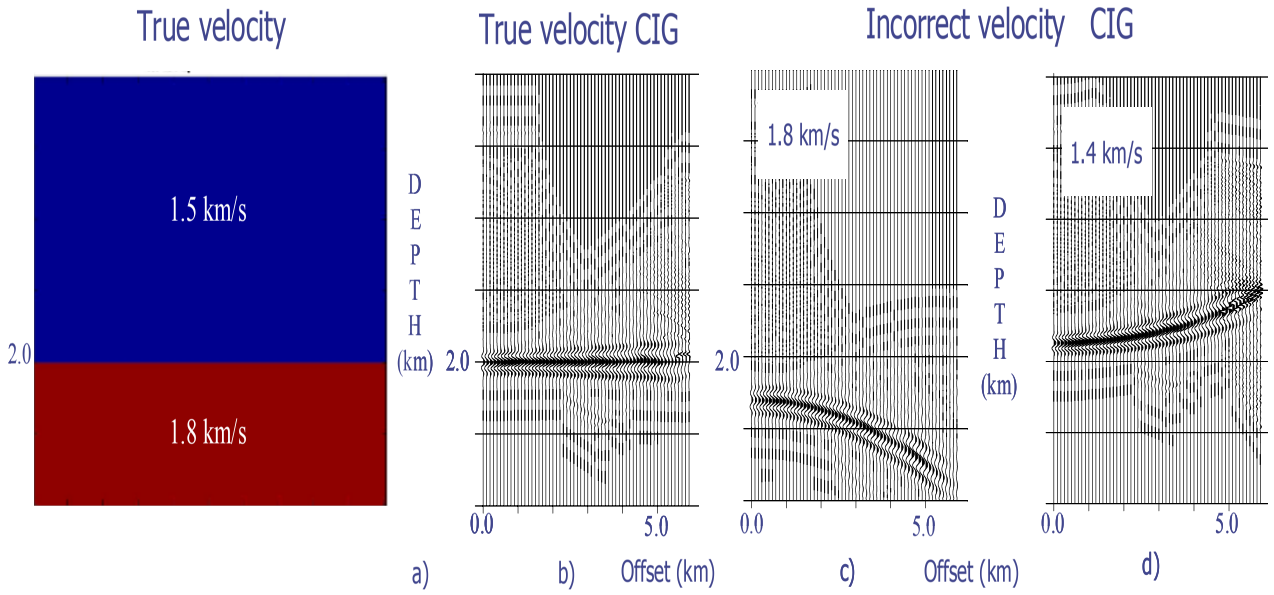

Figure 1.11 (a) A half space interval velocity model, (b) CIG migrated using the true velocity of Figure.1.11a, (b) CIG migrated using the incorrect velocity of 1.8 km/s, (d) CIG migrated using the incorrect velocity 1.4 km/s.

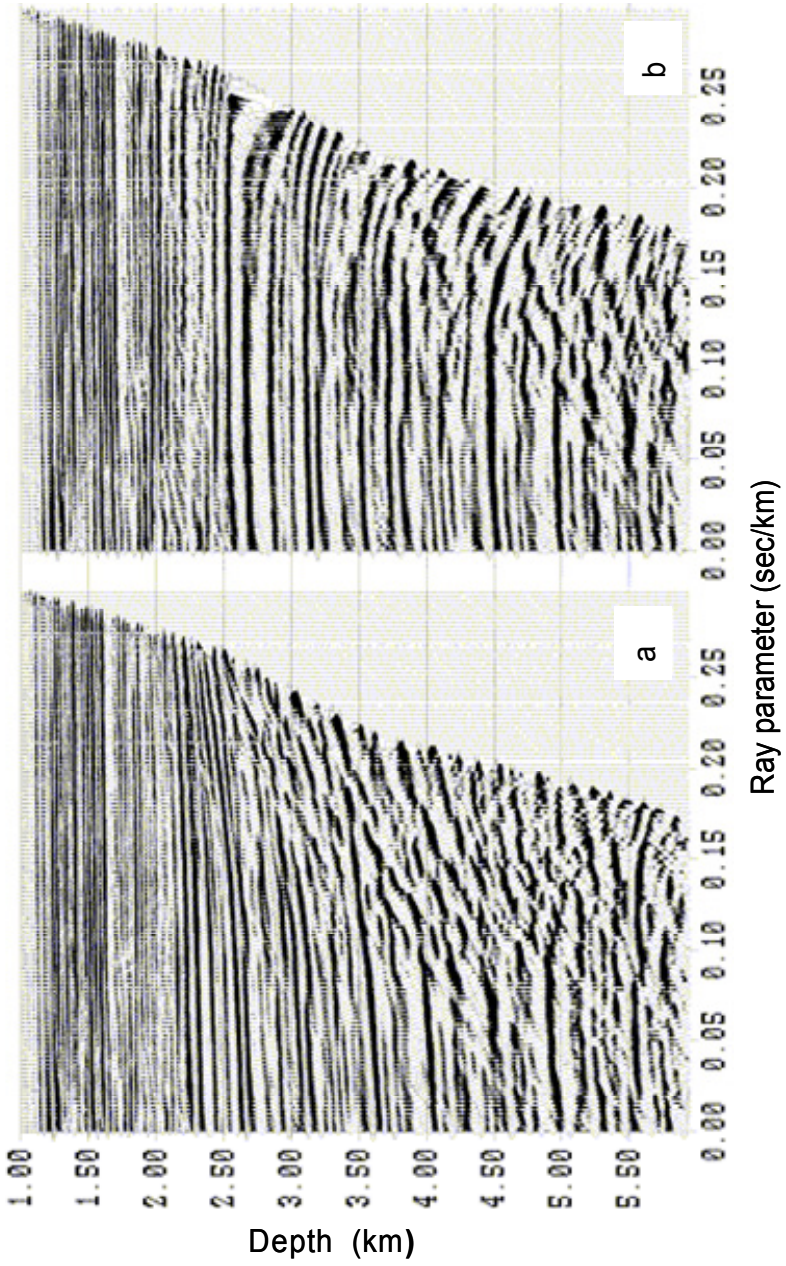

Figure 1.12. CIG (field data) before (a) and after (b) residual migration correction using Jiao's technique. The events on the CIG are much flatter after the correction (Jiao, 2002).

Chapter 2: Data processing of the Nicaragua MCS data set: Requirement for pre-stack depth migration

2.1 INTRODUCTION

In this chapter I discuss the basics of reflection seismology particularly the data processing. Then, I show post-stack migrated sections from Nicaragua and Costa Rica. I stress the need to do pre-stack depth migration in order to fulfill the detailed imaging objectives of this dissertation. Finally I will conclude this chapter by comparing some real data images based on post-stack time to pre-stack time to pre-stack depth.

2.2 REFLECTION SEISMOLOGY

The seismic reflection method utilizes seismic waves to derive information about the earth's interior. Different rocks in the earth have different elastic characteristics that, when combined with density, cause seismic waves to be reflected, refracted, and transmitted when the wave front encounters changes in rock properties. In other words, the contrasts in elastic properties and density effect seismic wave propagation (Aki and Richards, 1980), which makes the seismic method a powerful imaging tool. Snell's law controls the travel paths of seismic waves while the physical properties (elastic constants and density) of the rocks control the amplitudes of seismic waves. In the last seven decades, exploration seismology has developed various seismic exploration methods such as reflection, refraction, and transmission to determine earth structures. In a conventional 2-D multi-channel seismic survey the vibrations generated by a

source (typically an explosive charge or pneumatic airguns) propagate through the earth, get reflected from the subsurface and are recorded by an array of recorders called geophones or hydrophones placed along the same line with the source. The source point is then moved along the line along with the geophones on land. This procedure is repeated for a number of lines resulting in an areal coverage yielding a 3D image volume. Figure 2.1 is a cartoon showing 2D marine seismic acquisition where hydrophones are used to record the pressure wavefield. The data acquisition geometry might differ depending on the type of application. We might have detectors on either side of the shot or detectors arranged in an areal pattern, depending on whether the acquisition is on land or on sea, etc.. The signals recorded by each geophone or hydrophone correspond to a seismic trace at that location. Thus the conventional seismic data are expressed as a function of offset (distance for the shot or source of seismic energy at the detector) and recording time, this is referred to as the offset-time domain.

Traces recorded by all the detectors, which correspond to one “shot”, are grouped together and are referred to as a shot gather in the offset-time domain(Figure 2.2). Traces from different shots and detectors which have their geometric mid point in common can be grouped to form a CMP (common mid point) gather, also in an offset-time domain (Figure 2.3). Most of the conventional data processing techniques, like velocity analysis, NMO (Normal move out) correction and stacking are done on the CMP gathered data. Travel times of reflections from a horizontal flat layer are recorded as a hyperbola (time-offset domain) in a shot and the CMP becomes a CDP (Common depth point) gather

(figure 2.4). These data can then be corrected to the equivalent zero-offset reflection time, or corrected for Normal move out.

The main objectives of seismic data processing are improving the seismic resolution and increasing the S/N ratio. Velocity analysis (Figure 2.5) is performed on selected CMP gathers to estimate the stacking velocities of each reflection. The stacking velocities are used to remove the effect of offset from the reflections in each CMP gather (NMO correction). The NMO corrected traces in each CMP gather are summed over the offset coordinate (stacked) to produce a single trace.

Stacking is one of the most important data processing steps. Stacking improves the S/N ratio. However, stack sections are only approximations (Sonograms) to geologic sections and are difficult to interpret in structurally complex areas. This is because, no matter where in space the reflection actually occurs, each event on a stack section is plotted directly beneath the source-receiver midpoint. For example, a stack section (Figure 2.6b) of a syncline (Figure 2.6a) gives a characteristic bow tie image due to reflections from different locations arriving at the same receiver location. Figure 2.6c is obtained after applying a migration algorithm to the stack section (Figure 2.6b). We see that Figure 2.6c closely represents the syncline model in Figure 2.6a. The aim of migration is to move the reflectors to their true subsurface reflection position and is therefore a very important step in data processing. Migration is discussed in detail in the remaining sections of this chapter.

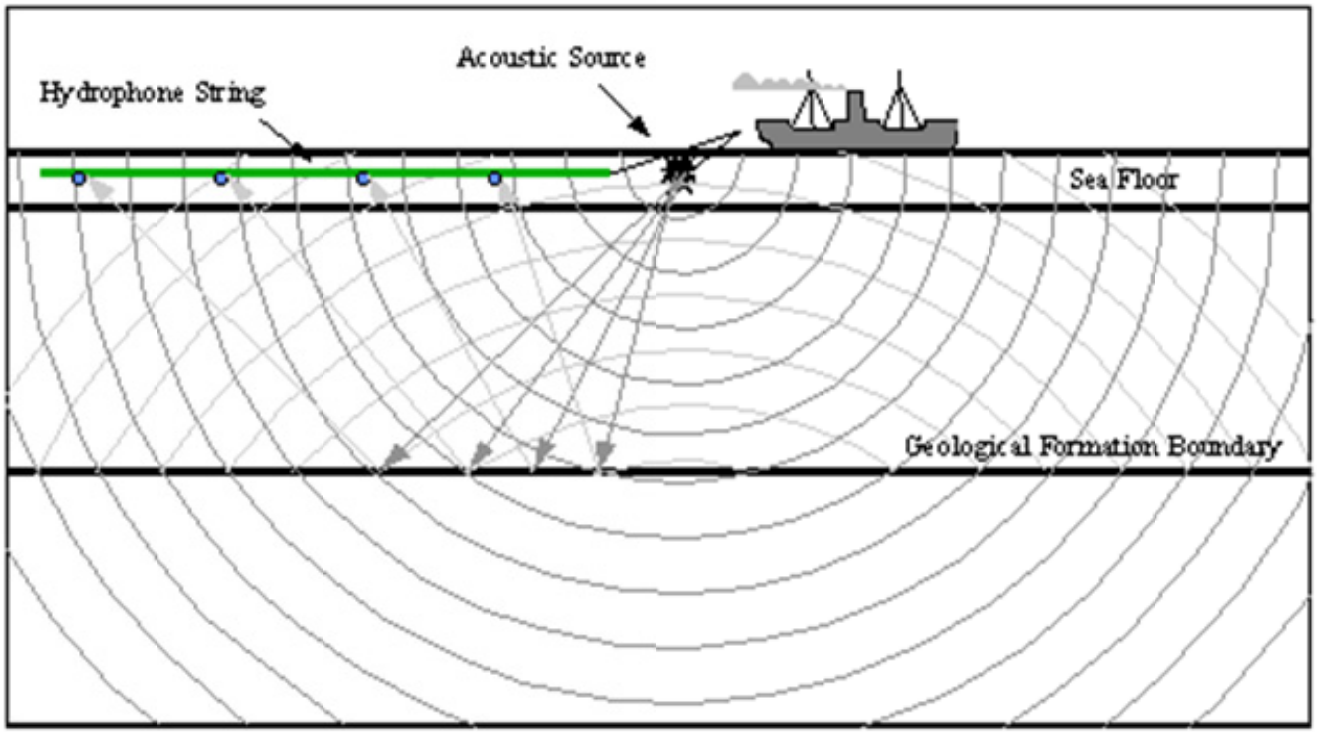

Figure 2.1. A cartoon showing marine seismic acquisition. Spherical waves generated by the source reflect from the subsurface and reach the detectors (hydrophones), where they get recorded. Each detector gives a seismic trace (the time history of the pressure it has been recording for a certain period of time).

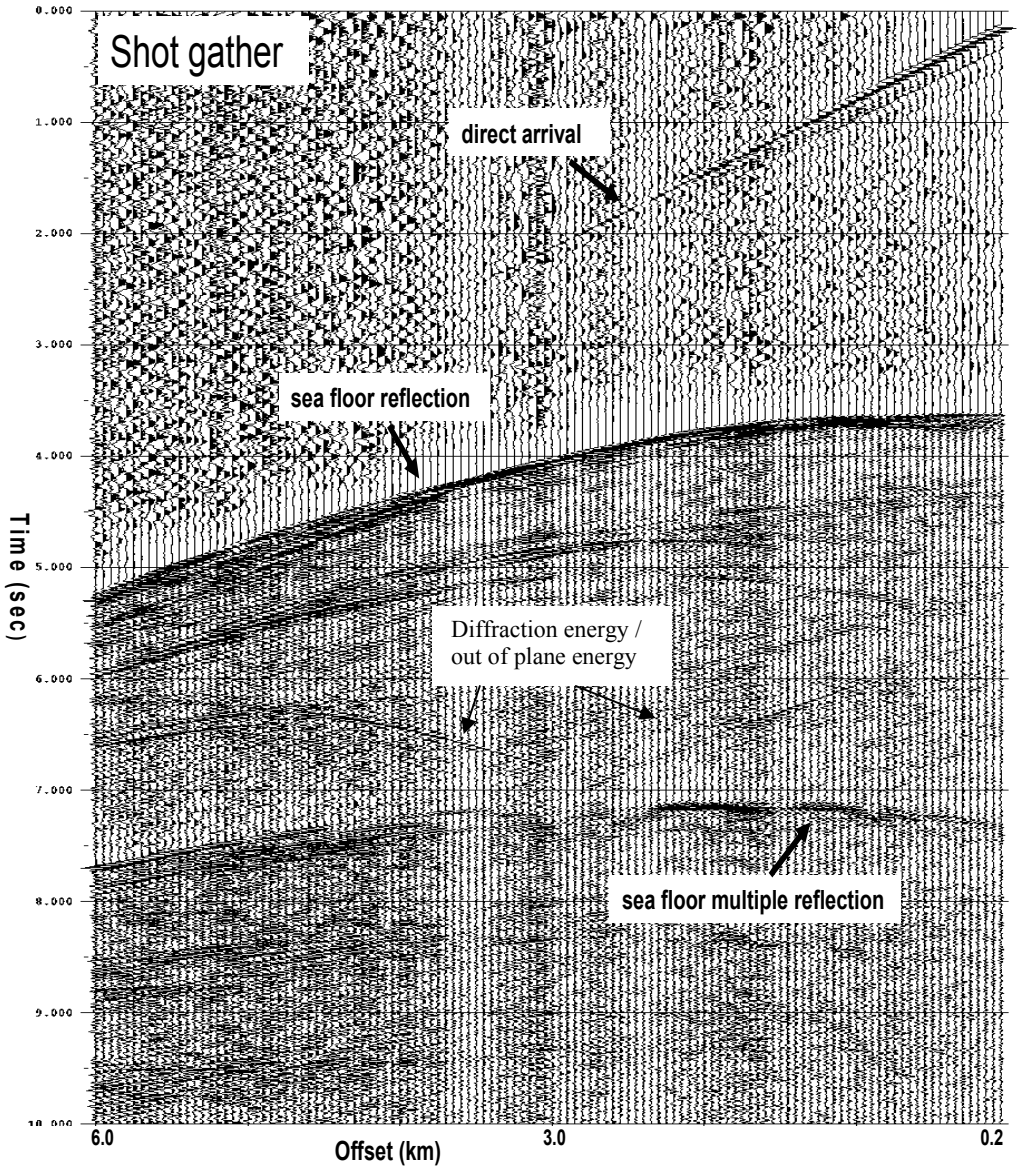

Figure 2.2. A shot gather example.

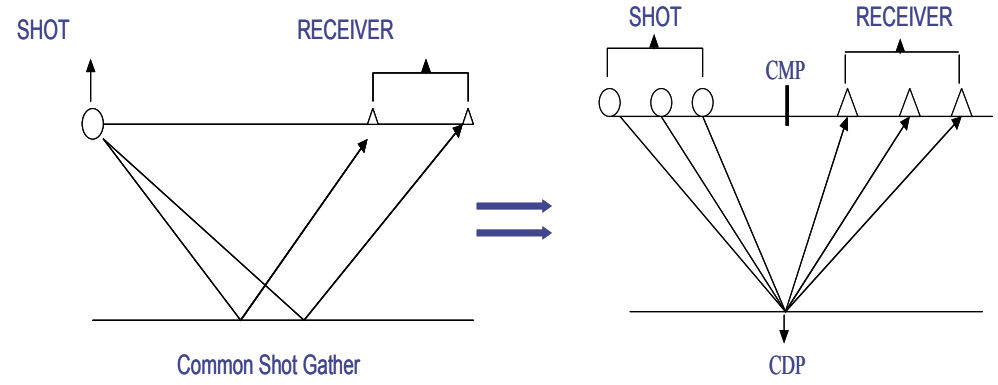

Figure 2.3. Sorting from a shot gather to a CDP gather geometry. CMP is the surface common mid point location between shot and receiver. If the subsurface comprises of horizontal reflectors then CMP is the vertical projection of CDP on the surface.

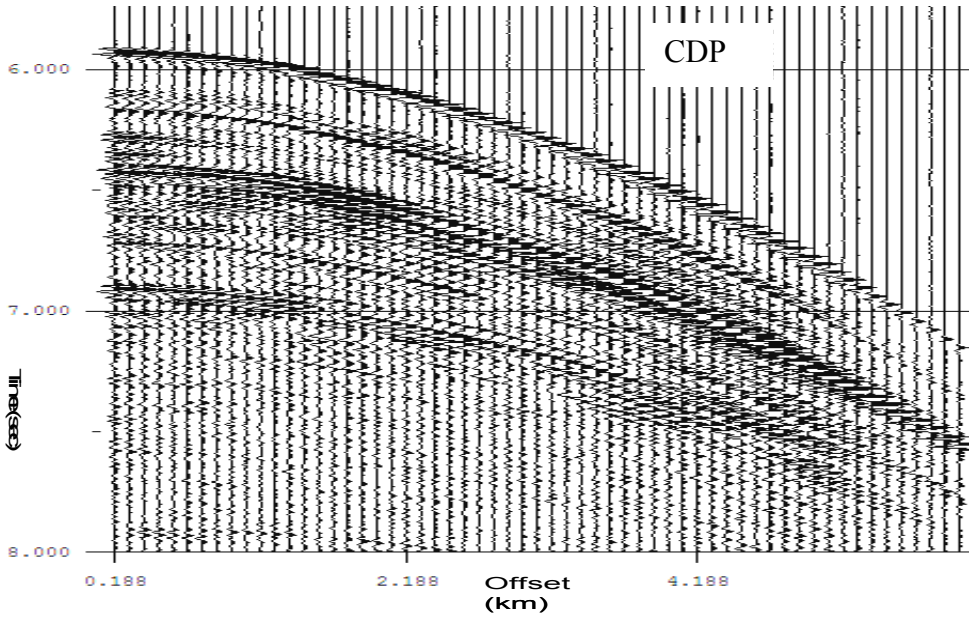

Figure 2.4. Example of a CDP gather. The reflections are observed as hyperbolic events in the gather.

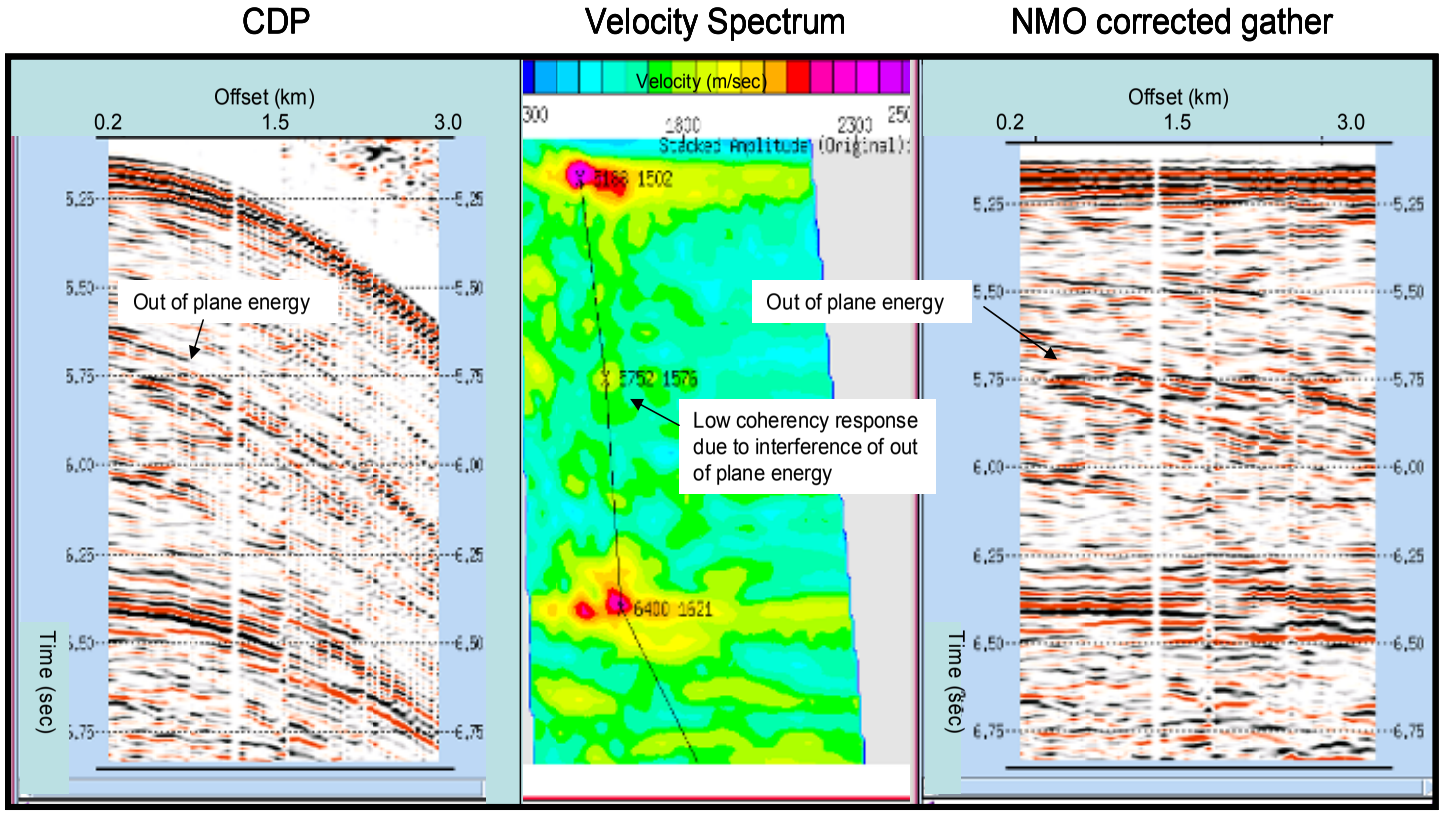

Figure 2.5. Velocity analysis for a CDP gather. The velocity spectrum (a colored display of coherency) is used for picking the velocity which will make the reflectors flat once we do NMO corrections. The NMO corrected gather with the picked velocity function is shown on the right.

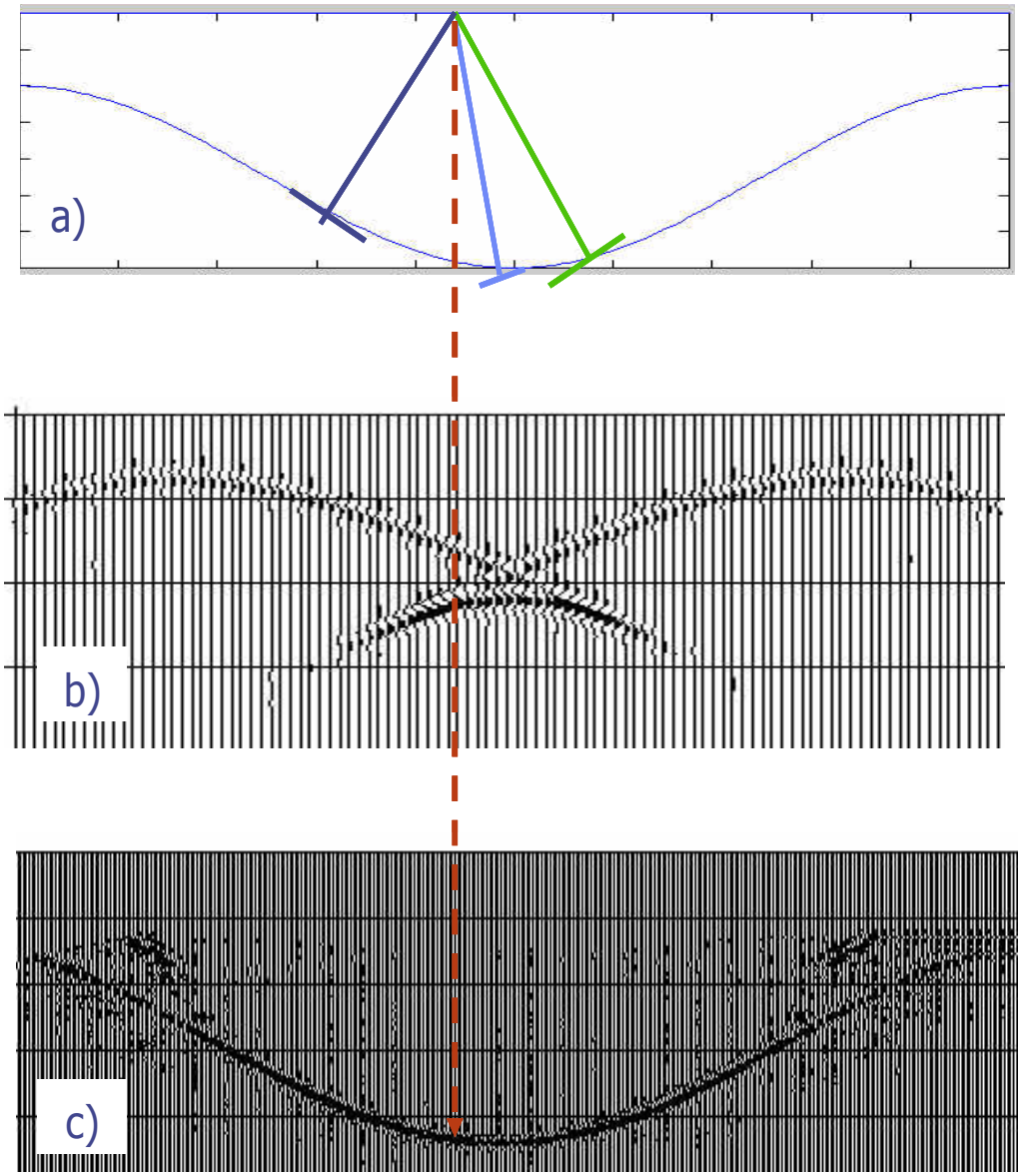

Figure 2.6. (a) A syncline model, (b) stacked section of the syncline model and (c) post-stack migrated result of stack section in (b). The migrated section closely resembles the syncline model in (a).

2.3 SEISMIC MIGRATION

The aim of migration is to reveal the true structure and geometry of the subsurface reflectors and to improve the spatial resolution of the seismic data by moving dipping reflectors into their true subsurface position. In addition, migration collapses diffractions caused by sharp edges or discontinuities within the earth. Existing migration methods can be classified according to several different criteria. First, migration algorithms can be classified according to the place of migration in the processing sequence, i.e., pre-stack migration (prior to summation of CMP gathers) or post-stack migration applied after summation of CMP gathers (Yilmaz, 1987; Claerbout, 1985). They can also be classified based on the extrapolation coordinate, i.e., time migration or depth migration. They can be classified on the basis of the extrapolation domain, which are time-space (t-x) migration (Schneider, 1978; Claerbout, 1985; McMechan, 1983), frequency-wavenumber (f-k) migration (Stolt, 1978, Gazdag, 1978, Gazdag and Sguazzero, 1984) or frequency-space (f-x) migration (Stoffa et al., 1990). Also, they can be classified based on the input for each extrapolation step, i.e., recursive migration (e.g. Phase Shift migration, Split Step Fourier migration) or non-recursive migration (e.g. Kirchhoff migration).

2.3.1 Post-stack Migration

In a zero-offset section (Figure 2.7a), each trace corresponds to a field acquisition geometry, where the sources and receivers are assumed to be coincident. One of the models for migration of stacked (CDP or CMP) seismic data is that the zero-offset section may be closely approximated by the output of a

hypothetical physical experiment based on exploding reflectors (Lowenthal et al., 1976). In this model every point in the subsurface is assumed to explode and emit up-going waves at time t=0 (Figure 2.7b), with an amplitude proportional to the reflectivity and with half the velocity between the diffraction point and the receiver at the surface. Since such data do not correspond to any wave field resulting from a single experiment, a zero-offset section provides an intuitive model for the post-stack migration case. The advantage of migrating stacked data is that the data volume is reduced by orders of magnitude (by the stacking process), has an increased signal to noise ratio compared to the original field data and in many cases it will collapse diffractions and position reflecting events with reasonable success. Since the sources and receivers are coincident in a zero-offset section, they can be downward continued simultaneously. As a result, post-stack migration of CMP data is considerably less expensive than migration applied before stack. On the other hand, there are situations where stacked data fail to mimic the zero-offset required for post-stack migration. The migration process that produces a migrated time section is called time migration (Taner and Koehler, 1977). Time migration requires rms (root mean square) or stacking velocities, which can vary both laterally (space) and vertically (time) so the resulting image is in the space and time domain. However, time migration is appropriate only as long as lateral velocity variations are mild to moderate. On the other hand, depth migration (Judson et al., 1980, Larner et al., 1981) requires detailed interval velocities and can handle significant lateral (space) and vertical

(depth) velocity variations. The resulting image from depth migration is in the true space and depth domain.

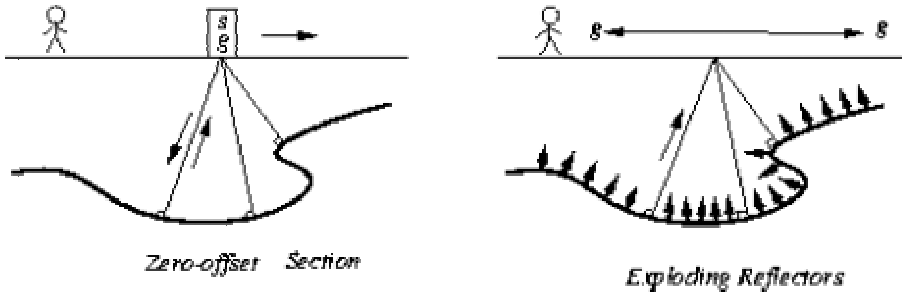

a) **b)**

Figure 2.7. Echoes collected with a source-receiver pair moved to all points on the earth's surface (a) and the ``exploding-reflectors'' conceptual model (b). (Claerbout, 1985)

I did the conventional processing up to and including post-stack time migration on most of the MCS lines offshore Nicaragua using a commercially available processing system, Paradigm's Focus software (available at the University of Texas Institute for Geophysics). The processing steps include trace editing, gain corrections, filtering, deconvolution, sorting into CMP gathers, multiple attenuation, velocity analysis, stacking and post-stack migration. Figure 2.8 show the location of the seismic lines. From post-stack migrated section of NIC-60 (Figure 2.9) it appears that the fault block rotation is preserved in the lower plate on subduction. The upper plate deformation near the lower slope of NIC-60 (Figure 2.9) also suggests the subuction of rotated fault blocks. It also seems that fault block rotation is preserved even at the deeper section (~20km) of NIC-80 after subduction as shown in Figure 2.10. In NIC-80 (Figure 2.10) we

observe a subducted seamount and we can observe the upper plate deformation. On the other hand there is little or no fault block rotation of the incoming plate shown in Figure 2.11 (CR-20). Also there is no fault block rotation after subduction. Based on these observations we have developed a hypothesis (Figure 2.12) that can explain the geochemical disparities offshore Nicaragua and Costa Rica. Basically, the horsts of the rotated fault blocks act as a conveyer belt to carry the sediments along the subducted plate surface to the volcanic roots.

A stacked seismic section is often not a good approximation to a zero-offset section in regions where steep dips and/or strong lateral velocity changes are present because hyperbolic moveout assumptions may not be appropriate for certain reflections (Yilmaz, 1987, Claerbout, 1985). Therefore, even though it will be more expensive, in such cases pre-stack migration is preferred (Yilmaz, 1987, Claerbout, 1985). The models (Figure 2.12) in our hypothesis have significant lateral velocity changes and are structurally very complex.

Providing the velocity field information for migration is vitally important. Depth migration (poststack or prestack) requires a detailed interval velocity model. It turns out that estimating the velocities to be used for depth migration is much harder than the problem of migration itself (Yilmaz, 1987). Migration velocity analysis is a powerful tool for updating interval velocity, but it requires analysis of Common Image Gathers (CIG) obtained from prestack depth migrations. Thus obtaining a true interval velocity of complex areas for migration provides additional motivation for doing prestack depth migration.

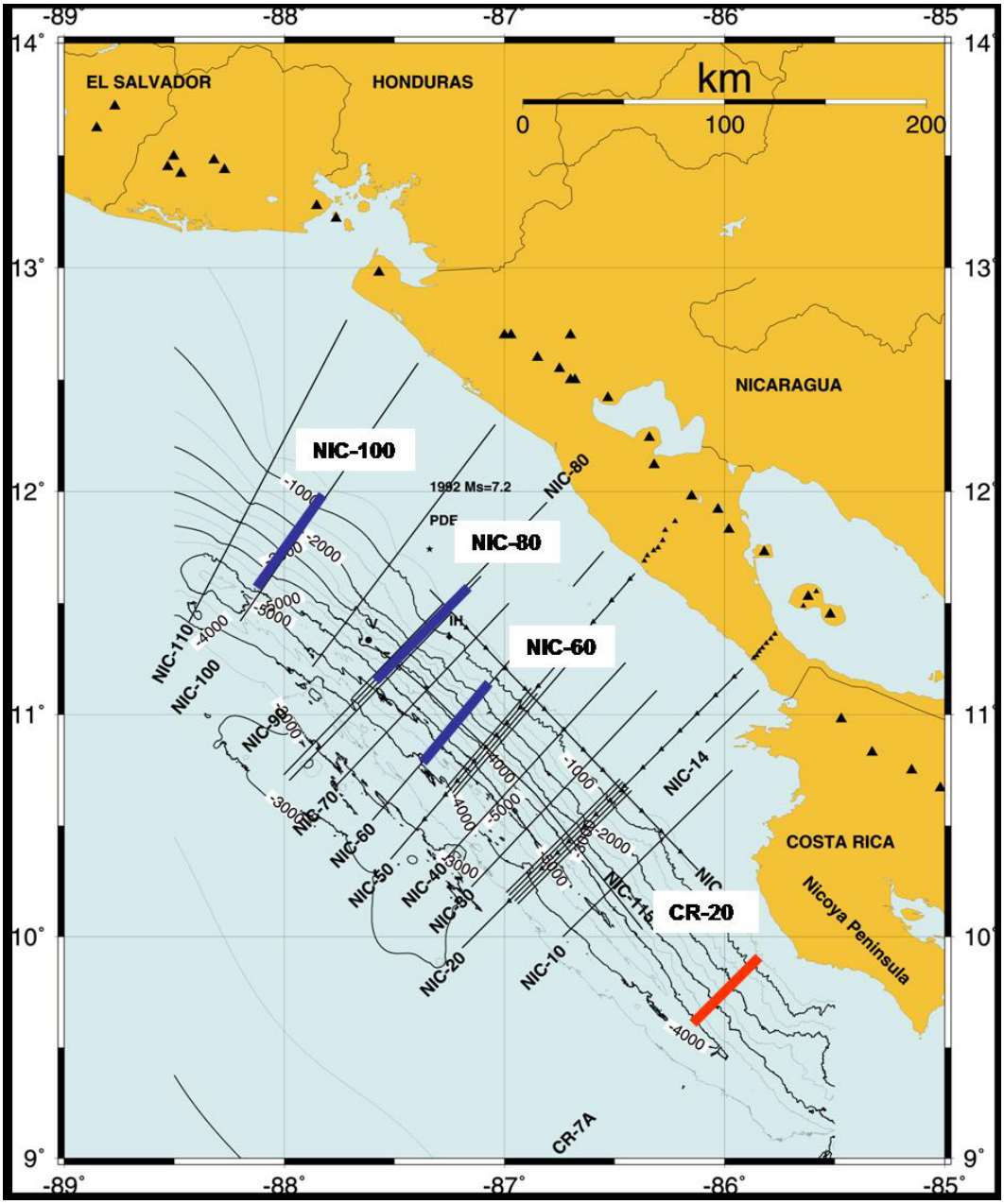

Figure 2.8 Map showing the location of MCS lines discussed in this chapter.

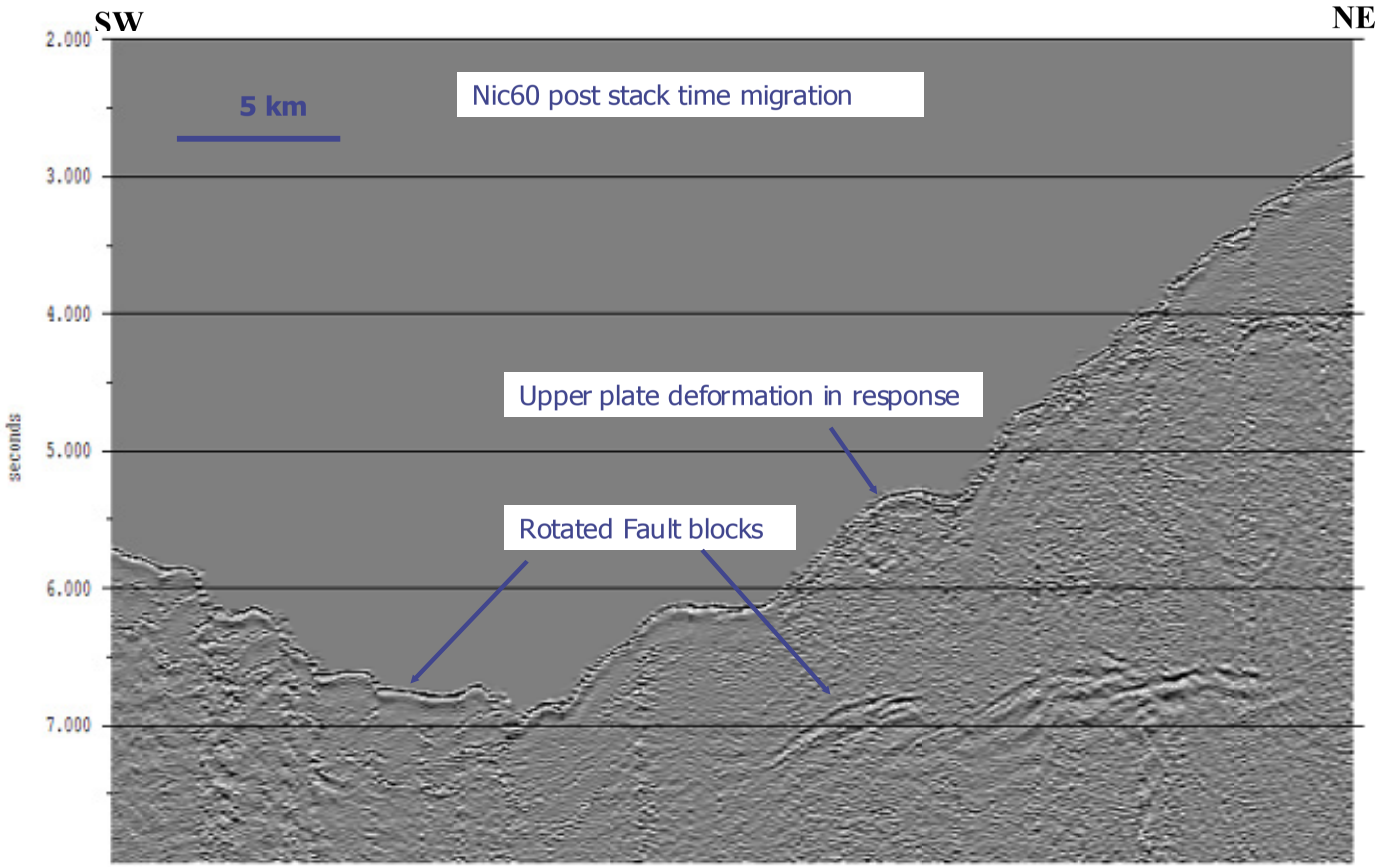

Figure 2.9 Post-stack time migrated image of NIC-60.

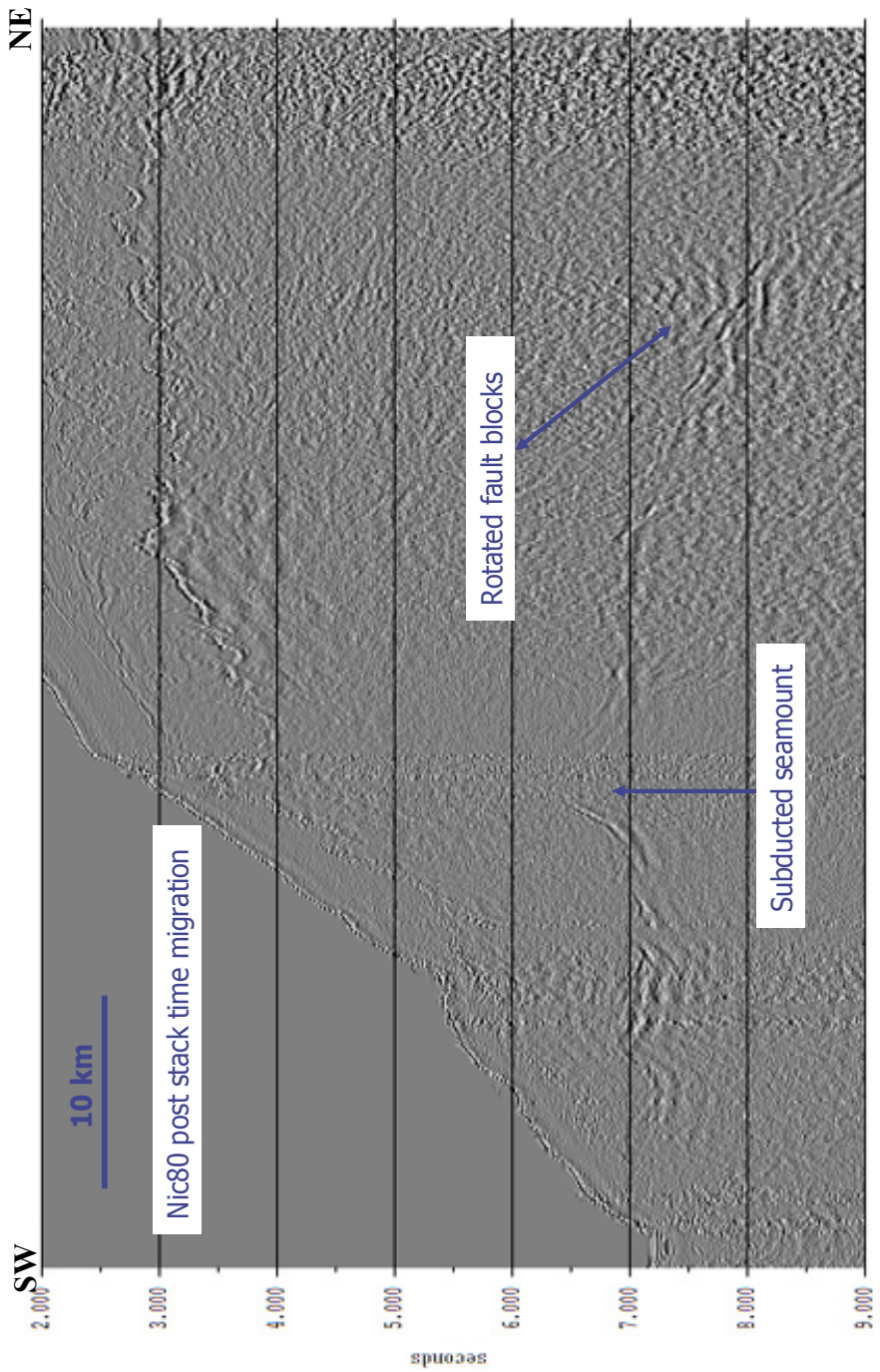

Figure 2.10. Post-stack time migrated image of NIC-80.

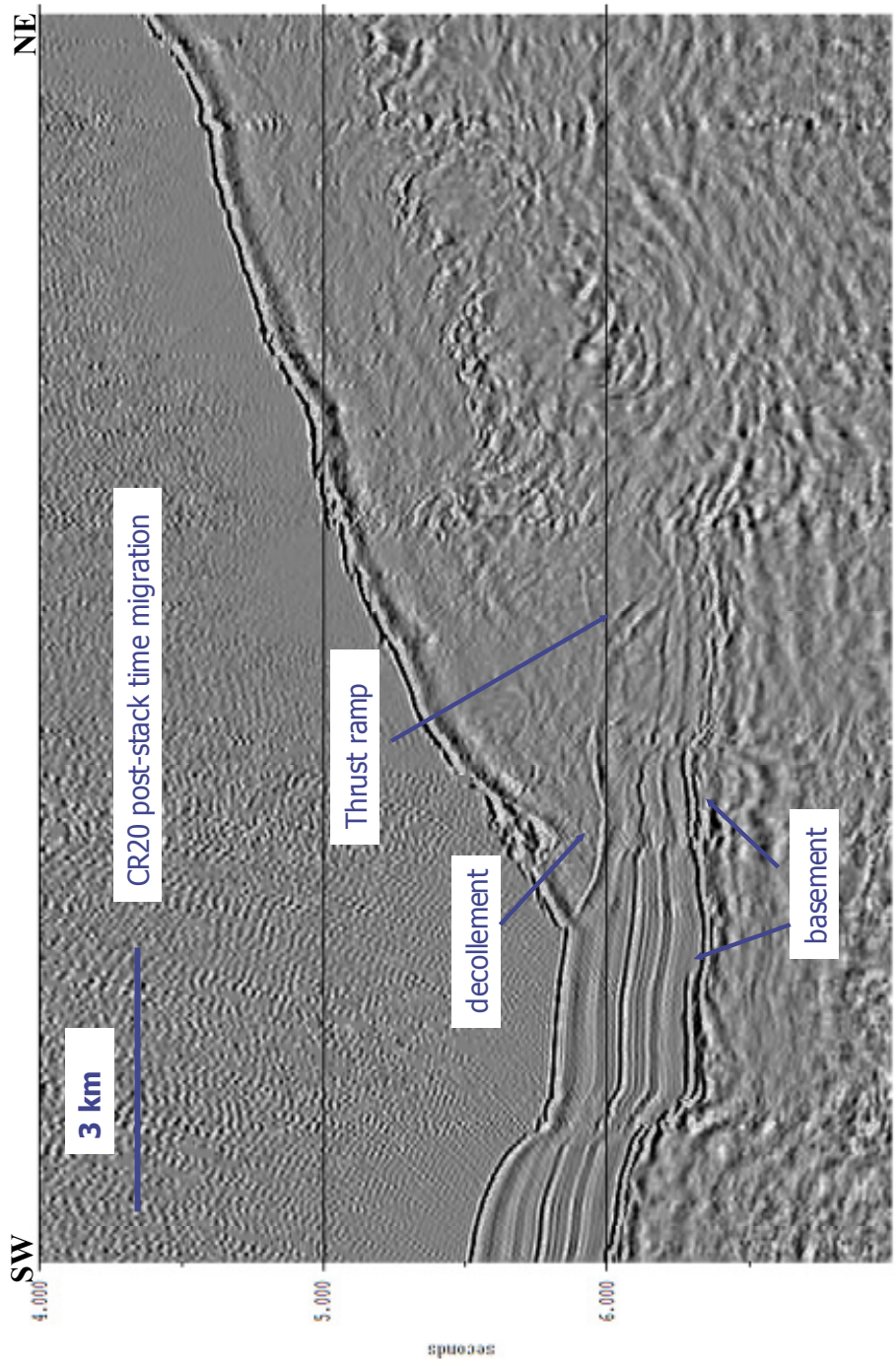

Figure 2.11. Post-stack time migrated image of CR-20.

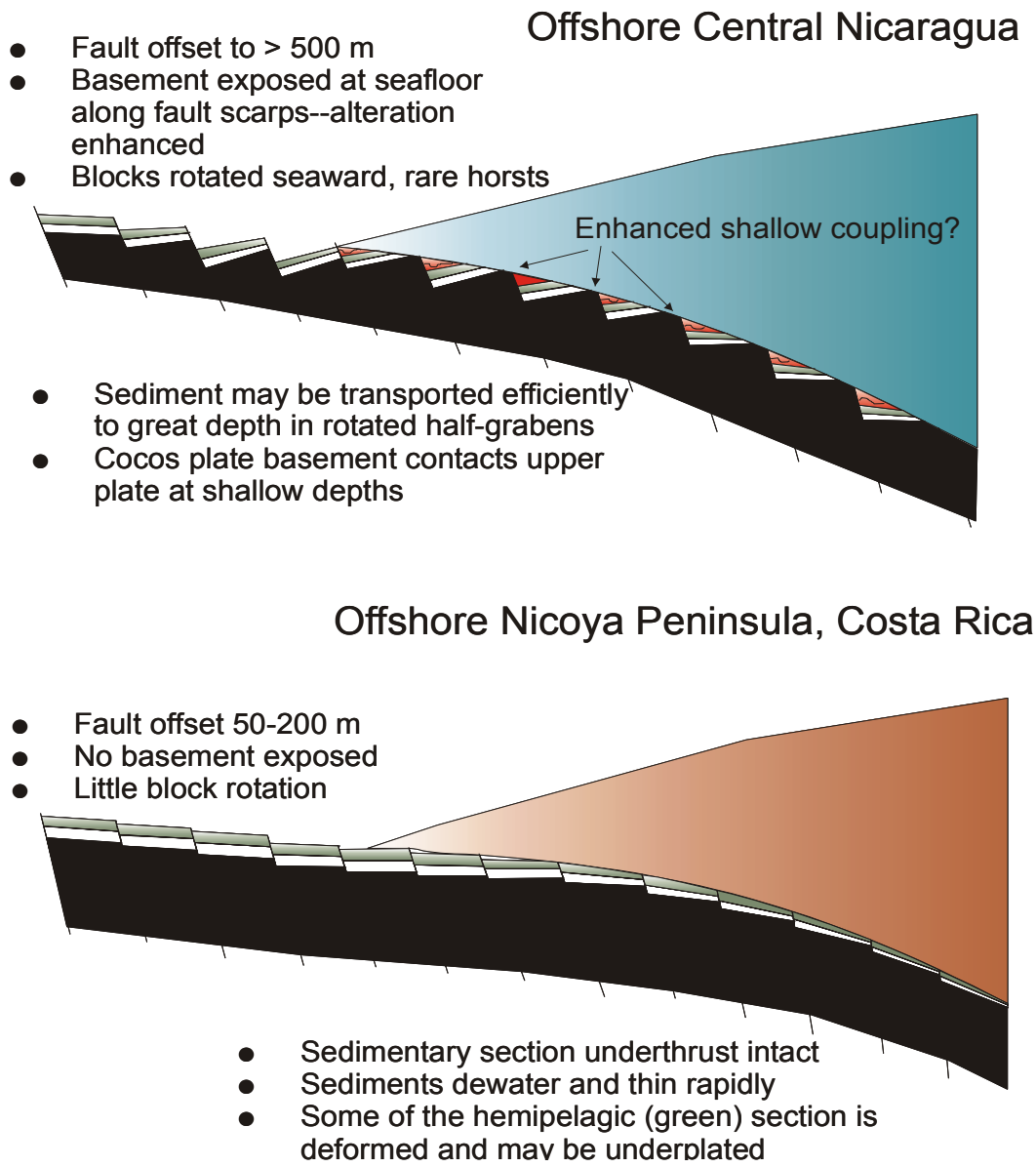

Figure 2.12. Cartoon showing and describing my hypothesis.

2.3.2 Pre-stack migration

Pre-stack migration creates an image of the earth's reflectivity directly from the original recorded data. It is an alternative to the ``**exploding reflector**'' (Lowenthal et al., 1976) concept that proved so useful in zero-offset migration. In **pre-stack migration**, we explicitly consider both the downgoing and upcoming waves.

A good starting point for discussing pre-stack migration is a scattering point within the earth. A wave incident on the point from any direction scatters waves in all directions (Trorey, 1970). This geometry is particularly important because any model is a superposition of such point scatterers. The point-scatterer geometry for a point located at (*x*,*z*) is shown in Figure 2.13.

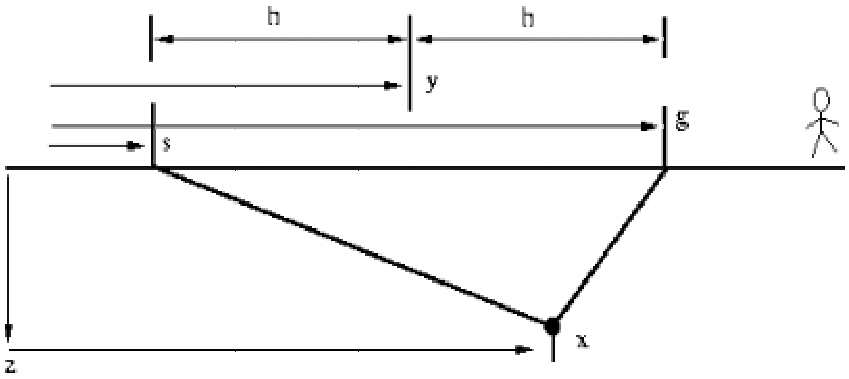

Figure 2.13. Geometry of a point scatterer. (Claerbout, 1985)

The equation for travel time *t*, the sum of the two travel paths is

$$tv = \sqrt{z + (s - x)^2} + \sqrt{z + (g - x)^2} \,. \tag{2.1}$$

We could model the recorded field data with equation (2.1) by superimposing scatterers from any point in (*x*,*z*)-space into (*s*,*g*,*t*)-space using the appropriate travel times and amplitudes. Alternatively we could form an image by stacking over all recorded offsets. This process would be called pre-stack migration. One problem here is that the velocity must be known. It is not satisfactory to use a constant or even horizontal layer velocity approximation to do migration in complex areas. Migration becomes even more sensitive to velocity variations when wide angle propagations are being imaged. Errors in the velocity will cause events to add out of phase and diminish the benefits that accrue from pre-stack (instead of post-stack) migration.

One of the most important pre-stack depth migration techniques is the Kirchhoff depth migration. Schneider, 1978 posed the migration as a boundary value problem, which led to an integral or summation algorithm in either two or three dimensions. The scalar wave equation is given by

$$\nabla^2 P(r,t) - \frac{1}{V^2}\frac{\partial^2 P(r,t)}{\partial t^2} = 0 \ , \tag{2.2}$$

where, $P(r,t)$ is the acoustic wave field at point $r(x,y,z)$ at time t and V is the velocity of the medium. Solution of the scalar wave equation based on Green's theorem is given by

$$P(r,t) = \frac{1}{4\pi}\int dt_0 \int dS_0 \left[G\frac{\partial}{\partial n}P(r_0,t_0) - P(r_0,t_0)\frac{\partial}{\partial n}G \right], \tag{2.3}$$

where, $P(r_0,t_0)$ is the wave field recorded at the surface, G is the Green's function and n is the outward normal vector to the surface S_0. Since $P(r_0,t_0)$ in equation (2.3) is equated to the observed seismic data on the surface, we require that $G=0$ on the surface (A_0) in order to eliminate the gradient in P. A Green's function

having the desired properties at the free surface consists of point source at r_0 and its negative image at $r_0^{'}$ or

$$G(r,t|r_0,t_0) = \frac{\partial(t-t_0-\frac{R}{V})}{R} - \frac{\partial(t-t_0-\frac{R^{'}}{V})}{R^{'}}, \tag{2.4}$$

where,

$$R = \sqrt{(z-z_0)^2+(x-x_0)^2+(y-y_0)^2},$$

and

$$R^{'} = \sqrt{(z+z_0)^2+(x-x_0)^2+(y-y_0)^2}\ .$$

Other choices of G are also possible. On substituting equation (2.4) into equation (2.3) and simplifying we get the following integral representation of the wave field $P(r,t)$ at any point in the image space in terms of observations of the wave field $P(r_0,t_0)$ on the surface,

$$P(r,t) = \frac{1}{2\pi}\int dt_0 \int dA_0 . P(r_0,t_0)\frac{\partial}{\partial z_0}\left[\frac{\partial\left(t-t_0-\frac{R}{V}\right)}{R}\right]. \tag{2.5}$$

The above equation is a rigorous statement of Huygen's principle and is commonly called the Kirchhoff integral. By interchanging the z_0 derivative with z derivative, which may be taken outside the integral, we get

$$P(r,t) = -\frac{1}{2\pi}\frac{\partial}{\partial z}\int dA_0 \frac{P\left(t-t_0-\frac{R}{V}\right)}{R}. \tag{2.6}$$

Equation (2.6) forms the basis of Kirchhoff migration. Equation (2.6) extrapolates the observed wave field from one z-plane to another which also can be written in 3D convolution form as,

$$P(x,y,z,t) = P(x,y,z_0,t) * \frac{1}{2\pi}\frac{\partial}{\partial z_0}\left[\frac{\partial\left(t \pm \frac{R}{V}\right)}{R}\right]., \qquad (2.7)$$

To obtain the image at a point *(x,y,z)*, we set t=0 in equation (2.6),

$$I(x,y,z) = P(x,y,z,0).$$

In this derivation V is a constant. In practice V is generally path dependent and can be explicitly taken into account.

The input seismic data used in Kirchhoff migration is organized either shot or common offset (CMP) gathers. Each gather is migrated independently to produce a partial image. Then these partial images are summed to generate a final image. In this method, there are major two steps:

- Traveltime computation
- Imaging

The traveltime computation is done usually by the finite difference solutions of the Eikonal eqauation (Schneider Jr. et al., 1992) or by ray tracing (Červený, 2001). The imaging is applied by mapping the amplitude of each trace into the image space with proper amplitude corrections (geometric divergence and source & receiver directivity). The amplitude correction *W* is given by the following equation (Aki and Richards, 1980)

$$W = (1/4\pi\rho v^2|s-x|)\times(1/4\pi\rho v^2|r-x|), \qquad (2.8)$$

where, ρ is the background density, *v* is the background velocity, |s-x| is the absolute distance between source and the image point and |r-x| is the absolute distance between receiver and the image point.

Figure 2.14 shows a schematic diagram illustrating this technique, s is the source location with respect to the grid and r is the receiver location with respect to the grid. x represents the scatterer location with respect to the grid. The shot and the receiver traveltimes are computed for all image positions in the grid and stored in a table. The objective in Figure 2.14 is to image point x. The traveltime t(s,x) from s (source) to x (scatterer) can be found from the shot traveltime table. The traveltime t(x,r) from the x (scatterer) to r (receiver) can be found from the receiver traveltime table. The total time t(s,r) is the sum of t(s,x) and t(x,r). Next we go to the trace produced by this shot and recorded by this receiver and we extract the amplitude that corresponds to the total time t(s,r) and we map it to location x in the image space. The corresponding amplitude correction (equation 2.8) is then applied. The procedure is then repeated at all grid points of the image space for all shots and for all receivers. The stacking of all partial images produces the final image. However if we use an incorrect velocity model then events don't map to the correct location in the image space as shown by green broken arrows in Figure 2.14. Therefore pre-stack migration is very sensitive to the velocity. An accurate velocity model (Versteeg, 1993) is very important for getting good pre-stack images. Therefore velocity analysis is a very important part of pre-stack migration. Once the data are migrated, errors in the velocity are manifested as residual depth errors in the imaged data for each offset of the same image point. Analysis of these residuals can be used to update the velocity (Yahya, 1989, Liu and Bleistein, 1992). I discuss a new residual migration velocity analysis technique in the depth-offset domain in the next chapter.

From Figure 2.15 through Figure 2.17 I compare the images from post-stack time migration to pre-stack time migration to pre-stack depth migration of MCS line NIC-100. Comparing these images we see an overall improvement in image quality from post-stack time migration to pre-stack time migration to pre-stack depth migration. In particular, the improvement in the image quality of the horst block near the trench before subduction and the horst block after subduction is noteworthy. These images further strengthen my belief that pre-stack depth imaging is necessary to achieve my interpretation objectives.

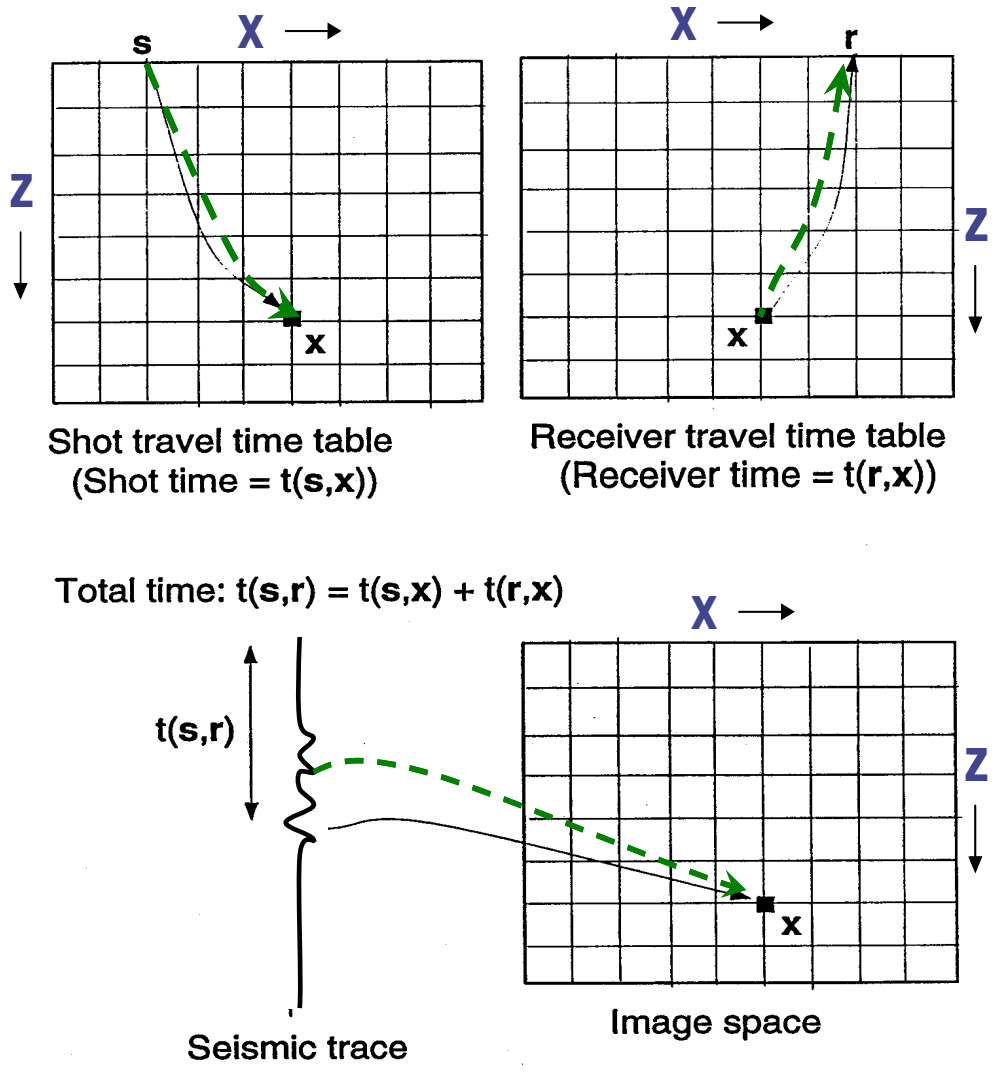

Figure 2.14. Conventional Kirchhoff depth migration. The broken arrows represent the incorrect mapping of events due to incorrect velocity model (modified from Akbar, 1997).

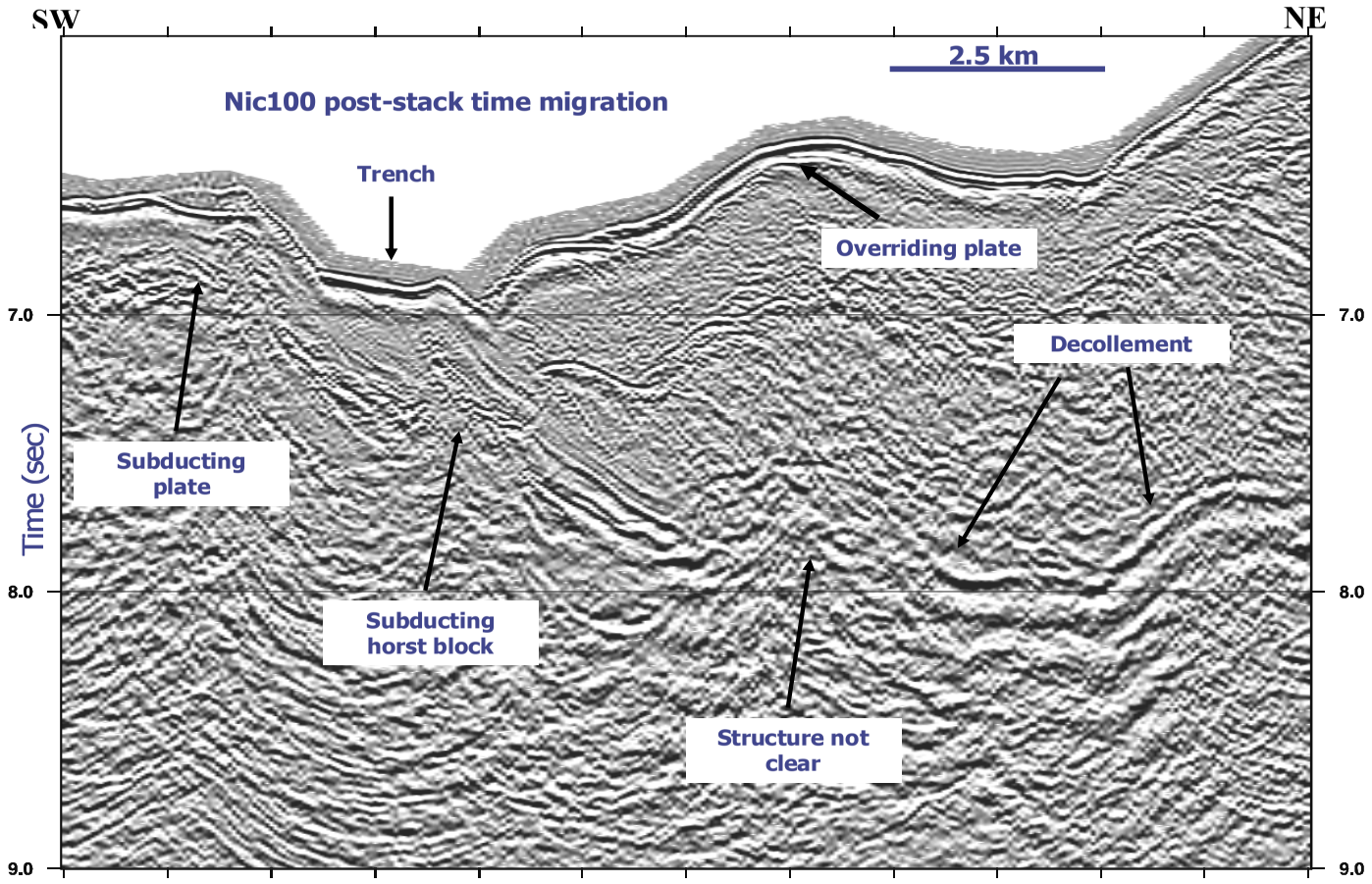

Figure 2.15. Post-stack time migrated image of NIC-100.

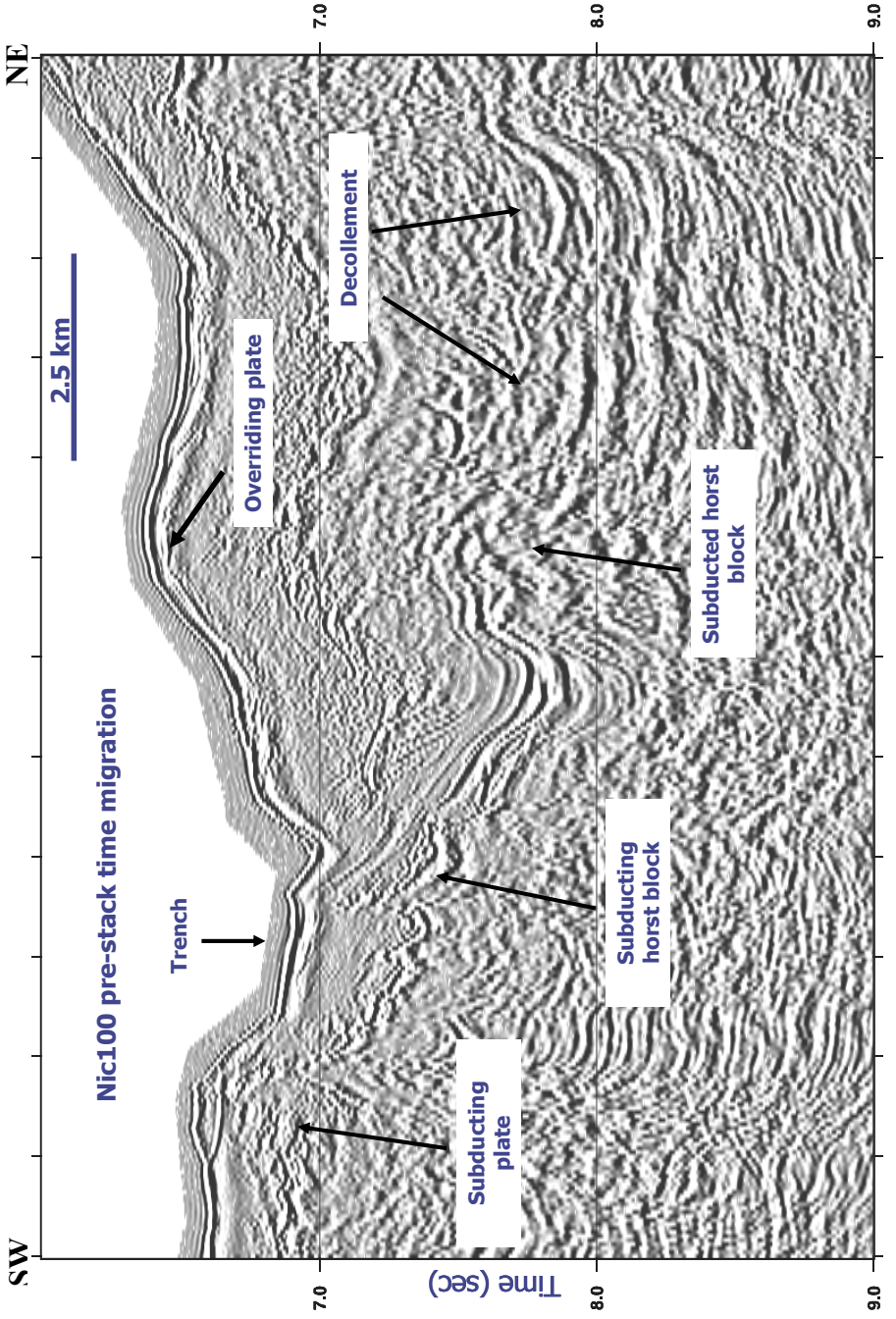

Figure 2.16. Pre-stack time migrated image of NIC-100.

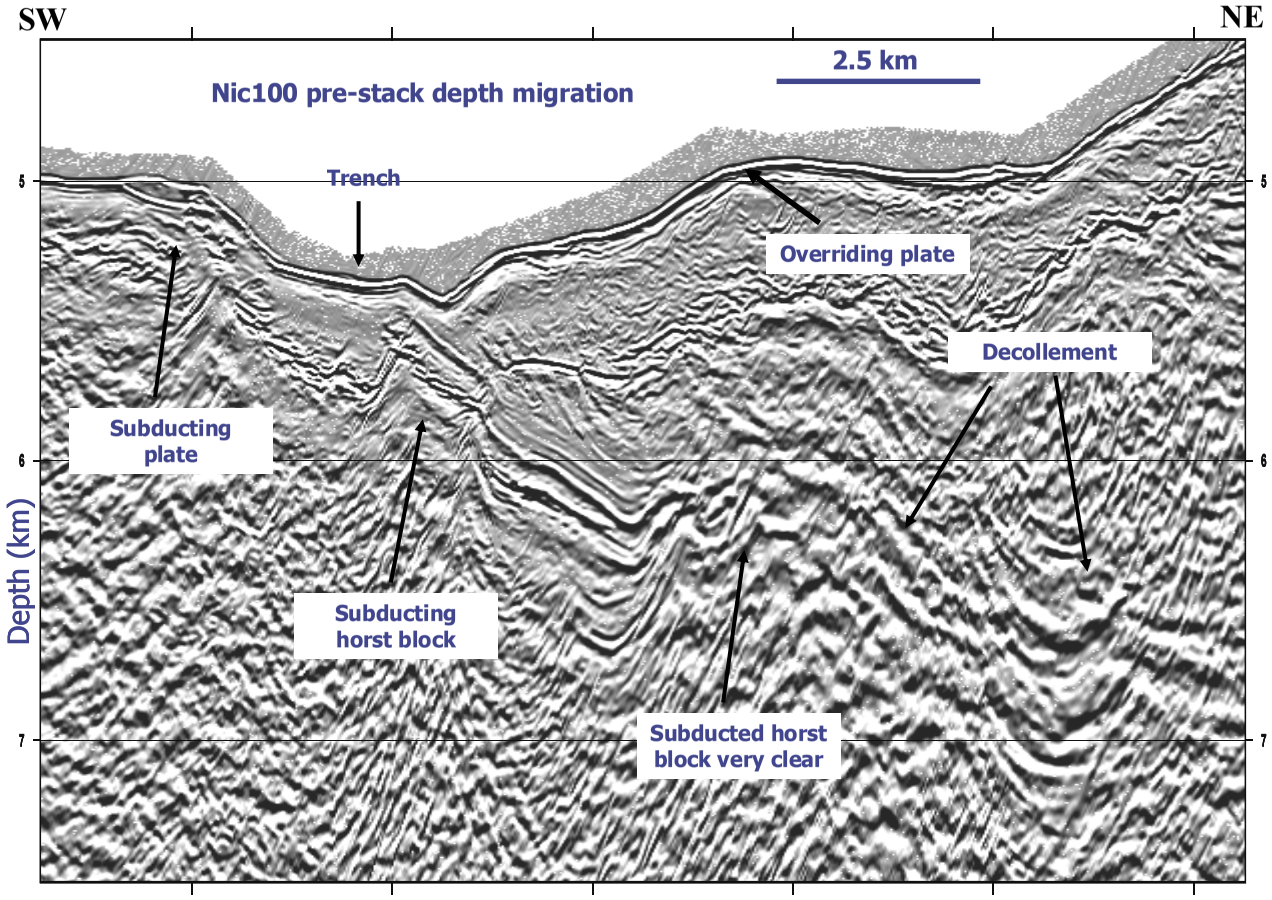

Figure 2.17. Pre-stack depth migrated image of NIC-100.

2.4 CONCLUSION

The aim of migration is to reveal the true structure and geometry of the subsurface and therefore it is one of the most important stages of seismic data processing. In this chapter I have discussed the basic theory of post-stack and pre-stack migration. I have also shown application of Kirchhoff post-stack and pre-stack migration. Through these images I have observed that for my objectives I need to do pre-stack depth migration. Pre-stack depth migration is very sensitive to the interval velocity. Therefore getting an accurate velocity depth model is very important to obtaining a good pre-stack depth image. In the next chapter I discuss a new and fast technique for getting a good interval velocity model.

Chapter 3: Residual migration velocity analysis in the offset-depth domain via the ray parameter-depth domain

3.1 ABSTRACT

Over the last few decades, residual migration velocity analysis has been an area of active research. Previous work on residual migration velocity analysis in the depth-offset domain required top down layer stripping migration in order to derive the interval velocities directly, hence making it very computationally intensive. Here we propose a new technique in which for each common image gather (CIG) we first create a table of offset-ray parameters -depth (*x*-*p*-*z*) using a local 1D assumption. Then we calculate the residual migration depth corrections in the *p*-*z* domain and finally map these depth corrections back to the *x*-*z* domain using the *x*-*p*-*z* table. Since we calculate the residual migration depth corrections in the *p*-*z* domain, the interval velocities are derived directly by top down residual migration. Hence we do not have to explicitly do the layer stripping migration followed by residual normal moveout to get the interval velocities. Results on synthetic data and real data tests are encouraging.

3.2 INTRODUCTION

Using wave theory, it is possible to decompose a spherical wave from a point source into a series of plane waves. Stoffa et. al. (1981) decomposed seismic reflection data from time-offset (*x*-*t*) into plane waves (τ-*p*) by slant stacking (τ-*p* transform) and showed many advantages of representing the data in this domain.

One of the most significant advantages is the ease of direct interval velocity analysis in the τ-p domain (Stoffa et. al., 1982). This is not possible in the x-t domain and we make use of this property in this work.

Research on prestack migration velocity analysis in the depth-offset domain began in the late 1980's (Yahya, 1989 and Liu, 1992), but was limited to mostly constant velocity, small dip and/or small offset. Later residual migration moveout analysis was extended to incorporate lateral velocity changes (Meng & Bleistein, 1999). These methods being in the depth-offset domain follow the top-down layer stripping migration using different trial velocities to derive the interval velocities and are therefore very computer intensive. Recently, Jiao et al. (2002) proposed residual migration velocity analysis in the plane-wave domain, which updates interval velocities directly in a top-down residual–difference correction for all layers after prestack depth migration instead of top-down layer stripping migration followed by residual velocity analysis. This is less computer intensive and thus can be used for 3-D residual migration velocity analysis.

However, most of the current reflection seismic data processing and analysis including migration algorithms are carried out in the depth-offset domain. Therefore it is quite natural that we implement the residual migration velocity analysis in this domain. Thus our goal here is to extend the concepts described by Jiao, et al. (2002) to the depth-offset (z-x) domain.

In this chapter I first discuss the basics of the analysis of seismic wave in the τ-p domain, then develop the theory of residual migration velocity analysis in

the depth-offset domain using the τ-p domain. Finally I show some applications on synthetic and real data using this new technique.

3.3 BASIC CONCEPTS

The space-time (x-t) domain shot gather can be decomposed into the plane wave domain, which is also called the τ-p domain. Tau (τ) refers to the sum of the vertical slowness-thickness products (vertical delay time) and p refers to the horizontal slowness or ray-parameter, which is a ratio of the sine of the angle of incidence and the velocity. Let us consider a plane wave traveling in a homogenous acoustic medium with velocity V in a direction specified by i, the angle of the ray with vertical (Figure 3.1).

Traveltime can be expressed in terms of these two components as:

$$\Delta T = p\Delta X + q\Delta Z \tag{3.1}$$

where

$$p = \frac{\sin i}{V}, \qquad q = \frac{\cos i}{V} \tag{3.2}$$

are horizontal and vertical components of the wave slowness respectively. According to Snell's law, p, the horizontal slowness, is constant along any ray propagating through a stack of layers. If we write the inverse of velocity V as u, also called the slowness, then the relationship between p and q is given by the following equation

$$q = (1/V^2 - p^2)^{1/2} = (u^2 - p^2)^{1/2}. \tag{3.3}$$

For a horizontal n-layer model with slowness u_j, thickness ΔZ_j and vertical slowness q_j for the j^{th} layer, the two-way traveltime of a ray with constant ray parameter p, for a point source and a receiver located at z = 0, can be obtained by summing over the n layers

$$T = pX + 2\sum_{j=1}^{n} q_j Z_j \,, \tag{3.4}$$

where the distance from the source to the receiver is X (Figure 3.2). Equation 3.4 describes a tangent to the travel time curve at the point (T,X) with slope p and intercept time τ (Figure 3.3) (Stoffa, 1981(b)) given by

$$\tau = 2\sum_{j=1}^{n} q_j Z_j = T - pX \,. \tag{3.5}$$

The contribution to τ from a single layer can be written as

$$\Delta\tau_j = 2Z_j(u_j^2 - p^2)^{1/2} \,. \tag{3.6}$$

The above equation describes an ellipse in the τ-p plane, having semi-axial lengths of $2Z_j u_j$, and u_j, the two-way normal traveltime and slowness of the layer. The mapping of the space-time domain data into tau-p domain ellipses is shown in Figure 3.3.

Finally, τ-p curves for a horizontal n-layer model are governed by the following equation

$$\tau_n(p) = \sum_{j=1}^{n} \Delta\tau_j(p) = \sum_{j=1}^{n} 2Z_j(u_j^2 - p^2)^{1/2} = \sum_{j=1}^{n} t_j(1 - V_j^2 p^2)^{1/2} \,, \tag{3.7}$$

where $t_j=2u_j\Delta Z_j$ is the two way vertical travel time for layer j. Equation (3.7) can be also written as

$$\tau_n(p) = \tau_{n-1}(p) + t_n(1 - V_n^2 p^2)^{1/2} \tag{3.8}$$

where t_n is the two way vertical travel time for layer n. equation (3.7) is fundamental for data processing in the τ-p domain.

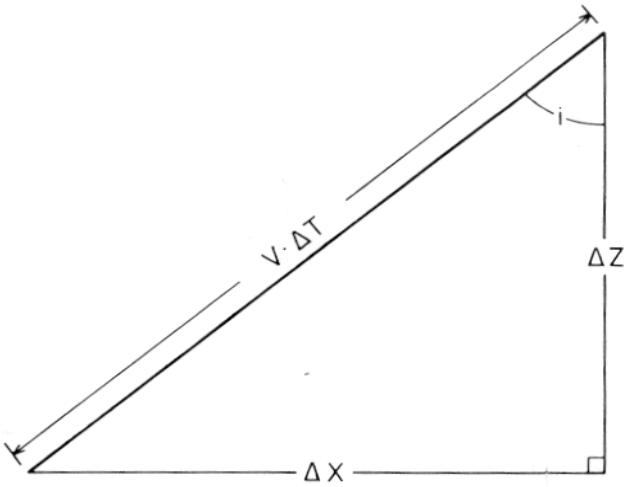

Figure 3.1. A portion of ray from a plane wave in a homogeneous medium with velocity V. The ray has a direction specified by the angle to vertical i. During the time ΔT, the ray traverse the distance VΔT, which is decomposed into its vertical component ΔZ and horizontal component ΔX (from Stoffa et al., 1981).

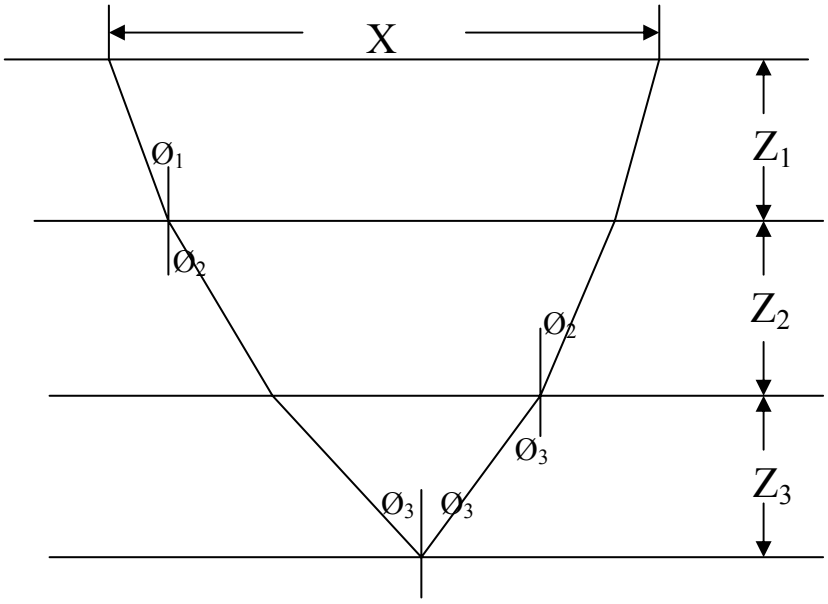

Figure 3.2. A stack of flat homogenous layers, showing the reflected ray path. The horizontal distance traversed is X. and the angle of the ray in each layer to the vertical is $Ø_j$.

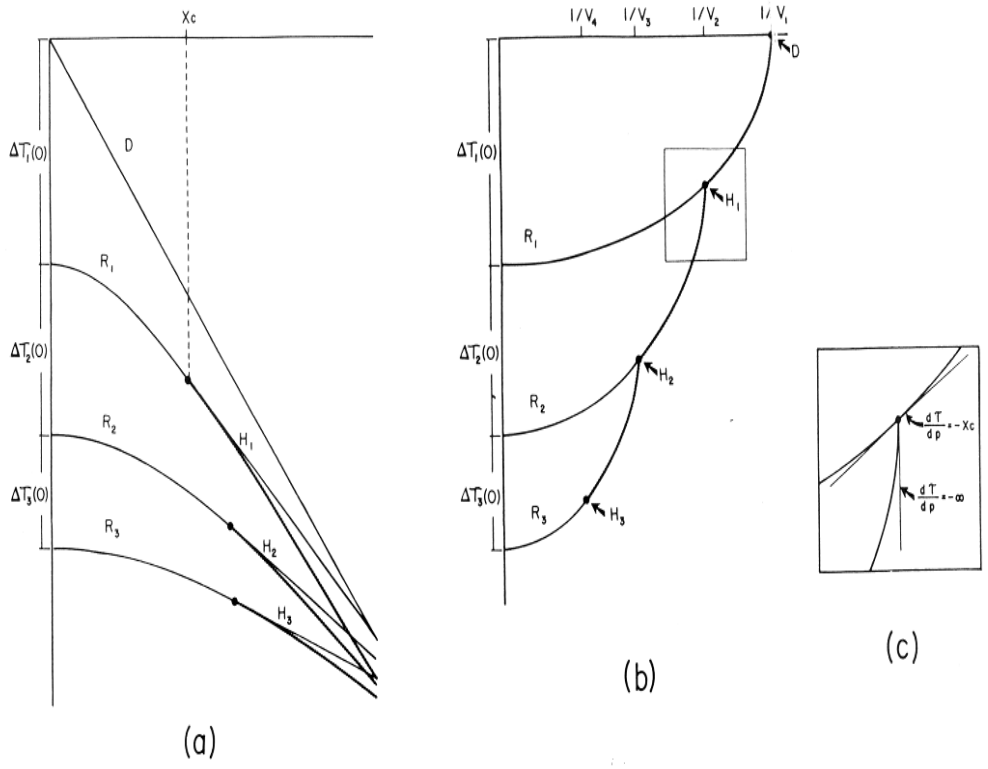

Figure 3.3 Relationship between the time space domain (a) and the τ-p domain (b). The travel time is plot in (a) for reflections and refractions in a 3-layer model (Figure 3.2) with two way travel times $\Delta\tau_j(0)$. The reflected arrivals are labeled R_j and are represented by the thicker lines post critical. Head wave refractions are labeled H_j. The Direct arrival is labeled *D,* and the range of the critical point of the first refraction is labeled as X_c. Figure 3.3b is the τ-p mapping of the X-T data of Figure 3.3a. On the τ-axis the p=0 intercepts are same as the vertical travel times of Figure 3.3a. The reflection mapping are marked and divided into sub and supercritical parts. The direct wave and the head wave refractions map as points. Figure 3.3c is a blow up of the τ-p mapping of the critical point for the head wave refraction H_1. The slope of the R_1 curve at this point is equal to the negative of the corresponding range X_c. The slope of R_2 curve as it approaches this point is minus infinity, corresponding to the range at which the R_2 travel time curve is asymptotic to H_1 (from Diebold and Stoffa, 1981).

3.4 THEORY

Equation (3.5) can be rewritten to obtain the equation for the depth of a n layer 1D model in the *z-p* domain as (Jiao et. al., 2002)

$$Z(p) = \sum_{i=1}^{n} \Delta Z_i(p) = \sum_{i=1}^{n} \frac{\Delta \tau_i(p)}{2(u_i^2 - p^2)^{1/2}}. \tag{3.9}$$

This equation relates the τ-p domain to the *z-p* domain for a 1D model for the true slowness values. Using equation (3.9), the depth of a reflecting horizon can be determined from the τ-p domain shot gather if the slownesses are known.

A trial slowness, u^m, is used to migrate the data, as the true slowness u is not initially known. The apparent depth, Z^m , at a given CIG is given by (Jiao et. al., 2002)

$$Z^m(p) = \sum_{i=1}^{n} \Delta Z_i^m(p) = \sum_{i=1}^{n} \frac{\Delta \tau_i^m(p)}{2((u_i^m)^2 - p^2)^{1/2}}. \tag{3.10}$$

The difference between the true slowness and the trial slowness will cause a misfit between the true depth Z and the migrated depth Z^m. This misfit is given by (Jiao et. al., 2002)

$$Z_{RMIG}(p) = Z(p) - Z^m(p) = \sum_{i=1}^{n} \Delta Z_i(p) - \sum_{i=1}^{n} \Delta Z_i^m(p)$$

$$= \sum_{i=1}^{n} \left[\frac{\Delta \tau_i(p)}{2(u_i^2 - p^2)^{1/2}} - \frac{\Delta \tau_i^m(p)}{2((u_i^m)^2 - p^2)^{1/2}} \right]. \tag{3.11}$$

In practice, $\Delta\tau_j$ and $\Delta\tau^m_j$ are acquired from every sample of the seismic data in the τ-p domain. Therefore, they are always equal to each other no matter what velocities are used for the migration and the uncertainty is only in the velocity and thickness. Therefore $\Delta\tau$ can be replaced by $\Delta\tau^m$. Then equation (3.11) becomes (Jiao et. al., 2002)

$$Z_{RMIG}(p) = \sum_{i=1}^{n} \Delta Z_i^m(p) \left[\frac{((u_i^m)^2 - p^2)^{1/2}}{(u_i^2 - p^2)^{1/2}} - 1 \right]. \tag{3.12}$$

For an n layer 1-D model it is possible to map to the offset-depth (x-z) domain for a CIG from a ray parameter-depth (p-z) domain CIG using the expression below (Aki and Richards, 1980)

$$x(p) = 2p \sum_{i=1}^{n} \frac{\Delta Z_i}{(u_i^2 - p^2)^{1/2}}. \tag{3.13}$$

Thus we can use the above equation to build a (x-p-z) table for a 1D model. The residual depth corrections calculated in the p-z domain using equation (3.12) can be mapped into the x-z domain using the (x-p-z) table calculated using equation (3.13). The cartoon in Figure 3.4 illustrates the above idea.

Equations (3.12) and (3.13) can be used to perform residual migration velocity analysis. We can use different trial slownesses in the residual migration, but only the residual migration corresponding to the true slowness will make the events flat in the CIG. However, the correct mapping will take place only if we

use the true velocity to create the *x-p-z* table. But since we do not know the true velocity to start with, if we use the incorrect velocity, the residual depth corrections calculated using equation (3.13) would be incorrect as well as the mapping because of the inaccurate *x-p-z* table. Thus the net effect is that we have non-flat events on the CIG. Theoretically, only the true velocity will give the correct answer. The examples in the next section illustrate our ideas.

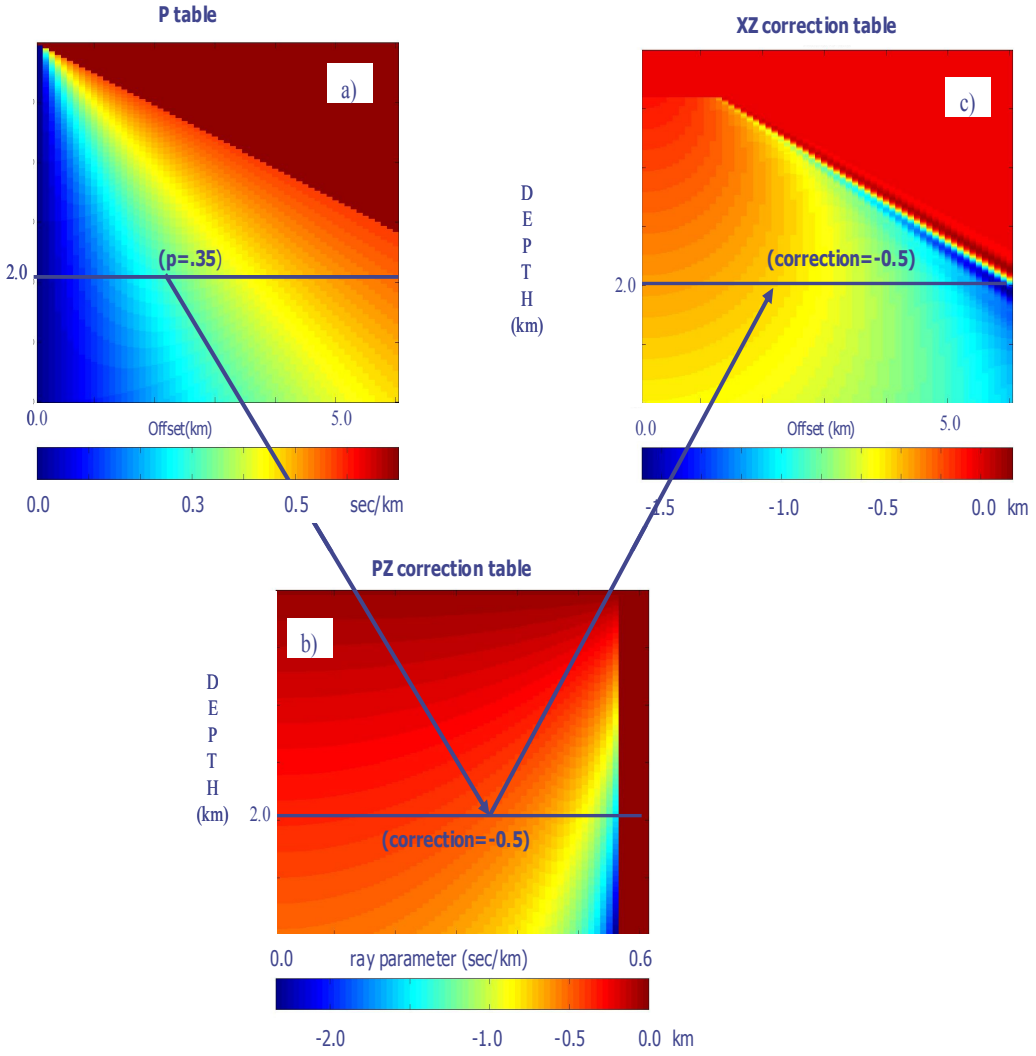

Figure 3.4 (a) the p table calculated using equation (3.13), (b) The depth correction in the p-z domain calculated using equation (3.12) and (c) the depth corrections in the x-z domain. In order to find the depth correction at a particular offset x and depth z. We first go to the p table (Figure 3.4 a) and find the p value for that (x,z) pair. Then we go to Figure 3.4 b and find the depth correction for that (p,z) pair. This is the depth correction in the space offset domain for the particular (x,z) pair.

3.5 EXAMPLES

Here we show examples of implementing our algorithm using several synthetic data sets, to demonstrate the effectiveness. In these examples, we first applied Kirchhoff pre-stack depth migration in the *x*-*t* domain with an incorrect velocity. Then we applied residual depth corrections in the *x*-*z* domain using different velocities following the ideas of Jiao, et al. (2002) but implemented these in the depth-offset (*z*-*x*) domain as described in the previous section.

The first example is that of a simple half-space with a flat reflector at 2 km depth as shown in Figure 3.5a. Figure 3.5b displays the incorrect velocity model that we used to migrate the shot gathers. Since we used too high a velocity for migration, the CIG in Figure 3.6a is curved downward and the zero offset response is at a deeper depth. The CIG in Figure 3.6b is obtained after applying the residual depth correction to the CIG in Figure 3.6a using the incorrect low velocity of 1.4 km/s. The depth corrected CIG shows an over correction, which is what we expect. The CIG in Figure 3.6c is obtained after applying the residual depth correction to the CIG in Figure 3.6a using the incorrect high velocity of 1.6 km/s. As expected, there is an under correction of the CIG. The results from using the correct velocity of 1.5 km/s to do the residual depth correction on the CIG in Figure 3.6a are displayed in Figure 3.6d. The correction has placed the reflector at the correct depth of 2 km and also the CIG is flat.

The next synthetic example simulates a 2D model. Figure 3.7 shows the velocity model used to generate the shot gather. It is a five layer model and has horizontal and opposite dipping reflectors. We used the incorrect constant

velocity of 1.5 km/s to migrate the data. Since we used lower velocities, the reflectors two to four in CIG at position 58 are all curved upward and are at incorrect depths (Figure 3.8a). Similar analysis, as in the previous example was done using this data. Figure 3.8b is the outcome of applying residual depth corrections to the CIG in Figure 3.8a using the true velocity. The events on CIG 58 are now flat and are at their correct depths.

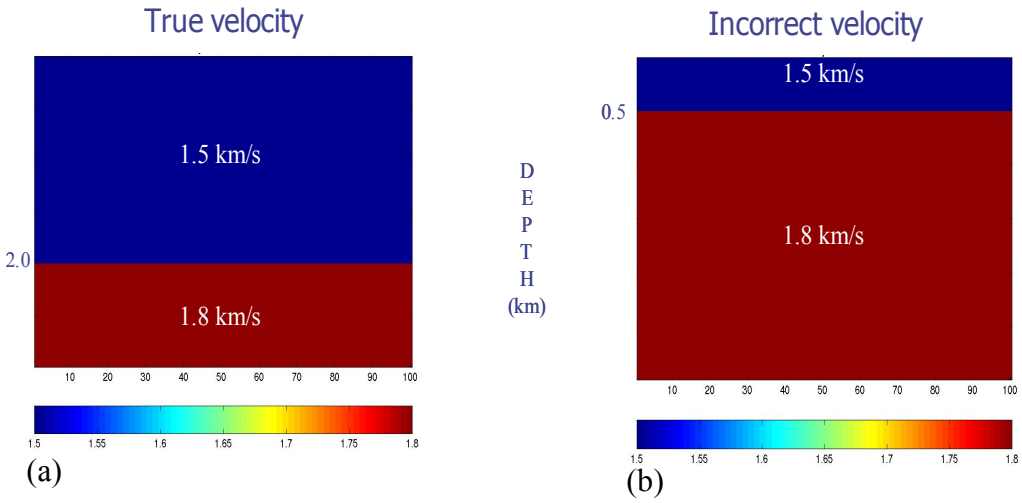

Figure 3.5. (a) Half-space velocity model. (b) Incorrect velocity model used for migration.

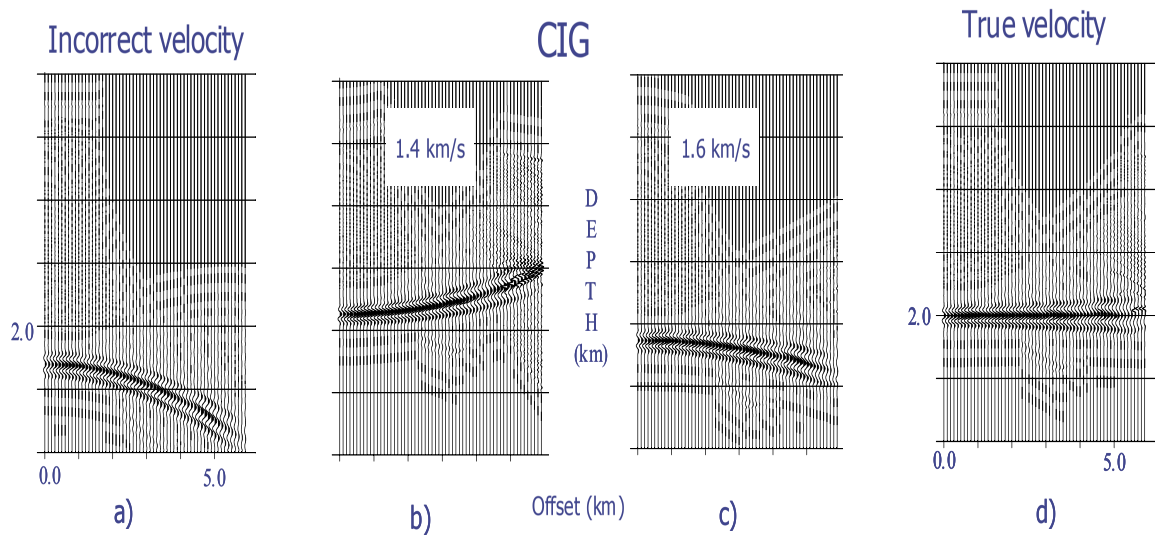

Figure 3.6 (a) CIG migrated using the incorrect velocity of Figure. 3.5b, (b) residual depth corrected CIG using the incorrect velocity of 1.4 km/s to do the residual depth correction to the CIG in Figure 3.6a, (c) residual depth corrected CIG using the incorrect velocity 1.6 km/s to do the residual depth correction to the CIG in Figure 3.6a, and (d) residual depth corrected CIG using the true velocity of 1.5 km/s to do the residual depth correction to the CIG in Figure 3.6a.

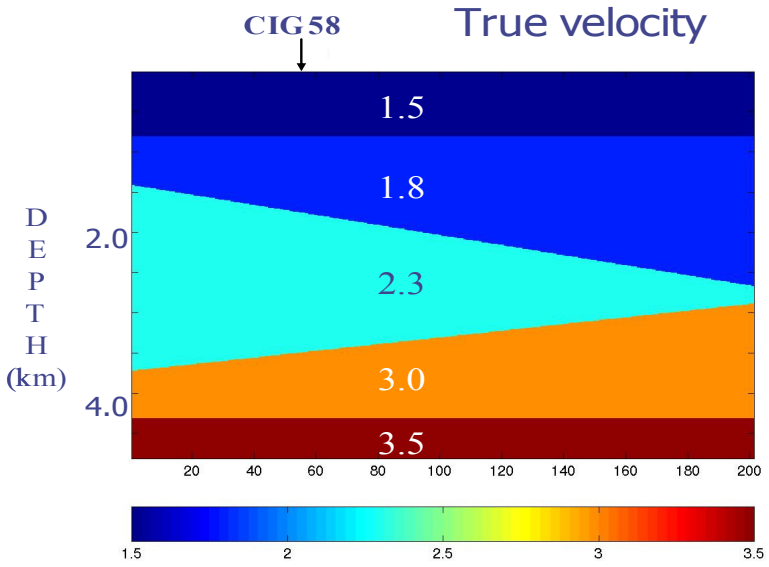

Figure 3.7. A five layer interval velocity model. The arrow is marking CIG58 shown in Figure below.

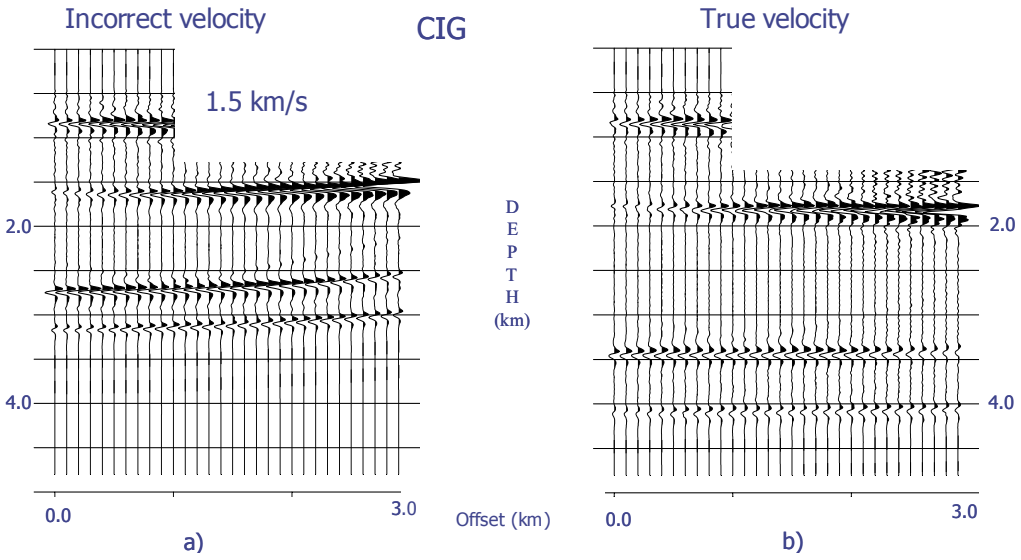

Figure 3.8. (a) CIG 58 using the incorrect constant velocity of 1.5 km/s, and (b) depth corrected CIG 58 using the true velocity of Figure 3.7.

3.6 IMPLEMENTATION OF THE RESIDUAL MIGRATION VELOCITY ANALYSIS:

I will demonstrate how to use equations (3.13 and 3.14) to develop a procedure to perform residual migration velocity analysis in the space offset domain which does not require a layer stripping process. The procedure is based on the condition that after pre-stack depth migration in the depth-offset domain with the correct velocity will generate horizontal events in the CIGS. On the other hand, velocity errors cause misalignment of the events in a CIG and only the true velocities can make residual migration give the flattest events.

3.6.1 Procedure for migration velocity analysis

First we require a starting interval velocity model, which can be obtained from stacking velocities or we can start with a smoothly varying velocity. The closer we are to the true velocity model, the fewer the iterations of residual migration velocity analysis that will be required to determine the true velocity or to approximate to true velocity model. First we perform pre-stack depth migration in the depth-offset domain for all depths and save the CIGs for residual velocity analysis. Next we apply residual migration to the individual CIG. We need to start the residual migration for the first or the topmost layer using a suite of residual velocities. The closer the derived velocity to the true velocity the flatter will be the events in the corrected CIG. Therefore we can use any of the standard procedures to determine the quality of the flatness of the events, such as, stack, semblance, etc. We can also interactively investigate the results of residual migration on a workstation screen to visually pick the best possible residual

velocity: such real time implementation is computationally tractable because of the efficiency of the formulation. After finding the best possible correction for the first layer we proceed in the same fashion to the next layer and so on. To obtain interval velocities directly, we only need to do top down layer stripping residual migration after migration for all depths instead of top down layer stripping migration and residual migration simultaneously for each individual layer. After finishing all the layers for one CIG we move on to the next selected CIG and repeat the procedure for all the selected CIGs. Then based on the new interpreted velocity functions we obtain a new velocity depth model by interpolation. We use the new velocity depth model to migrate the data again. The CIGs resulting from the new model should have flatter events then the previous one. If we are not satisfied with the results we repeat the process. The flowchart in Figure 3.9 summarizes the procedure.

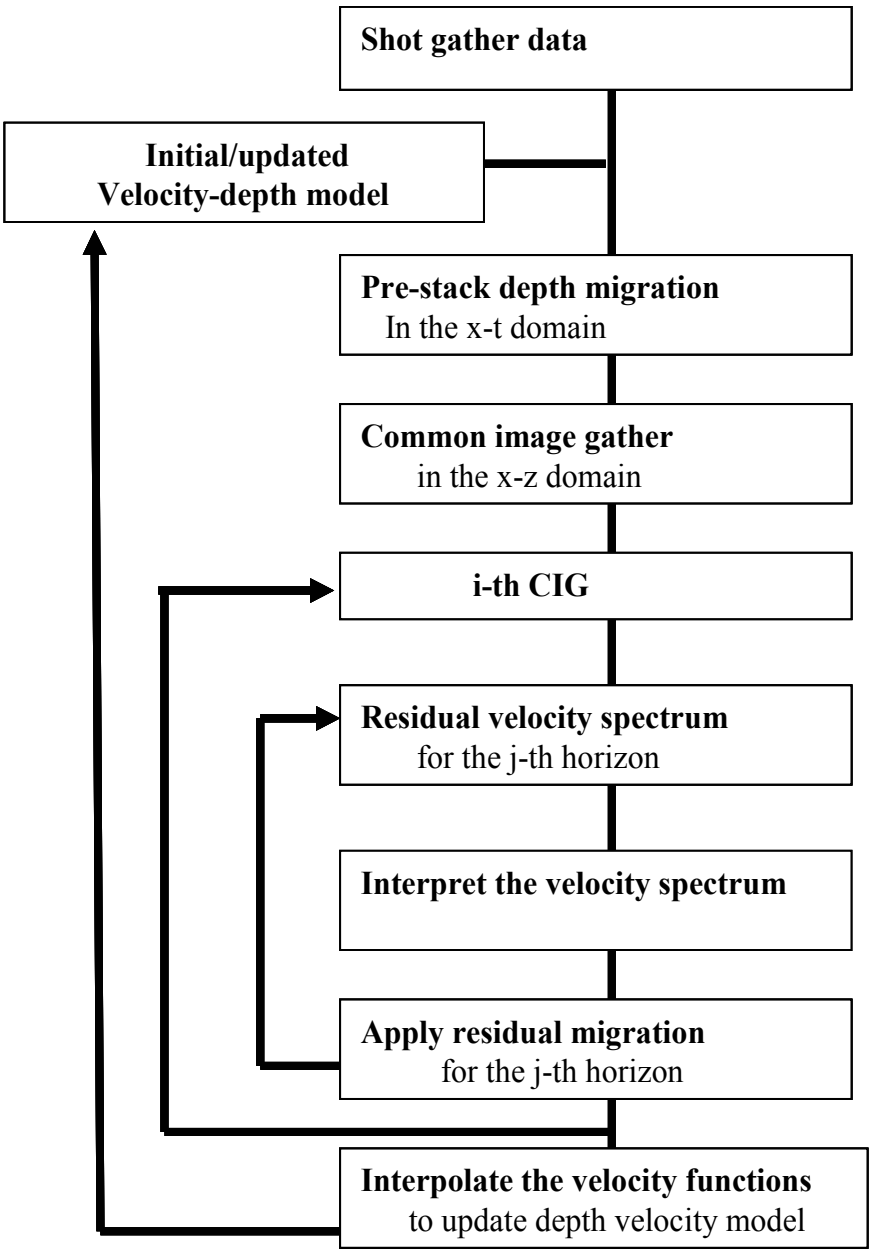

Figure 3.9 Flowchart for residual migration velocity analysis in the depth-offset domain.

3.6.2 Interactive updating of a velocity-depth model using residual migration in real time

To take advantage of the computational efficiency of the new residual migration velocity analysis method, an interactive graphic software package has been developed. This package performs the **horizon loop** and the **CIG loop** in the flowchart (Figure 3.9) interactively and in real time. Figures 3.10 through 3.13 show the major functions of this package which includes data loading and display, interactively changing velocity on the work station screen, real time residual migration, updating the velocity depth model, and outputting the new model and CIGs before and after residual migration.

To perform the analysis, the following data are loaded and displayed: CIG, semblance, original and changed velocity grids, and original and changed velocity models. There is a layer matching function which supplies the facility to change the thickness and the depth of a layer from the original model to match the reflecting events on the CIG or the stack section or the semblance.

To obtain higher resolution, velocity analysis can be performed on a zoomed window (Figures 3.11 and 3.12). An interpreter drags the blue dot to change the values of depth and velocity so that the semblance (in the second column) is a maximum. After the blue dot is released, the velocity and depth are updated and displayed in red. The residual migration process takes place in real time. This process can be repeated as many times as needed until the velocity is obtained which makes the event the flattest.

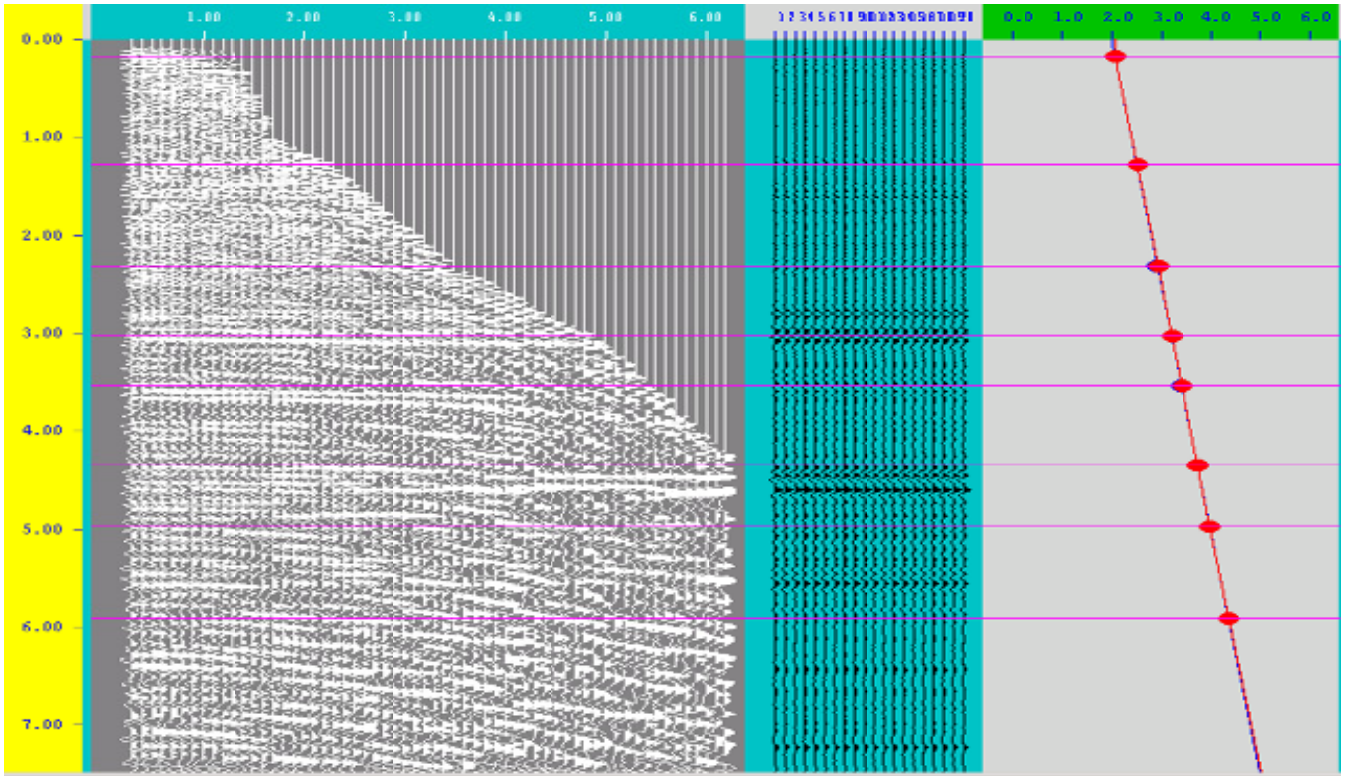

Figure 3.10. The user interface for Residual Migration velocity Analysis (RMVA). To perform the analysis, the following data are loaded and displayed: CIG (left in white), semblance (middle in blue), original and changed velocity grids (blue lines and red lines, which overlap at the start of the experiment, right), and original and changed velocity models (blue and red dots overlapping the velocity grids).

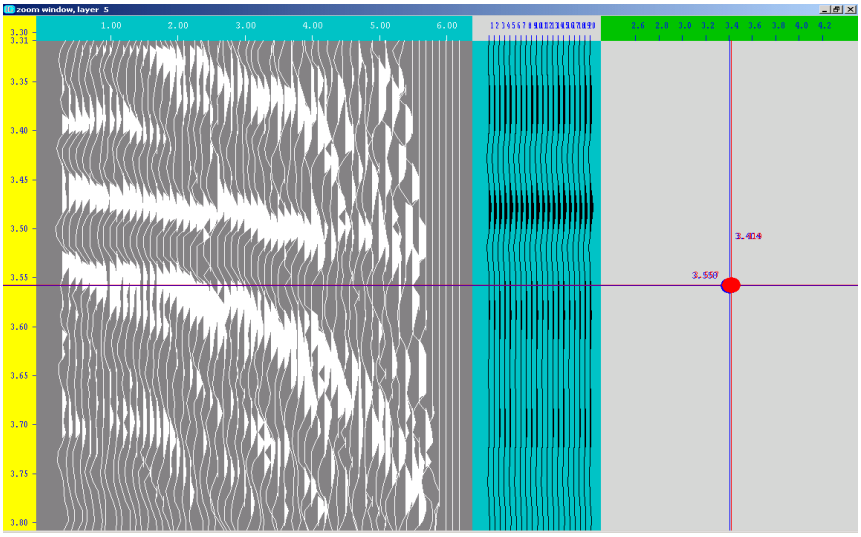

Figure 3.11. Zoomed window of RMVA for residual migration with original data displayed

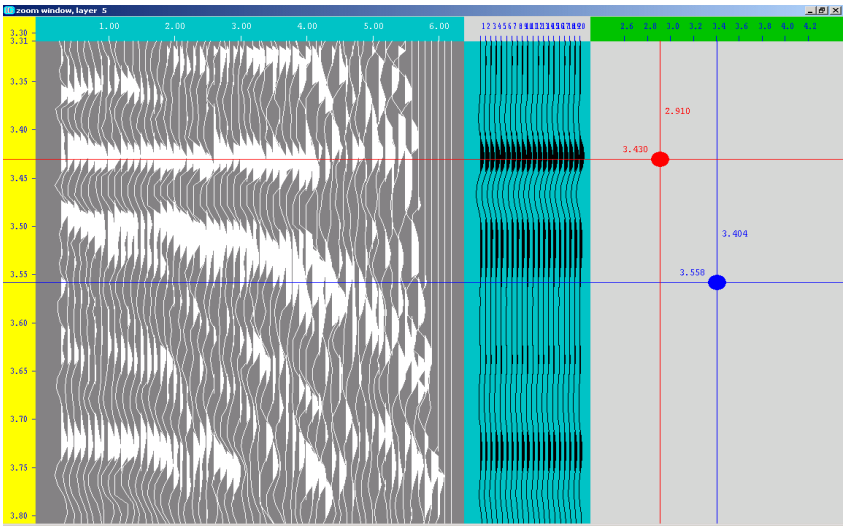

Figure 3.12. Zoomed window of RMVA. The blue dot and line are for original velocity and depth. An interpreter drags the blue dot to change the values of depth and velocity so that the semblance (in the second column) is a maximum. After the blue dot is released, the velocity and depth are updated and displayed in red.

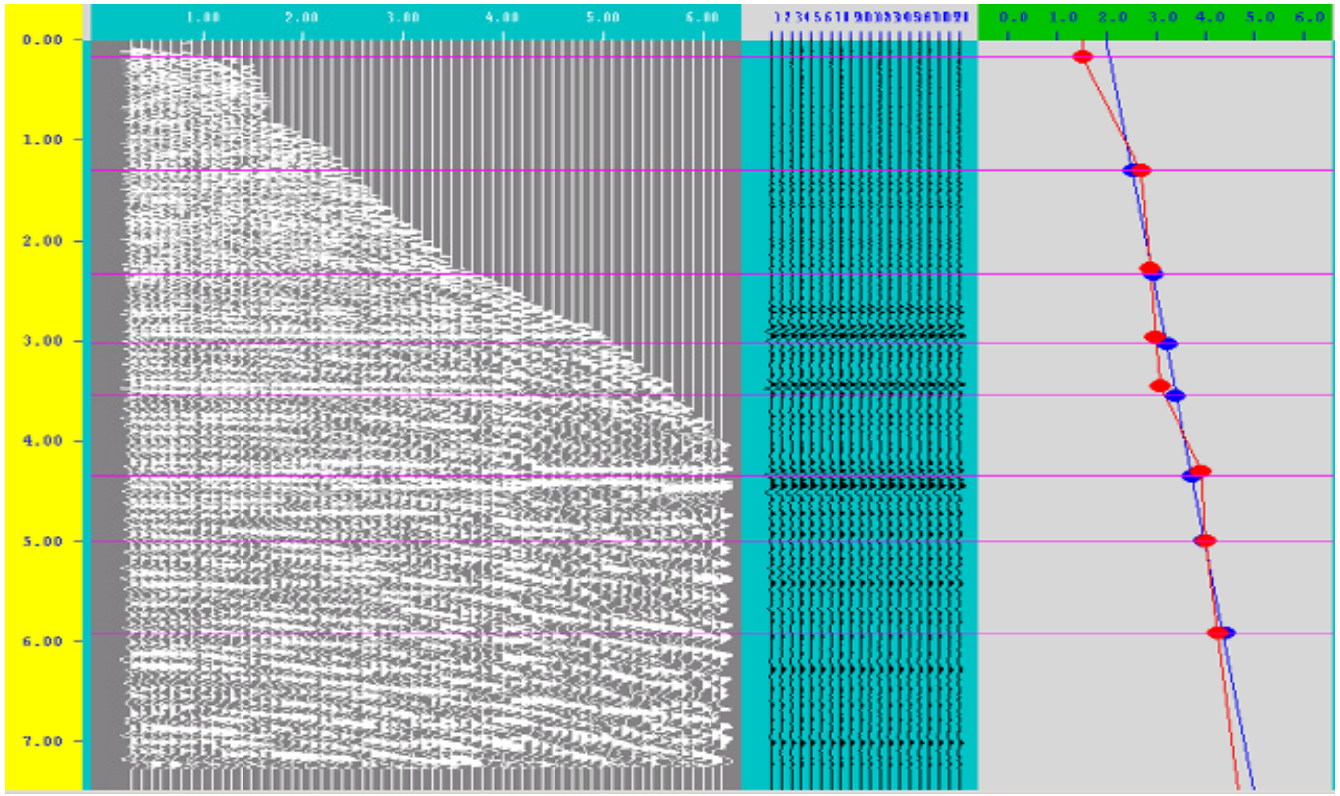

Figure 3.13. The user interface for Residual Migration velocity Analysis (RMVA) after RMVA is performed and residual migration is applied to the current CIG. Compared to the original CIG (Figure 3.10), the quality of the image is significantly improved and a new velocity model (red dos) is also obtained.

3.7 APPLICATION ON SYNTHETIC AND FIELD SEISMIC DATA

Combining the interactive software that performs residual migration velocity analysis (RMVA) with the Geodepth software, from Paradigm Geophysical for performing prestack depth migration, I am equipped with a powerful tool to build velocity depth models and obtain high quality images of geological structures with a high degree of efficiency and low computational cost. I will now apply the new method to both the 2D synthetic and field data.

3.7.1 Synthetic data example: The SEG/EAEG salt model

The synthetic data are from the SEG/EAEG salt model (Aminzadeh et al., 1997). Finite difference modeling was used to generate the shot gathers. This model is based on a typical Gulf Coast salt structure and is used to test seismic imaging algorithms with the velocity field defined by the following equation:

$$V(x,y,z) = V_0 + zK(x,y) - GP \tag{3.14}$$

where V_0 is water velocity(1.5 km/s), GP is the deceleration term chosen as -0.46 km/s, and the salt velocity is 4.481 km/s. $K(x,y)$ is a spatially varying velocity gradient. The velocity model is shown in Figure 3.14.

Kirchhoff pre-stack depth migration in the x-t domain was performed on the shot gather. The image produced using the true velocity model is shown in Figure 3.15. We can see that the structures are well imaged by migration using the true (i.e., known) velocity model.

The choice of initial velocity depth model is not critically important for this residual velocity analysis technique since it is based on the analysis of the

residuals. To test the new method I started with 1-D gradient velocity model (Figure 3.16a) with the velocity varying from 1.5 km/s at the surface to 4.2 km/s at a depth of 2.1 km. The initial velocity chosen is quite different from the true velocity especially in the salt region and below the base of the salt (Figure 3.16b). The true velocity at the depth of 2.1 km is 2km/s. Also the true velocity in the salt region is about 4.481 km/s but the initial value in this region ranges from 2 km/s to 3 km/s. As expected, the images on the migrated stack section (Figure 3.17) are seriously distorted especially at the base of the salt and the reflectors below the salt.

I performed residual migration velocity analysis at every 25th CIG (0.25 km) using eight horizons. Interactive residual migration was performed in the "zoomed" window on the first horizon with different velocities repeatedly until the event became flat on the corrected CIG. After saving this velocity the above step was carried on the remaining horizons of the same CIG, one by one in a top-down fashion. Then this procedure was performed on the next picked CIG and so on. After finishing the analysis for the entire 2D line, the new velocity functions were interpolated onto a gridded velocity depth model. This model was then used for the next iterations. Figure 3.18a shows the velocity model derived after performing seven iterations of my new RMVA technique. This new velocity model approximates the true velocity model to the percentage errors shown in Figure 3.18b. Importantly the salt region shows up quite well and is also located at the correct depths. Figure 3.19 is the migrated stack section using the velocity

derived after seven iterations. Overall it has a good structural resemblance with the image in Figure 3.15 derived using the true velocity model.

After each iteration of RMVA, there is an improvement in the flatness of the events in a CIG. Figure 3.20 shows an example of CIG 250 and Figure 3.21 is an example of CIG375. These CIGs were chosen because they cross the salt dome and most of the horizons. There is a noticeable improvement of the events from the base of the salt and the horizontal reflector (2 km depth) below the base of the salt. Also after one iteration of RMVA, the events corresponding to the sedimentary structure and the top of the salt showed significant improvement. We observe this because the starting velocity was close to the true velocity for these events and also the velocity is closer to a 1D model for these events.

Imaging below the base of the salt is a challenging job (O'Brien et al., 1996) and any improvement in the methodology for this problem is given a lot of importance in the seismic imaging world. I began RMVA using a 1D model quite different from the target. After seven iterations of the RMVA, the final velocity model very closely represented the true velocity model, except for some minor differences. Also the image generated using this velocity model is of good quality. Therefore, the new method can indeed converge, even if we begin with an initial model far from the target model.

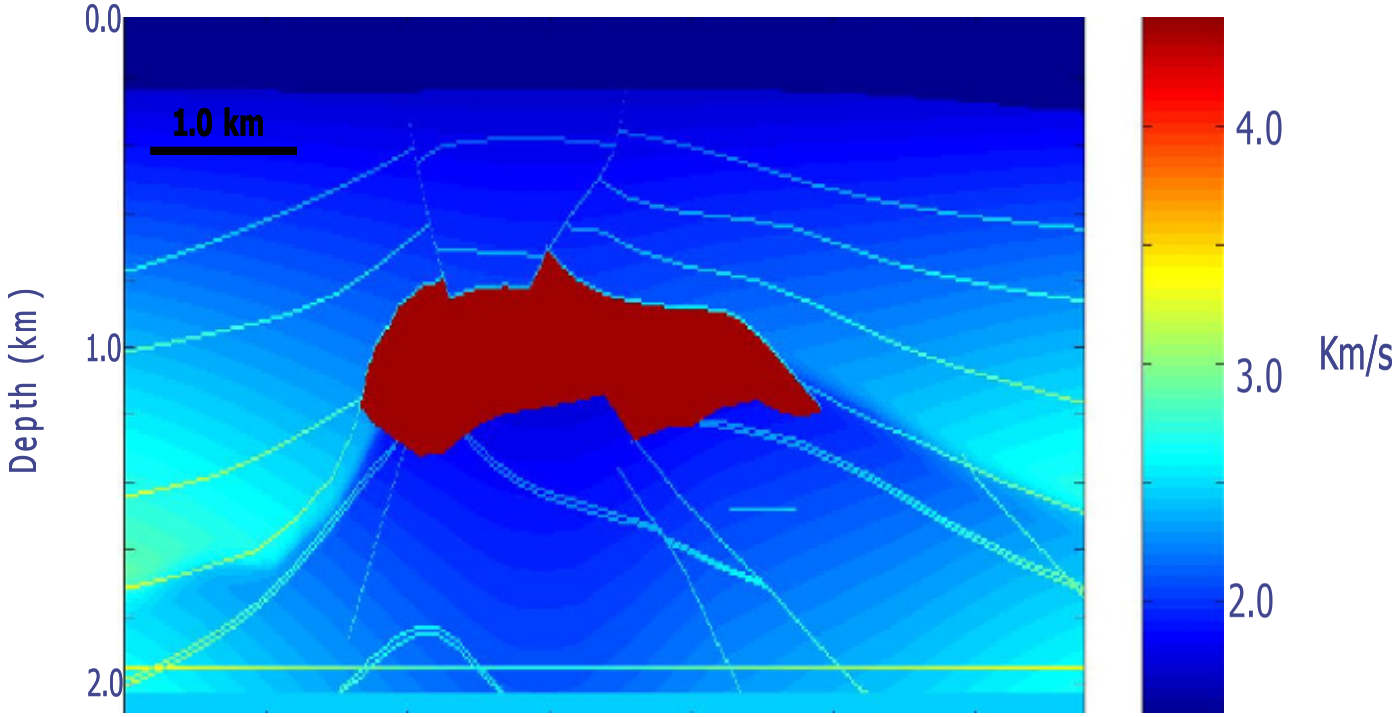

Figure 3.14. True 2D SEG/EAEG salt velocity model.

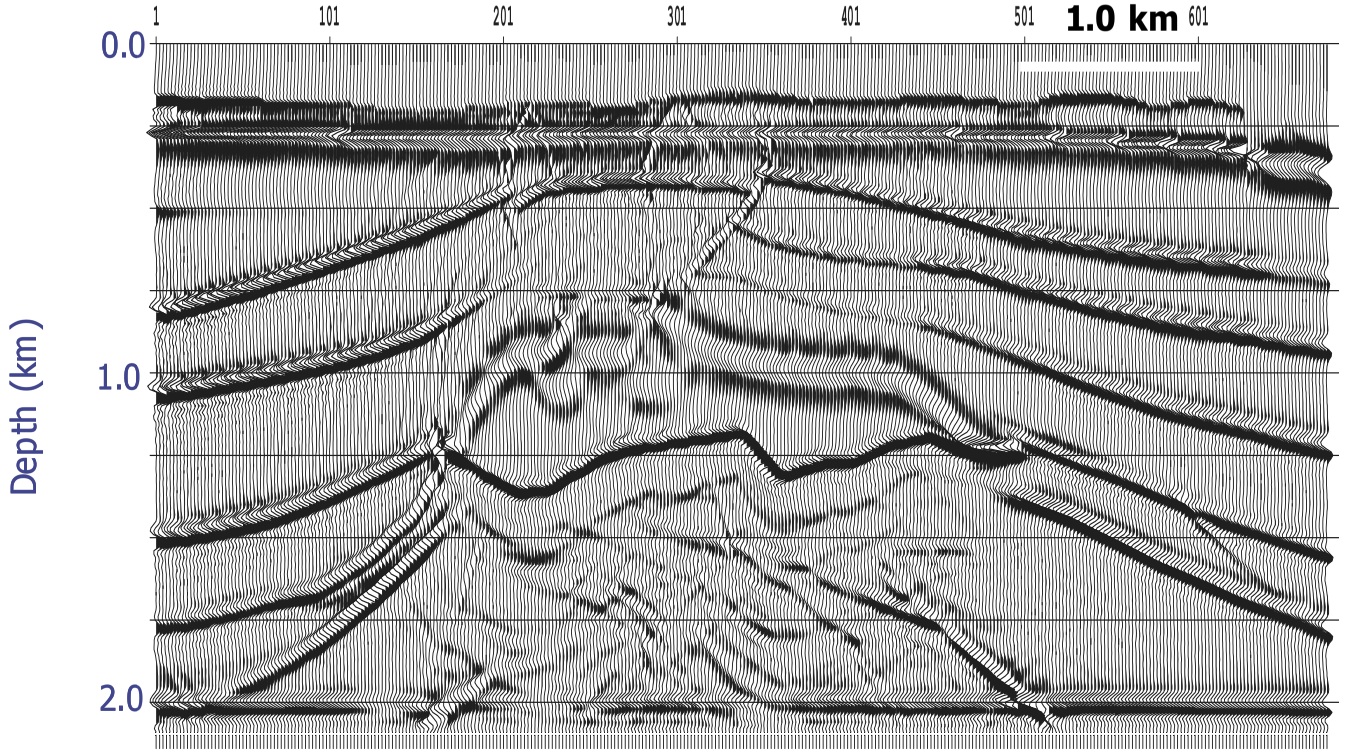

Figure 3.15. Prestack depth migrated (Kirchhoff) stack section using the true (known) 2D SEG/EAEG salt velocity model. The structures in the velocity model (Figure 3.14) are well imaged in this figure.

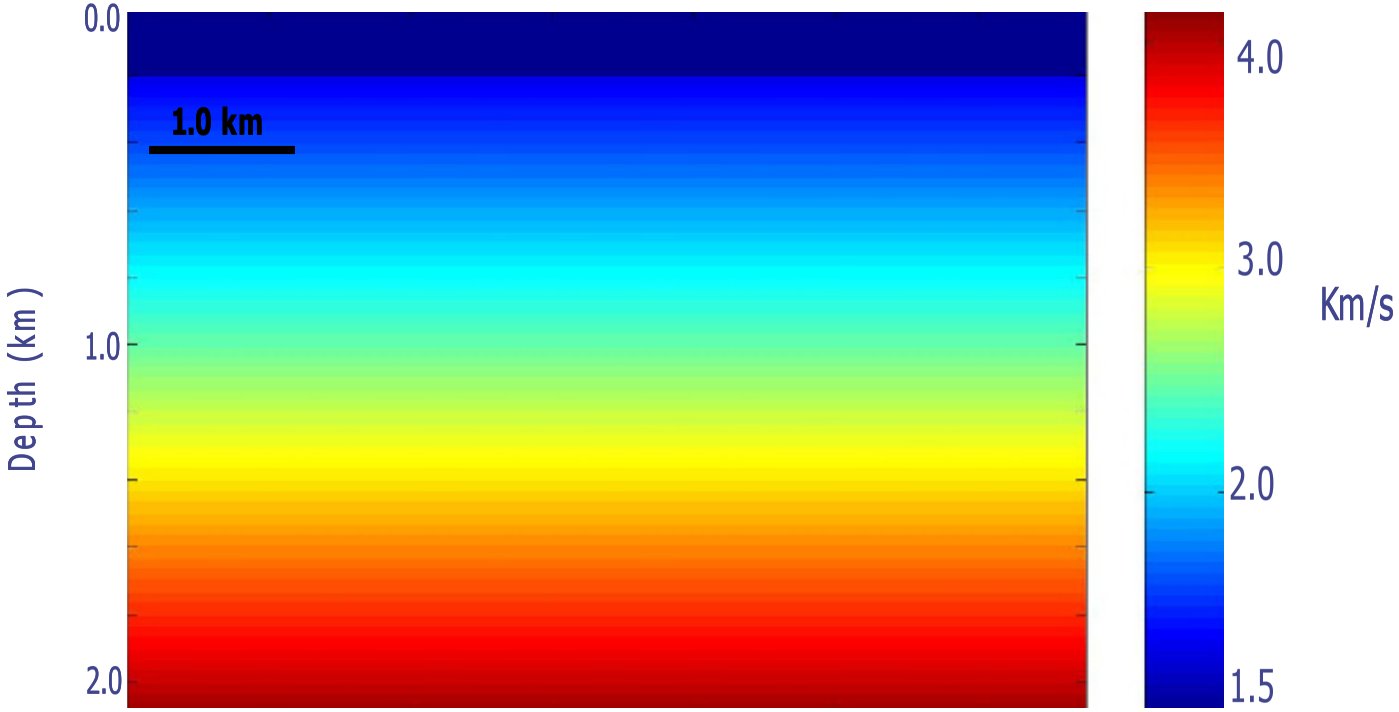

Figure 3.16. (a) Staring 1D gradient interval velocity model used for RMVA.

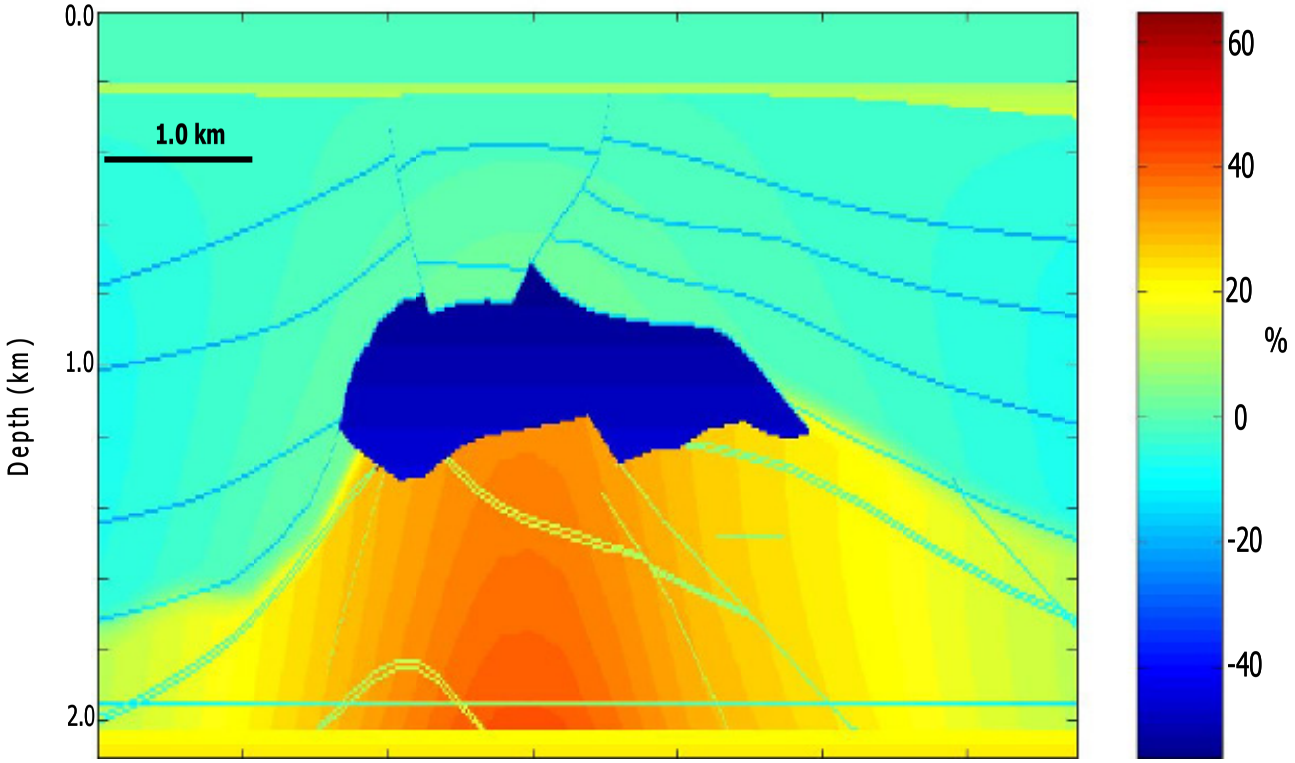

Figure 3.16. (b) Percentage difference plot between the initial and the true velocity model.

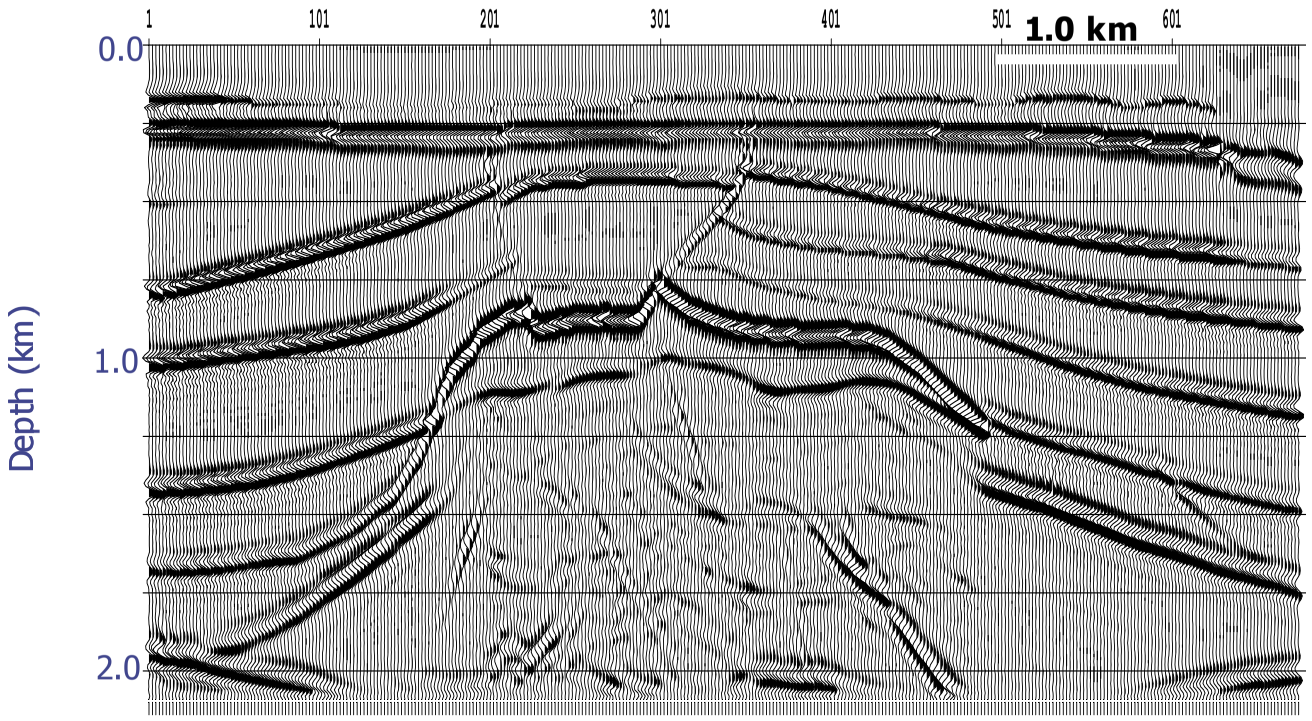

Figure 3.17. Prestack depth migrated (Kirchhoff) stack section using the initial 1D gradient interval velocity model. The base of the salt is not imaged properly and the horizontal reflector below the salt is not imaged at all.

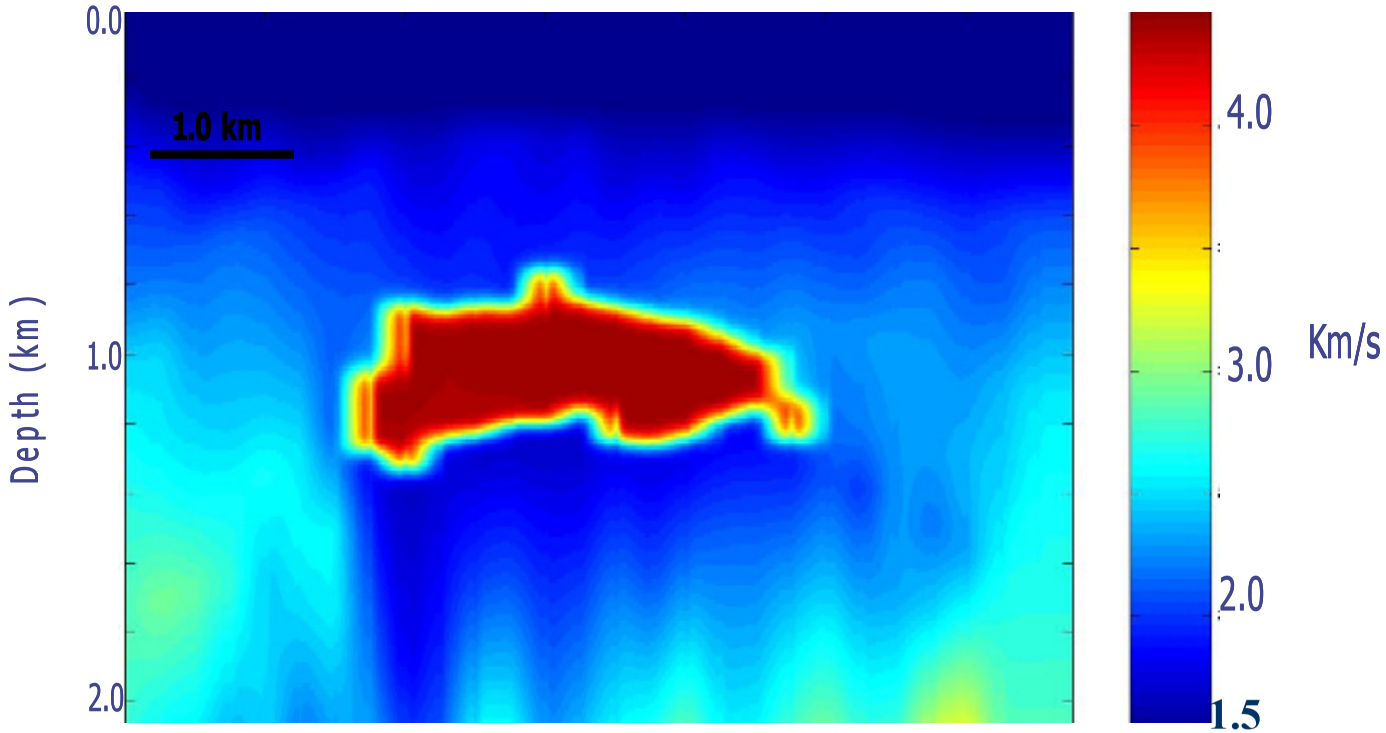

Figure 3.18. (a)Interval velocity model after seven iterations of RMVA. It shows a very close resemblance with the true velocity model (Figure 3.14.).

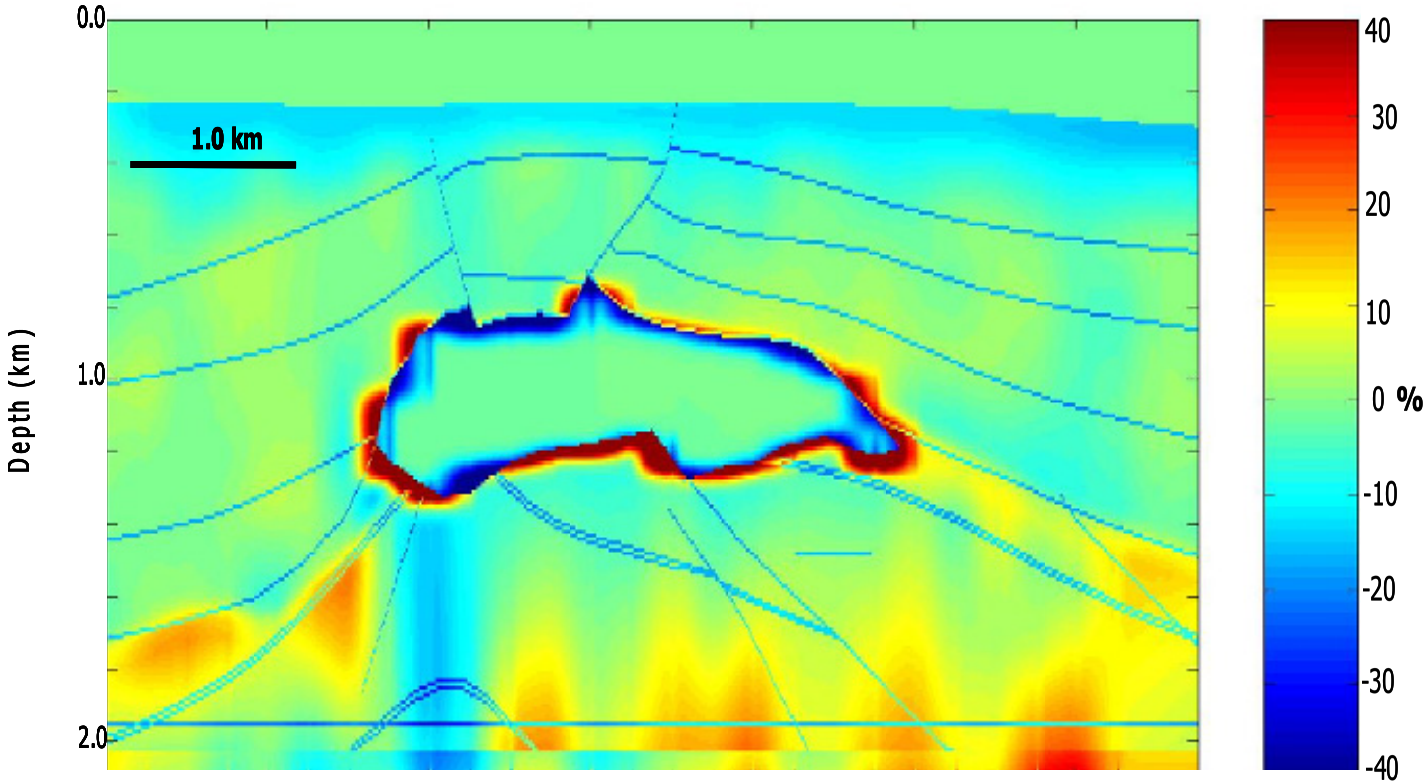

Figure 3.18. (b) Percentage difference plot between the velocity models derived after eight iterations of RMVA and the true velocity model.

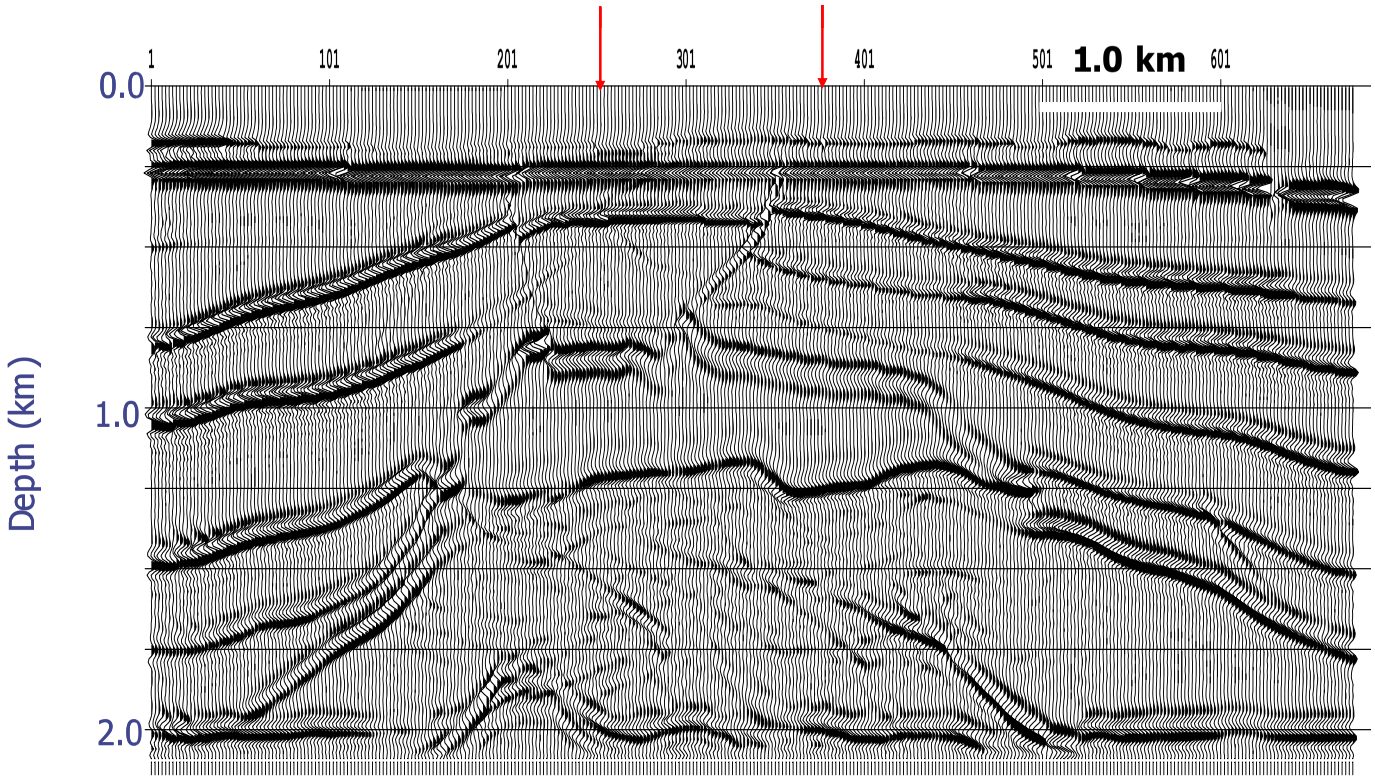

Figure 3.19. Prestack depth migrated (Kirchhoff) stack section using interval velocity derived after seven iterations of RMVA. This image compares very favorably with Figure 3.15, where the known velocity was applied to the Kirchhoff migration algorithm. The arrows are the location of CIG250 and CIG375. These CIG are analyzed in Figure 3.20 and 3.21 respectively.

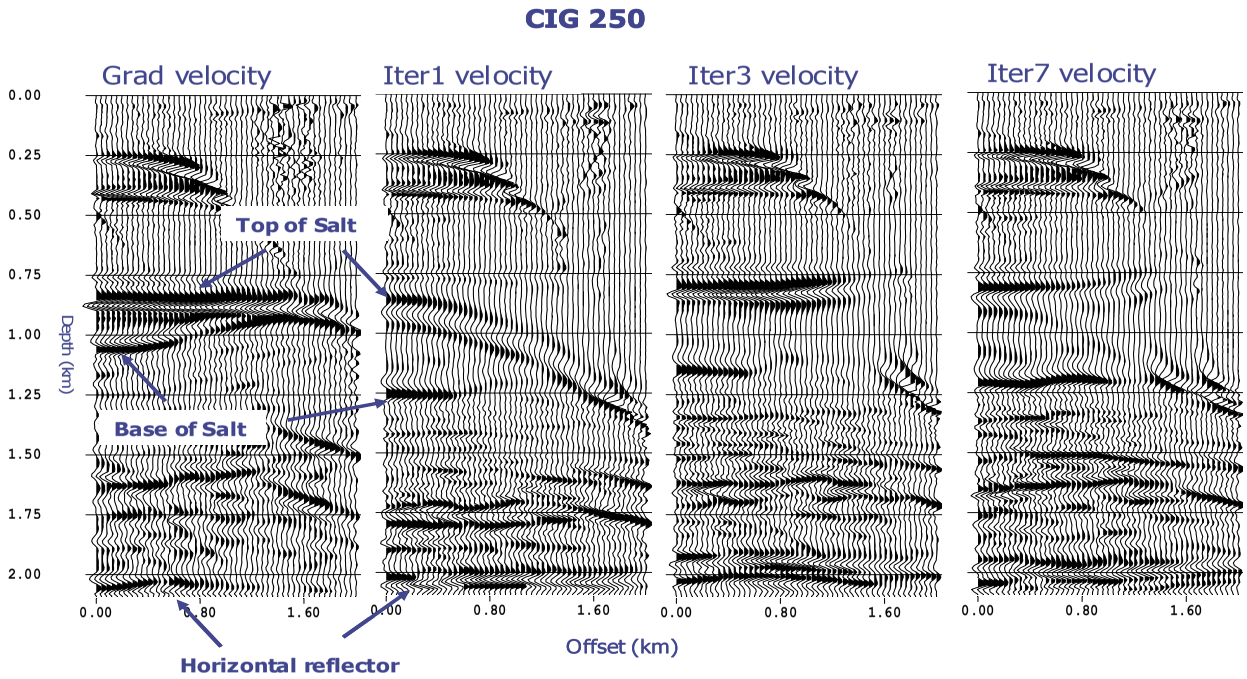

Figure 3.20. Improvement in the flatness of the events on CIG250 as we progress from starting gradient velocity to the velocity derived after seven iterations of RMVA. Especially note the improvement in the top of the slat reflector, the base of the salt reflector and the horizontal reflector at the depth of 2 km.

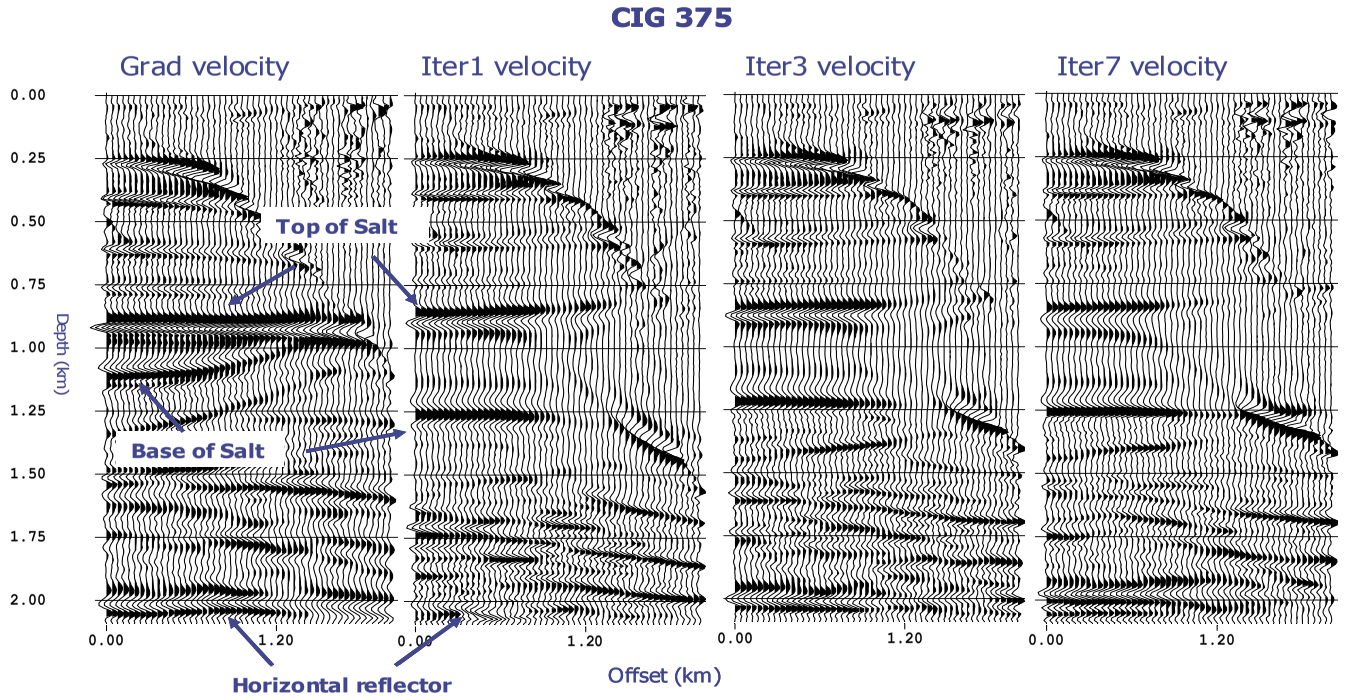

Figure 3.21. Improvement in the flatness of the events on CIG375 as we progress from starting gradient velocity to the velocity derived after seven iterations of RMVA. Especially note the improvement in the top of the slat reflector, the base of the salt reflector and the horizontal reflector at the depth of 2 km.

3.7.2 Field data example: offshore Nicaragua

This example is from MCS line NIC-50 collected offshore Nicaragua. Figure 3.22 shows the location of the 2D line. Figure 3.24a shows a CIG from the shelf region of this margin, where the water depth is shallow. The CIG was generated by migration with a preliminary interval velocity model (Figure 3.23). The event at 2.5km depth on the CIG is curved upwards, suggesting our initial velocity model has lower values than the true model. Figure 3.24c shows the best residual depth correction result possible from handpicking of the velocities. This figure shows quite an improvement on the CIG gather. In Figure 3.23 the light curve is the initial velocity model and the bold curve is the best possible handpicked velocity model. Figure 3.24b shows the semblance calculated for the original CIG. Figure 3.24d shows the semblance calculated for the depth corrected CIG. We can see that the semblance for the CIG due to the changed velocity is higher than that of the original velocity, indicating through this quick experiment that the residual migration velocity analysis has improved the velocity function.

As in the synthetic data example, I started with a 1-D gradient velocity model (Figure 3.25) for the real data example. It varies from 2 km/s at the surface to 4.8 km/s at 7 km depth. I performed Kirchhoff pre-stack depth migration in the x-t domain on the shot gathers using this gradient velocity model. Figure 3.26 shows the migrated stack section. I performed residual migration velocity analysis of every 30^{th} CIG (0.375 km) using eight horizons. Figure 3.27 is the migrated stack section after one iteration of my new RMVA technique. On comparing the

two images, we see significant improvements in the quality of the image produced from the velocity model after only one iteration of RMVA. Overall the image is much cleaner; the reflectors are more continuous and have higher amplitudes and are better defined. The faults are also better defined. The interval velocity model after one iteration of RMVA is shown in Figure 3.28.

To get a better picture of the improvement in the image quality after RMVA, we compare details from two different places along this seismic line. The first is from the portion of the seismic line where the structure is mostly flat to gently dipping, with some faults offsetting the reflectors. Figure 3.29 is the image produced from the gradient velocity and Figure 3.30 is the image produced by using the interval velocity after one iteration of RMVA. We clearly observe the improvements discussed while comparing the unzoomed versions before. Seeing flat events on a CIG always means our interpretations are improving the overlying velocities. Figure 3.31 is a comparison of a CIG from this line (CIG801). We observe that the events on the CIG have become flatter after one iteration of RMVA and they are also placed at their deeper depths. The second detail is from that portion of the seismic line where the structure is more complex, having greater dips and more faults. Figure 3.32 is the image produced from the gradient velocity and Figure 3.33 is the image produced using the interval velocity after one iteration of RMVA. We clearly observe the improvements in the image quality, especially the faults are better focused. Figure 3.34 is a comparison of a CIG from this line (CIG1821). We observe that the events on the CIG are much

better aligned after one iteration of RMVA and the depths of the events have changed.

The application of my new RMVA technique on real data also shows good results, concurring with the results observed in the synthetic data example. The improvement in the image quality was observed from geologically simple to geologically complex areas. So we have confidence in our new RMVA method that when it is combined with careful interpolation it will give us a good and geologically interpretable interval velocity model.

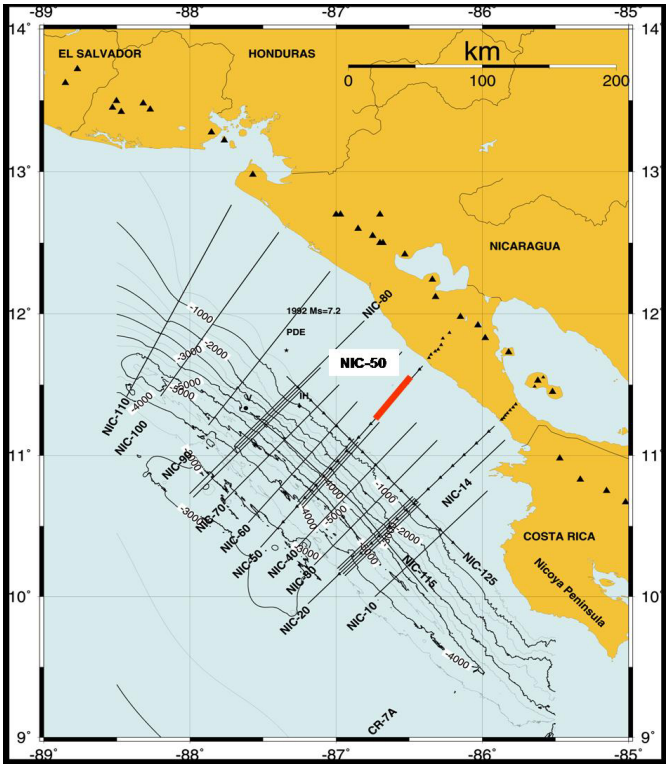

Figure 3.22. Map showing the study area with the 2D seismic profiles. The red line is the location of seismic line NIC-50

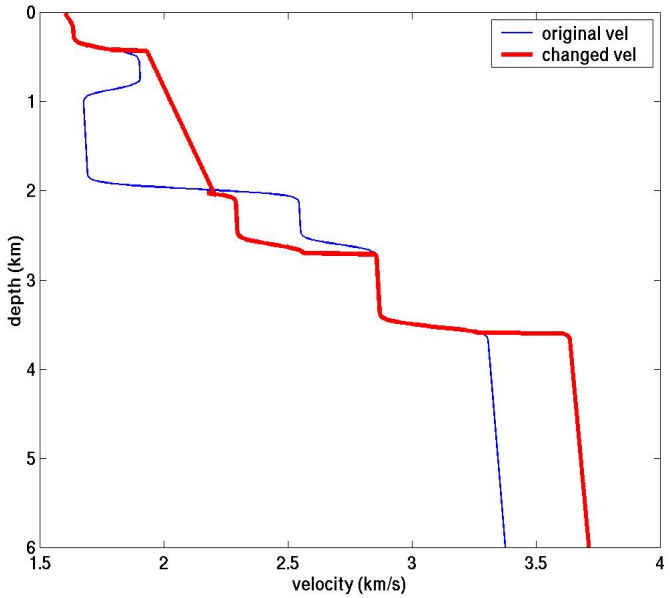

Figure 3.23. Blue curve is the original velocity model and Red curve is the hand picked velocity model.

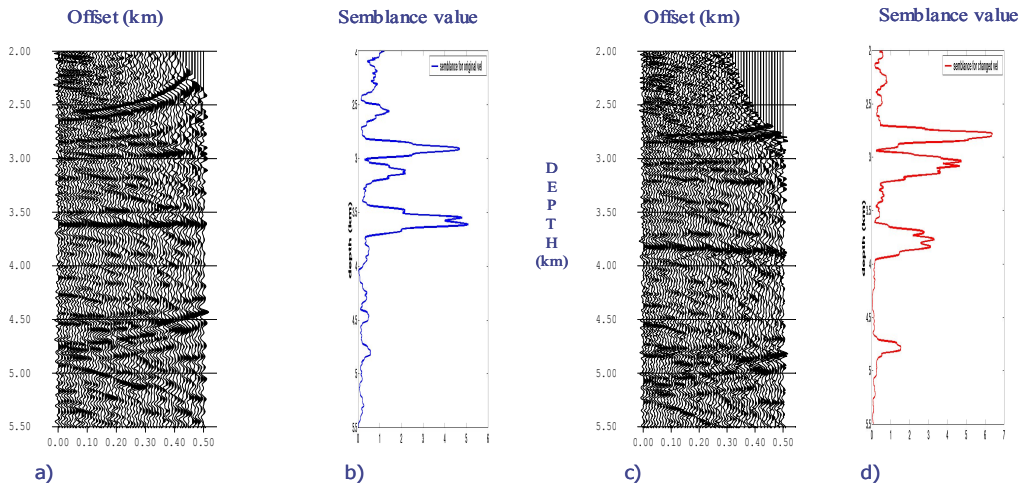

Figure 3.24. (a) CIG generated by doing migration using the original velocity model, (b) semblance plot calculated for the original CIG in Figure 3.24a, (c) The best possible residual depth moveout analysis using handpicked velocities, and (d) semblance plot calculated for the depth corrected CIG with the changed velocity.

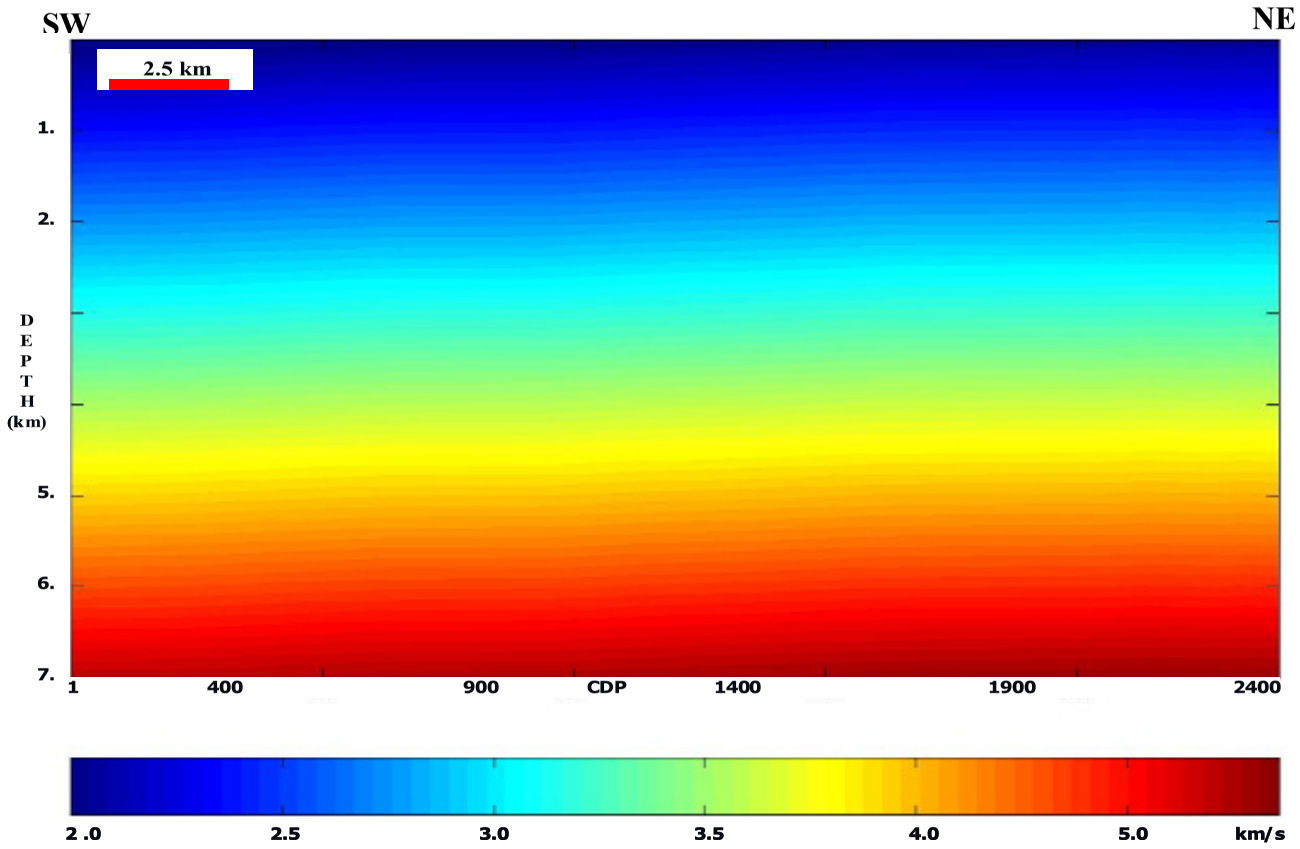

Figure 3.25. Staring 1D gradient interval velocity model used for RMVA.

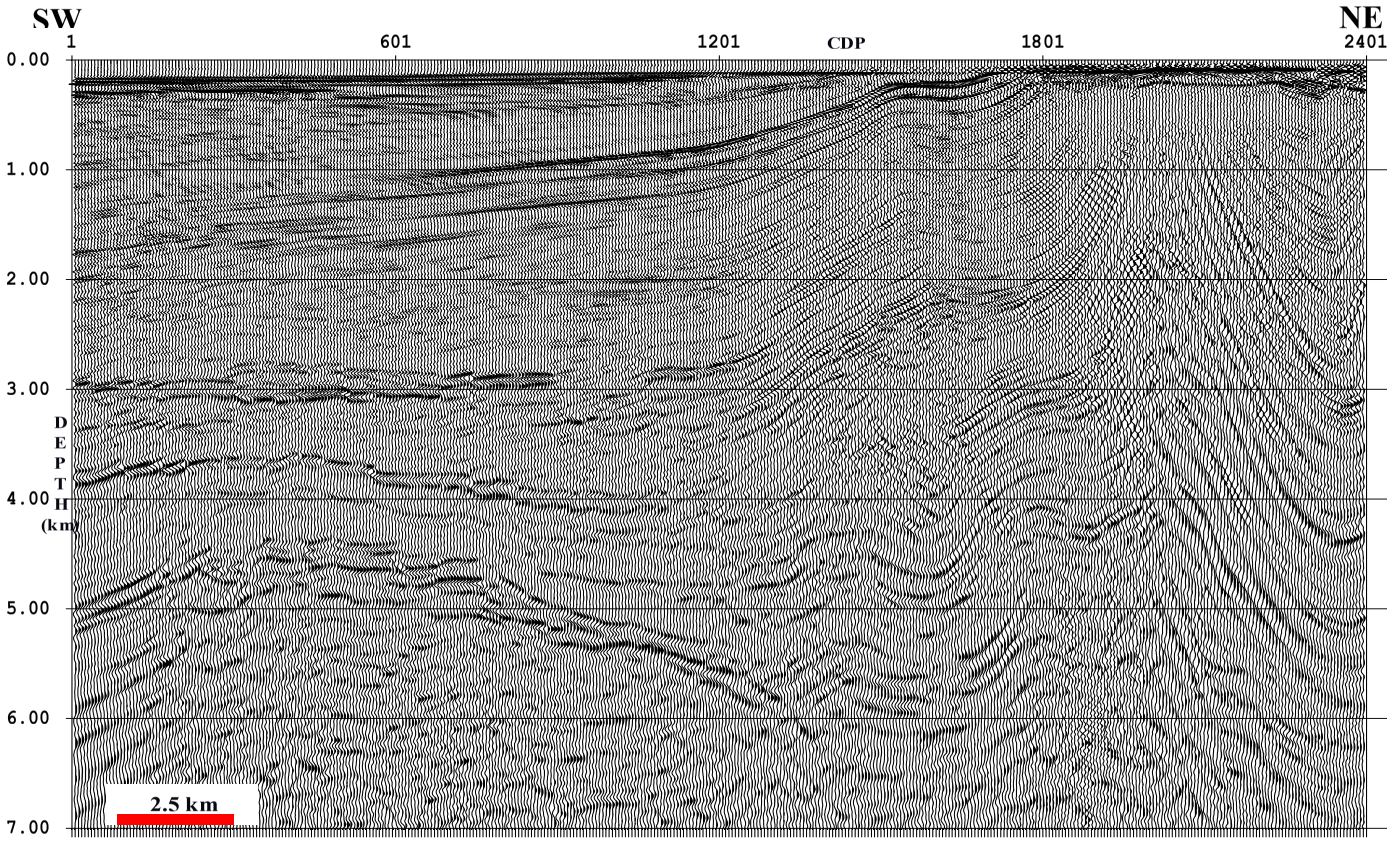

Figure 3.26. Prestack depth migrated (Kirchhoff) stack section using 1D gradient interval velocity model.

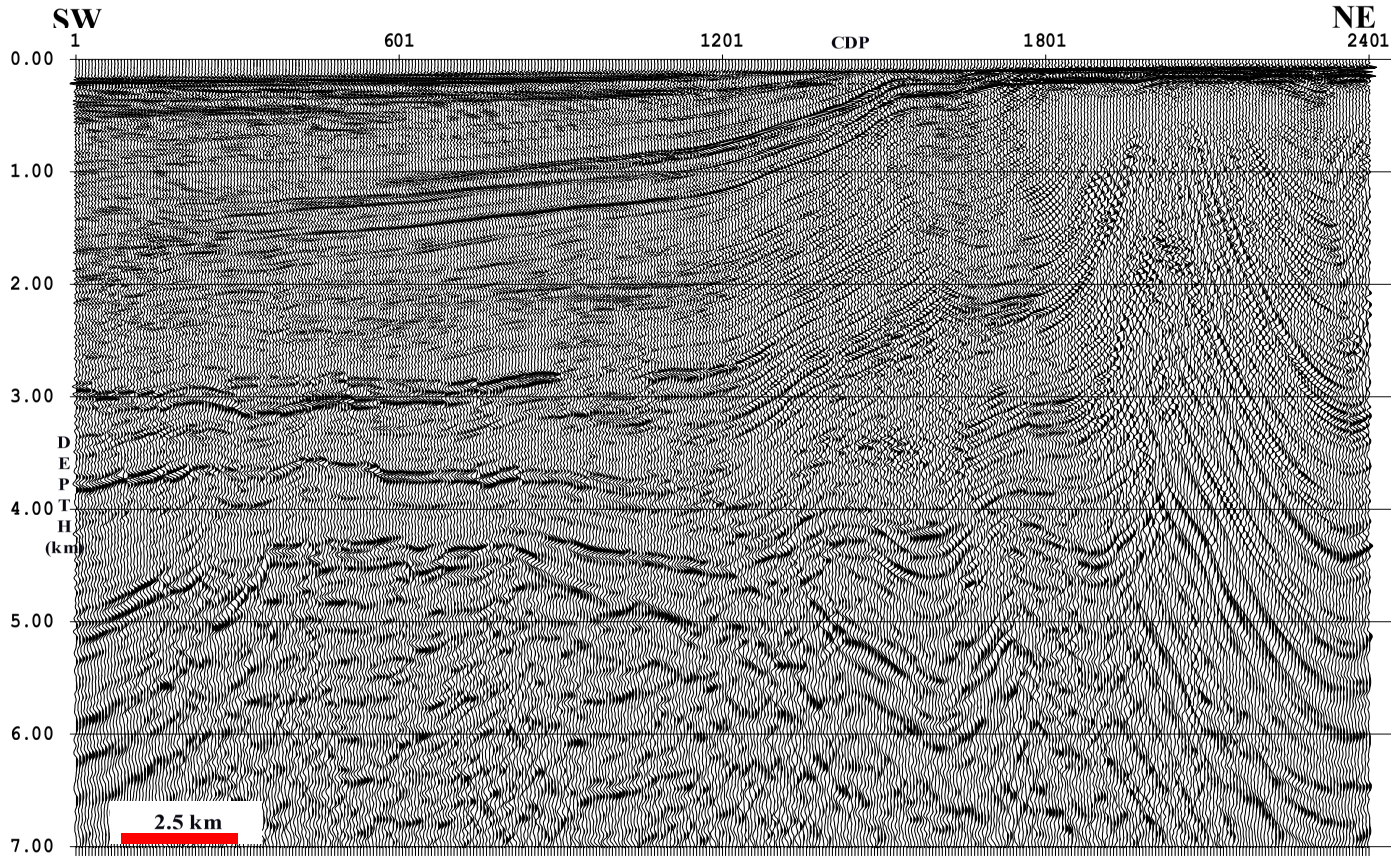

Figure 3.27. Prestack depth migrated (Kirchhoff) stack section using the interval velocity model from one iteration of RMVA. Over all the quality of this image is better than the gradient velocity image (Figure 3.26). The reflectors are more continuous and realistic. The faults are focused.

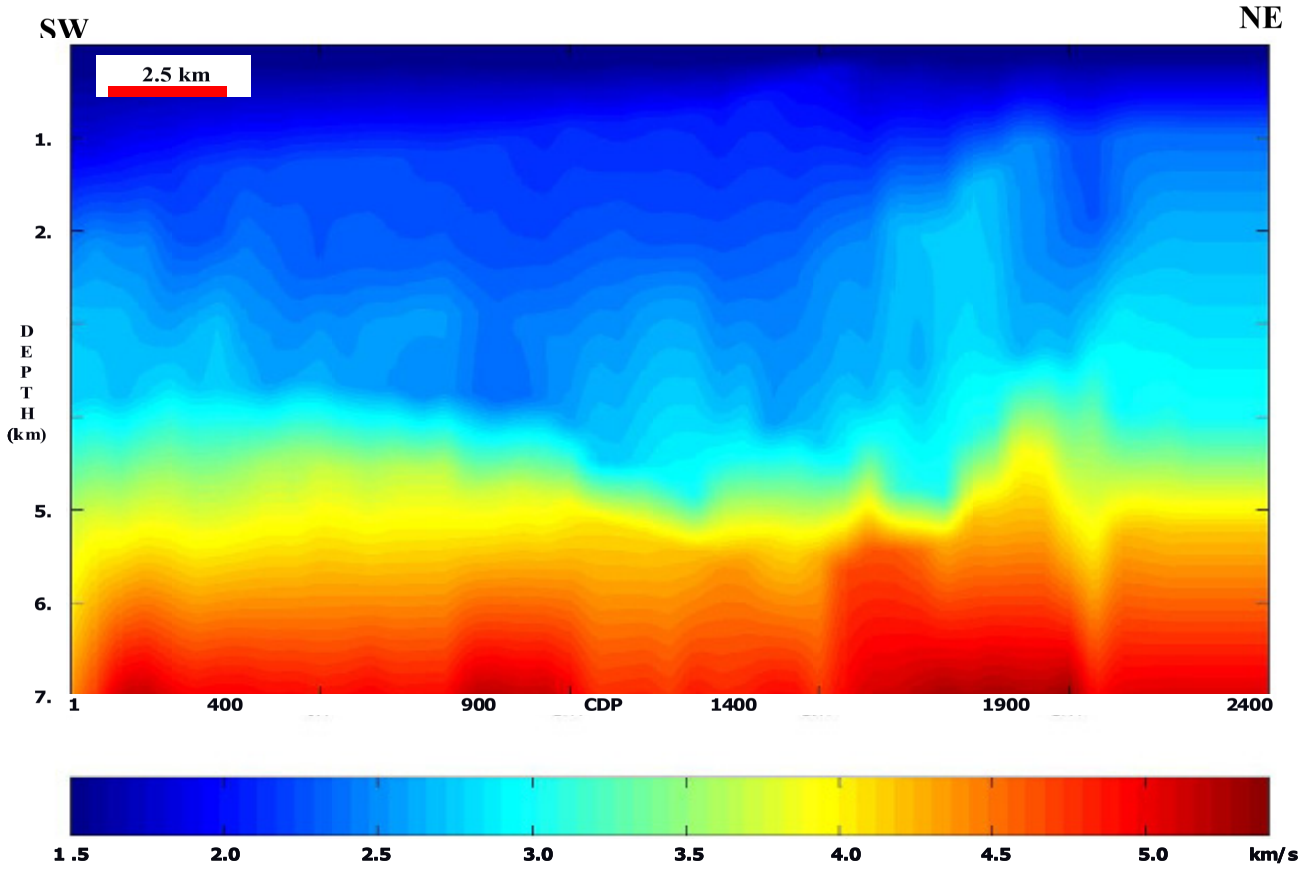

Figure 3.28. Interval velocity model after one iteration of RMVA. The velocity follows the structure of the image in Figure 3.27.

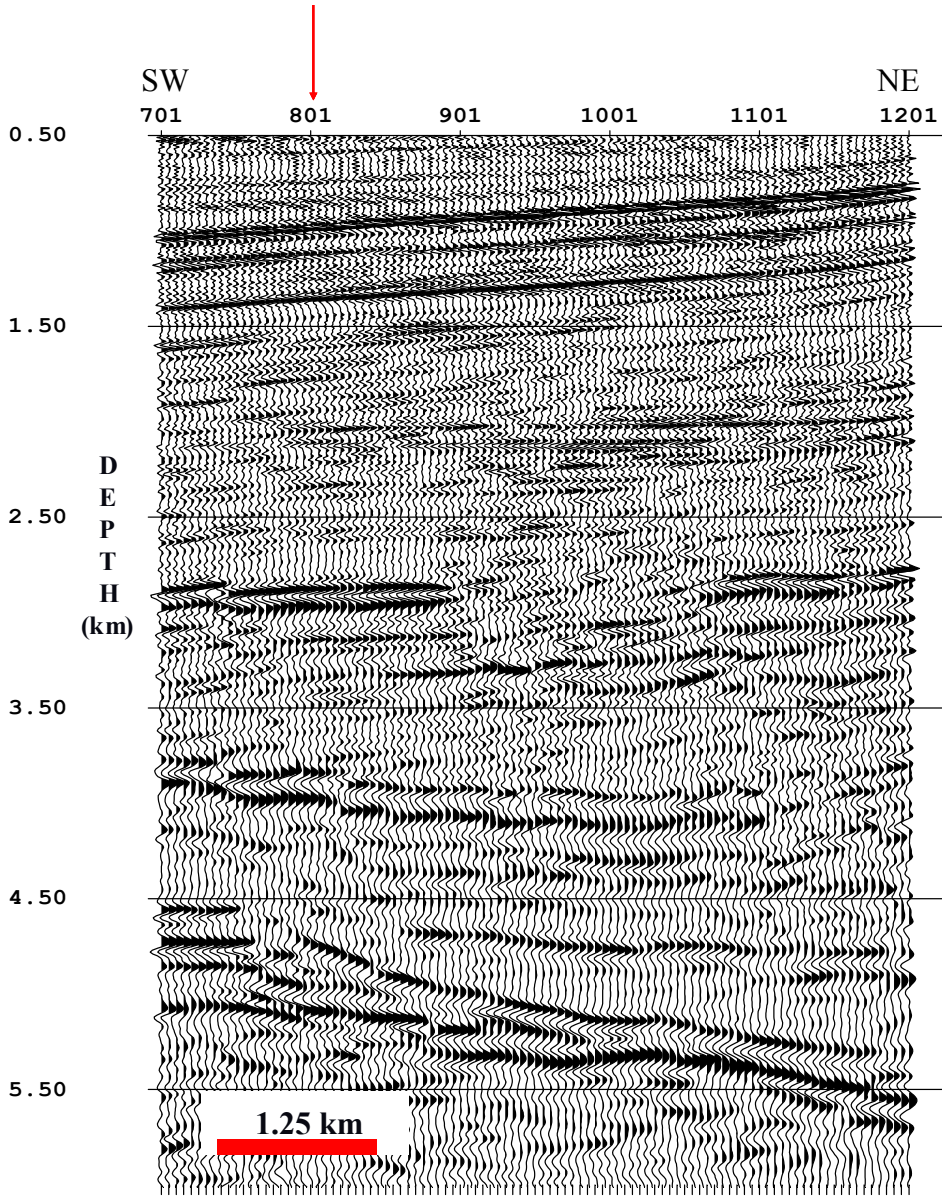

Figure 3.29. Zoom of the gradient interval velocity (initial velocity model) image. The section is from the portion of image in Figure 3.26., where the structure is not complex. The arrow points to CIG801, which is shown in Figure 3.31

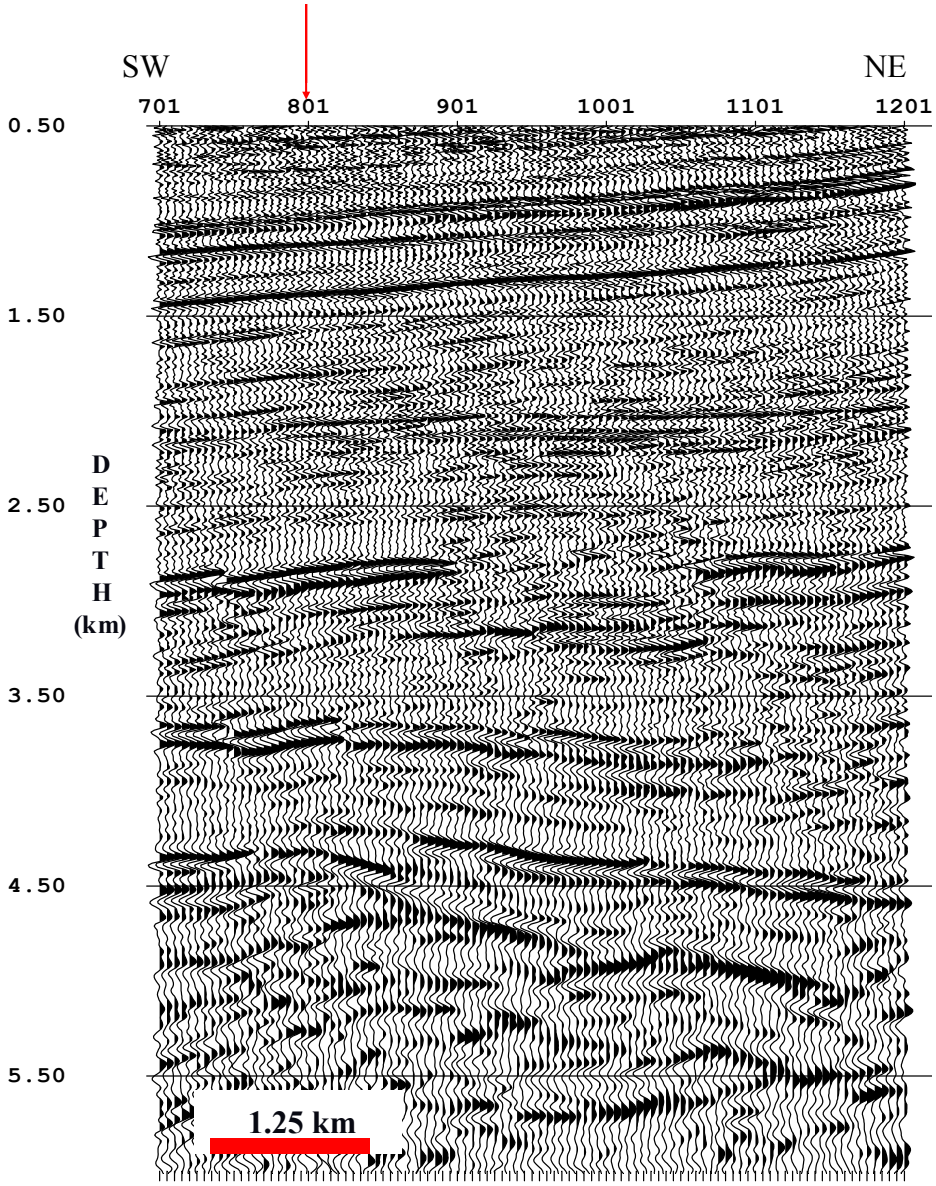

Figure 3.30. Zoom of the after one iteration RMVA interval velocity image. The section is from the portion of image in Figure 3.27., where the structure is not complex. The arrow points to CIG801, which is shown in Figure 3.31.

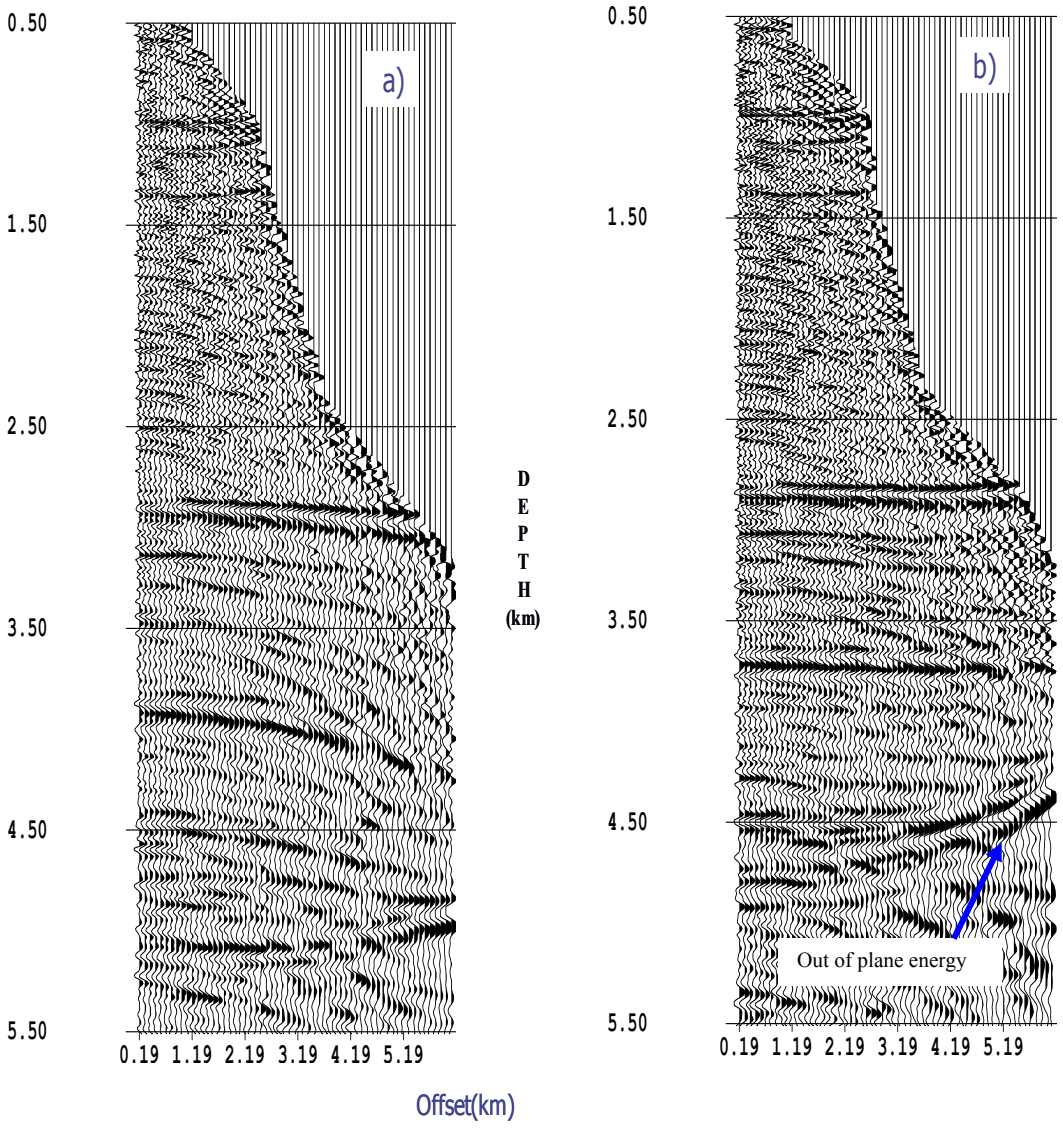

Figure 3.31. CIG801 generated after migration with gradient interval velocity (a) and with iteration1 RMVA interval velocity (b). The events on the CIG are much flatter in (b) than in (a).

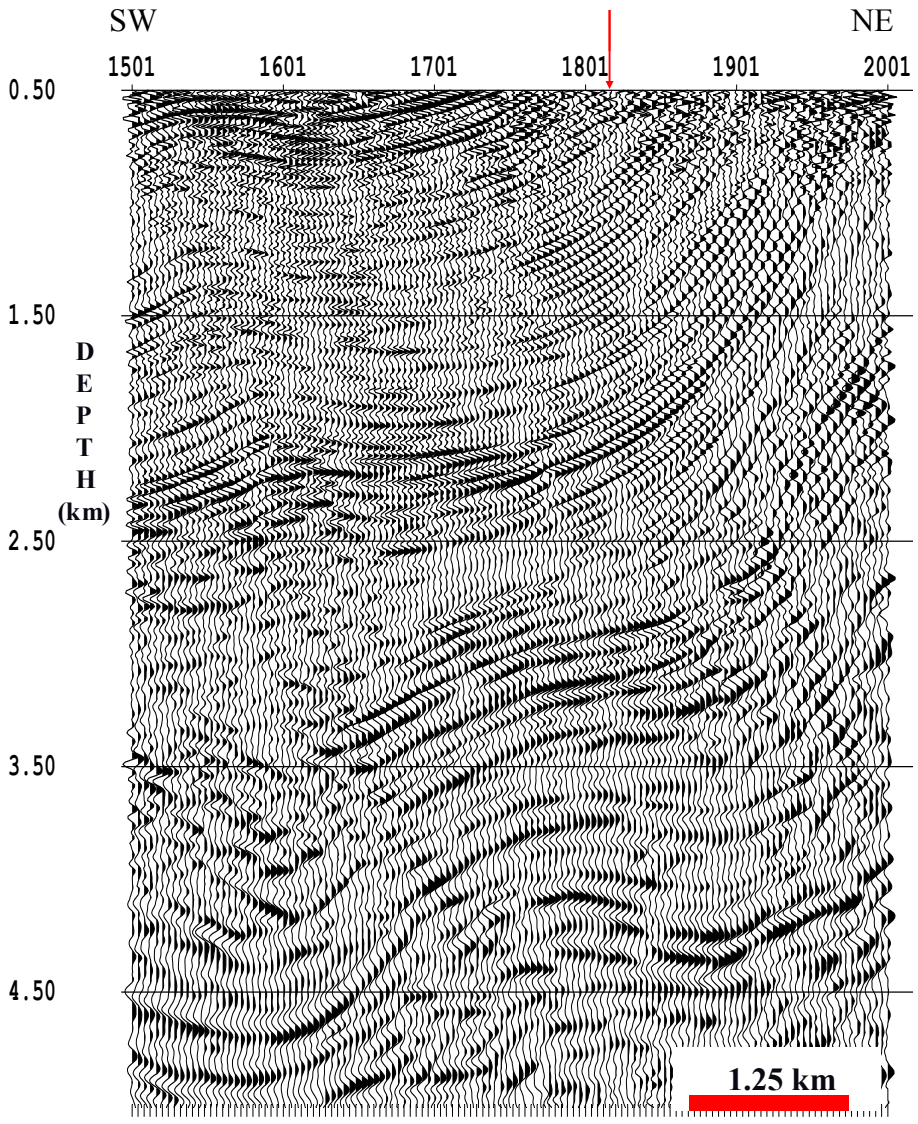

Figure 3.32. Zoom of the gradient interval velocity (initial velocity model) image. The section is from the portion of image in Figure 3.26., where the structure is more complex. The arrow points to CIG1821, which is shown in Figure 3.34.

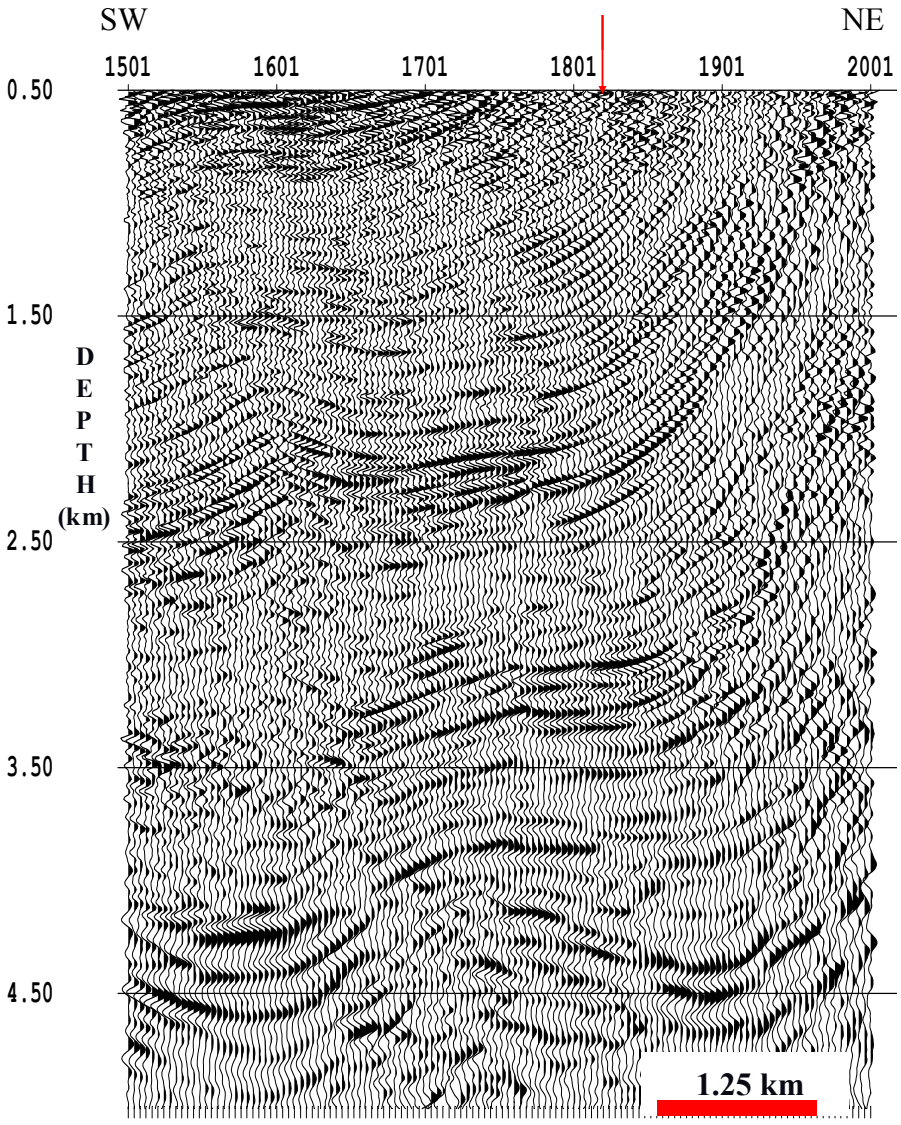

Figure 3.33. Zoom of the after one iteration RMVA interval velocity image. The section is from the portion of image in Figure 3.27., where the structure is more complex. The arrow points to CIG1821, which is shown in Figure 3.34.

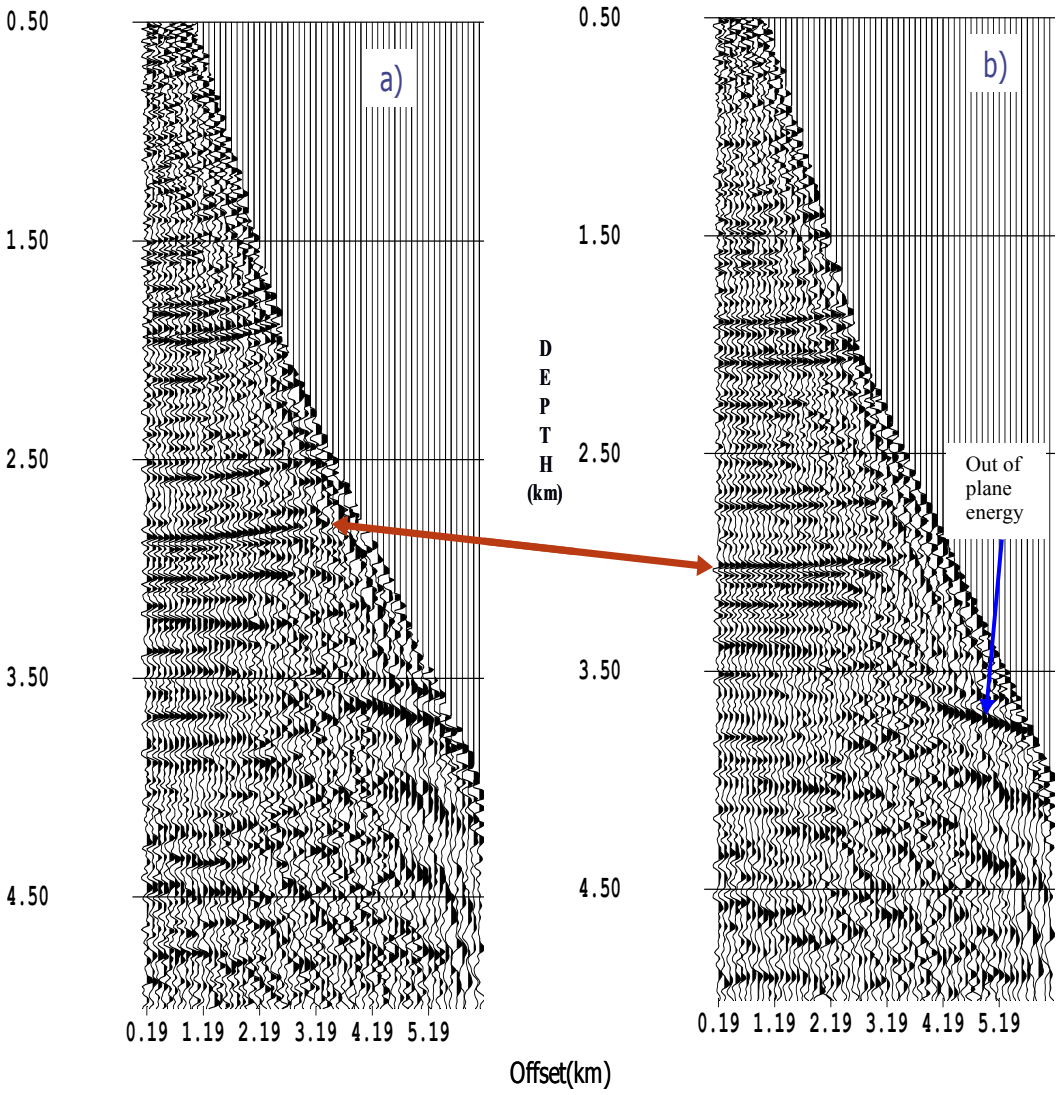

Figure 3.34. CIG1821 generated after migration with gradient interval velocity (a) and with iteration1 RMVA interval velocity (b). The events on the CIG are much flatter in (b) than in (a), they are also placed at deeper depths in (b).

3.8 CONCLUSIONS

We have developed a method for residual migration velocity analysis in depth-offset domain via the method of plane-wave domain residual migration velocity analysis. The implementation of the original plane wave theory is made possible by calculating the *x-p-z* table and mapping the residual depth corrections from the *p-z* domain to the *x-z* domain using this table.

Residual migration velocity analysis is a powerful tool for interval velocity analysis. I have done the implementation of this residual migration velocity analysis in an interactive manner, using the interactive software package that I have developed. The results on the synthetic and real data show good agreement with the theory and the original work of Jiao et al.(2002).

Chapter 4: Geophysical evidence of preferential complete sediment subduction offshore Nicaragua compared to offshore Costa Rica.

4.1 INTRODUCTION

The Central American convergent margin volcanics exhibits nearly the complete global range in geochemical indicators of the subducting plate (e.g. ^{10}Be, Ba/La) (Morris et al., 1990). In particular this margin shows dramatic variations in the radionuclide ^{10}Be, which is an excellent tracer for the recycling of the uppermost sediments at convergent margins (Morris et al., 1990, Kelly, 2003). These variations can be explained by the understanding of the processes of sediment subduction, sediment accretion and subduction erosion along this convergent margin. There have been two schools of thought explaining these variations. The first suggests the transition from nearly complete sediment subduction beneath Nicaragua to significant underplating of the surficial sediment beneath Costa Rica as the probable explanation (Tera et al., 1986; Morris et al., 1990; Valentine et al., 1997). On the other hand, the second school of thought prefers dilution by subduction erosion of the older sedimentary prism or igneous wedge material, with a lower rate of subduction erosion beneath Nicaragua (Ranero et al., 2000, Vannuchi et al., 2001) as the probable cause. However, both these theories are based on observations from Costa Rica data and lack evidence from Nicaragua.

UTIG (University of Texas Institute for Geophysics) collected MCS data offshore Nicaragua in May 2000. These data from Nicaragua and Costa Rica are thus available to provide a geophysical support to either of the above theories.

In this chapter I have seismically imaged the lower slope offshore Nicaragua and Costa Rica using seismic propagation velocities derived by a new RMVA technique to structurally identify the processes of mass transfer (sediment subduction, accretion and erosion) and how they might relate to the geochemical variation along the Nicaragua and Costa Rica convergent margin. In the following sections I will discuss my observations followed by discussions on the data and methodology used. Then I will show interpreted pre-stack depth migrated images from offshore Nicaragua and Costa Rica, and draw conclusions about the subduction process.

4.2 OBSERVATIONS

Moderate ^{10}Be enrichment in Guatemala progresses to a peak in Nicaragua and abruptly falls to values slightly above background in Costa Rica (Morris et al., 1990) (Figure 1.7). ^{10}Be has a relatively short half-life (1.5 x 10^6 yrs) (Arnold, 1956), and therefore it is only found in significant concentrations in the youngest marine sediments (<10 Ma) (Tera et al., 1986). Considering average sedimentation rates along this Central American margin of Nicaragua and Costa Rica, this corresponds to the upper tens to a few hundreds of meters of sediment thickness. The wide range of variations in ^{10}Be content in arc lavas cannot be accounted for through simple relationships between arc ^{10}Be and a single subduction parameter such as convergence rate, plate age, plate thickness or slab dip angle. Also there is no clear-cut relationship between sediment thickness on the incoming plate or recent sedimentation rates and arc ^{10}Be variations (Tera et al., 1986). The lavas from island arc volcanoes are too young to acquire their ^{10}Be signature through cosmic-ray bombardment or near-surface alteration. Near-surface hydrothermal fluids are unlikely to mobilize sufficient ^{10}Be, because ^{10}Be is fairly immobile in fluid (Morris et al., 1990). Therefore presence of high ^{10}Be in arc volcanic requires that the youngest sediment to be subducted to the arc volcanic roots, and the absence of ^{10}Be in arc volcanic can be explained by accretion or underplating of the youngest part of the incoming sediment (Tera et al., 1986; Morris et al., 1990; Valentine et al., 1997), and/or dilution by subduction erosion of the older sedimentary prism or igneous wedge material (Ranero et al., 2000; Vannuchhi et al., 2001).

As illustrated in chapter 1 (Figure 1.6), there is a marked transition in the bathymetric features of the subducting plate close to the trench from Nicaragua to Costa Rica. The origin of the Cocos plate lithosphere offshore Nicaragua is along the East Pacific Rise (EPR). The abyssal hill fabric of the EPR crust is oriented at shallow angle to the trench. Therefore flexural extension reactivates and augments the abyssal hill fabric and relief. This facilitates the development of large scale extensional faults in the incoming plate offshore Nicaragua. On the other hand the origin of the Cocos plate lithosphere offshore Costa Rica is along the early Cocos-Nazca spreading center. The fabrics are oriented northeast-southwest here and not parallel to trench axis (northwest -southeast). Therefore new faults are formed across existing tectonic grains and thus the incoming plate offshore Costa Rica has moderate to low scale extensional faults due to flexural bending of the plate. Also here the plate is modified by magmatism related to Galapagos hot spot. Multi-channel seismic (MCS) data image similar sediment thicknesses along the Cocos plate as it enters the trench (400–500 m), but the sediments are more continuous offshore Costa Rica then offshore Nicaragua because the basement fault throw offshore Costa Rica (<250-300 m) is far less compared to that off Nicaragua (<500-700 m) (von Huene et al., 2000; Ranero et al., 2000).

The large to moderate scale extensional faults on the downgoing slab can generate horst and graben features, rotated fault blocks or half-grabens as off Costa Rica and Nicaragua, at the trench. If the thickness of the subducting sediment column is less than or comparable to the basement fault throw then grabens could trap sediments and enhance subduction of the downgoing sediment.

Otherwise, frontal accretion or underplating may be more prevalent when the fault throw in the subducting plate is minimal or small in comparison with the downgoing sediment thickness (Hilde, 1983). The structural modifications on the incoming plate suggest these features (grabens) may play an important role in the sediment subduction across this margin. This is one of the hypotheses I sought to test during this project.

4.3 DATA AND METHODS

UTIG collected the MCS reflection data and wide-angle data offshore Nicaragua in a recent cruise (June 2000). The survey map with 2D seismic traverses is shown in Figure 4.1. There are also other datasets from offshore Costa Rica collected by UTIG, 1991. Both data acquisitions projects were funded by National Science Foundation (NSF). These profiles are marked in Figure 4.1. The data offshore Nicaragua were collected using a single 6km long streamer with 240 receivers spaced 25m apart. Shot spacing was 50m, giving a CMP gather with coverage of 60 fold. The data offshore Costa Rica were collected using a single 3km long streamer with 96 receivers spaced 33.33m apart and the shot spacing was 50m, providing a CMP gather with coverage of 48 fold. I used two MCS reflection lines from each of these surveys to apply prestack depth migration. The particular MCS lines selected are off central and southern Nicaragua, and off central Nicoya peninsula.

I did the routine MCS processing using the commercial Focus software processing package from Paradigm Geophysical. The processing steps include trace editing, gain corrections, filtering, deconvolution, sorting into CMP gathers, multiple removal, velocity analysis, stacking and post-stack migration. The flowchart for the conventional processing is shown in Figure 4.2. Although we acquired high quality seismic data, it remained difficult to image the lower slope and subducting plate structure in detail with conventional processing techniques. Several characteristics of this environment pose seismic imaging problems: the area is heavily faulted, adjacent reflection boundaries have contrasting dips, and

the velocity structure changes rapidly both laterally and vertically (Figure 1.2). In this environment the common midpoint (CMP) gathers do not represent a collection of true common subsurface reflection points. To realize an interpretable image of the lower slope offshore Nicaragua and Costa Rica, I applied the more rigorous pre-stack depth migration (PSDM). A good PSDM image requires an accurate earth velocity model. Therefore one of the most important aspects of PSDM is velocity analysis. In the previous chapter, I developed a new residual migration velocity analysis (RMVA) technique. The images discussed in this chapter were generated by performing PSDM using the velocities derived from this RMVA technique. The images of the selected lines are analyzed in the next sections.

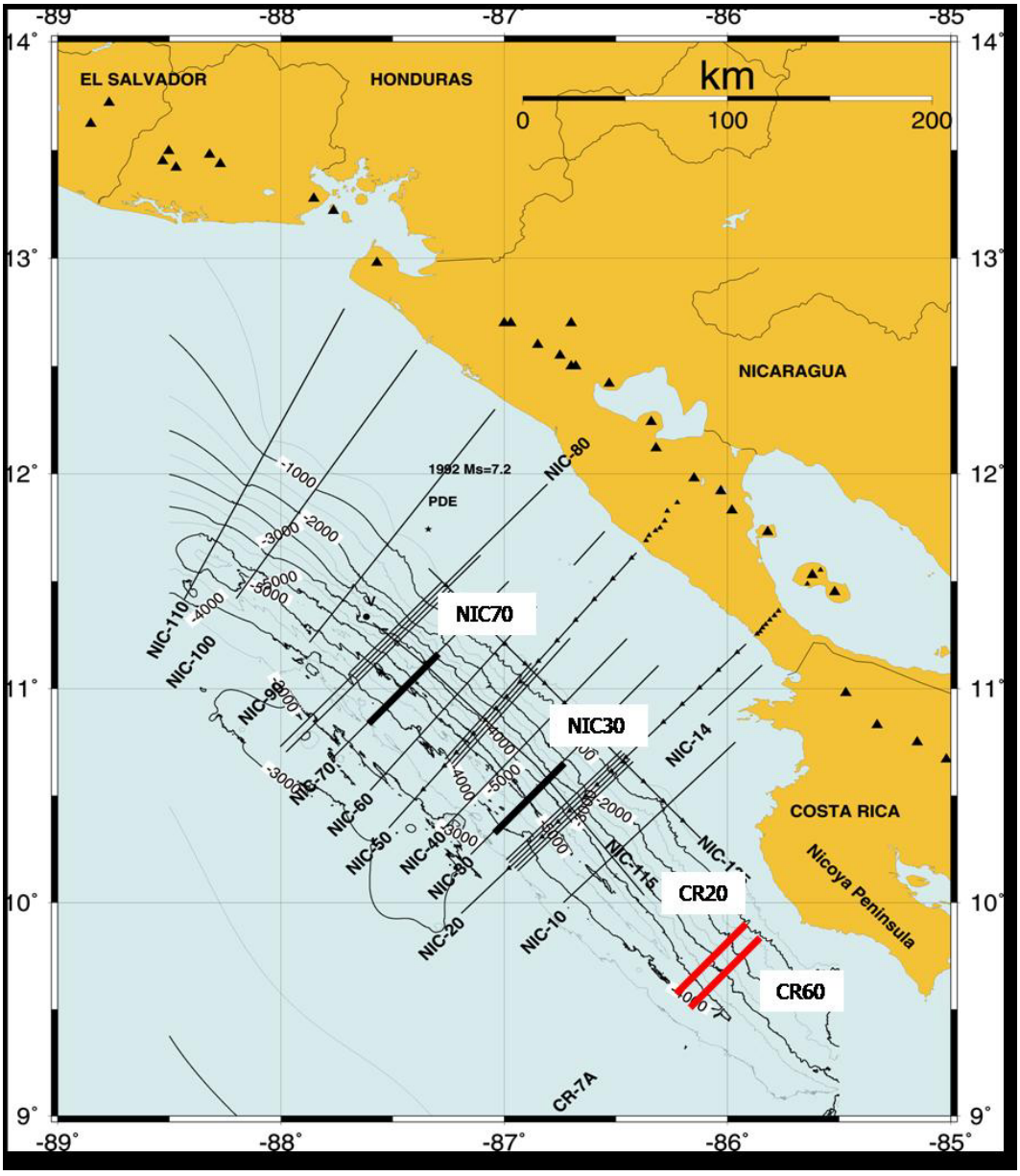

Figure 4.1 Map showing the study and the 2D MCS survey. Prestack depth migration (PSDM) was done on the selected lines above.

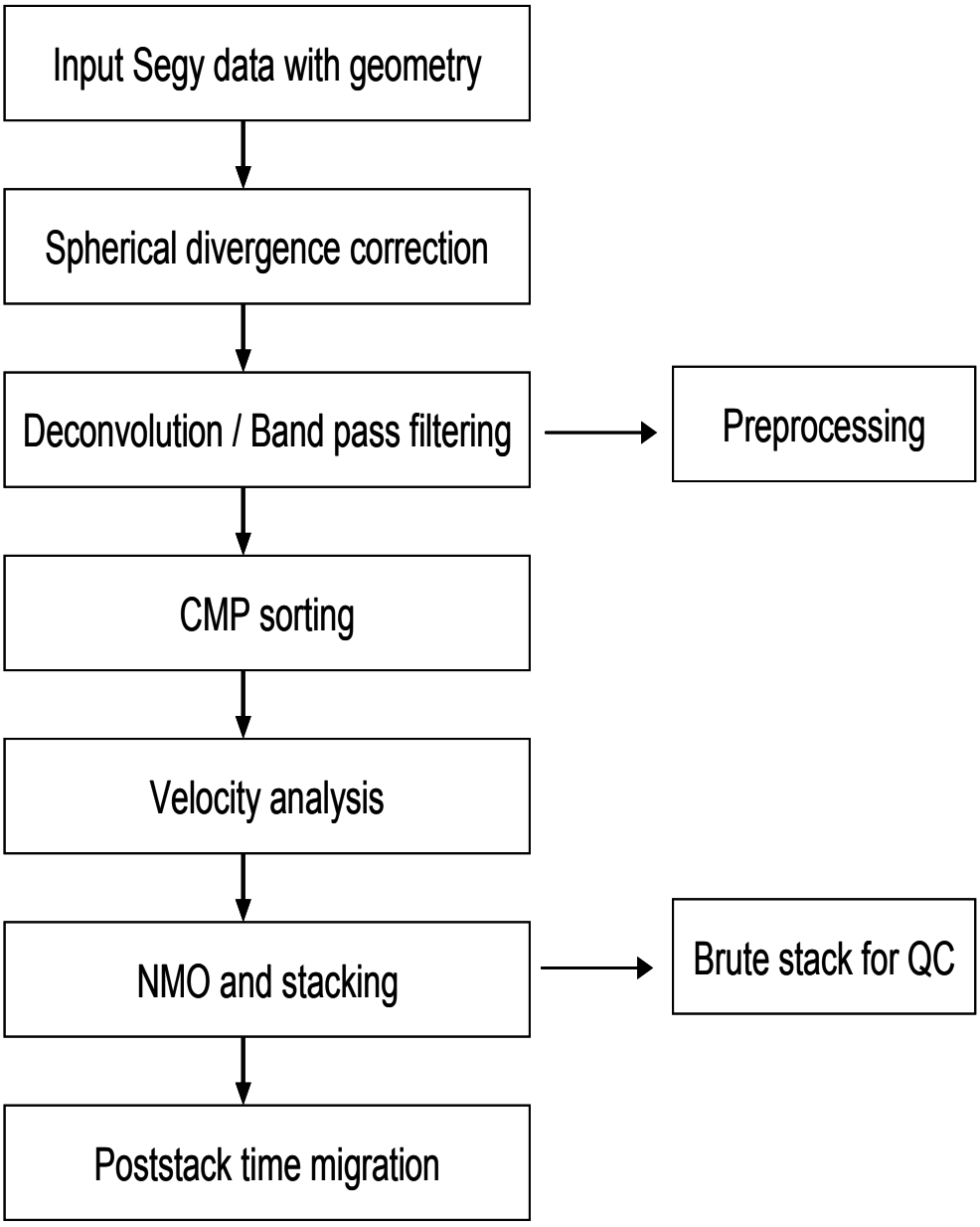

Figure 4.2. Flowchart for conventional seismic data processing.

4.4 SEISMIC IMAGES AND INTERPRETATION

One dimensional gradient velocity model hinged from the sea floor was chosen as the starting velocity model to apply the prestack depth migration (PSDM) algorithm on these MCS profiles. The common image gathers (CIGs) generated by applying PSDM were used for residual migration velocity analysis (RMVA) to update the velocity models. The RMVA process was repeated till a satisfactory velocity model for PSDM was obtained. I discuss the images off Nicaragua and Costa Rica in the subsections below.

4.4.1 Images offshore Nicaragua

Figure 4.3 is the pre-stack depth migrated image of the MCS profile NIC-30 off central Nicaragua using the 1D gradient velocity model in Figure 4.4. As expected the structure of the incoming plate is visible before subduction but there are only hints of it beneath the underthrust plate after undergoing subduction. This is because the gradient velocity is quite close to the true velocity of the incoming plate before subduction, but the velocity through the underthrust is much more complex than a simple gradient velocity seaward from the trench. Figure 4.5 is the prestack depth migrated image after two iterations of RMVA were used to construct the imaging velocity model. There is considerable improvement in the image quality compared to Figure 4.3. The pre-thrust sediments are very well imaged, and the rotated fault blocks can be observed both before and after subduction. The incoming sediment section is discontinuous because of large fault throws. It is very difficult to construct a good image at the toe of the trench. However, the RMVA technique has done well in generating a velocity model that

has produced a very good image of the toe of the trench. An important thing to notice here is that the images are constructed in depth, so what we are seeing is actual spatial representation of the subsurface. Figure 4.6 is the prestack depth migrated image after three iterations of RMVA. This image shows a slight overall improvement from the image after two iterations (Figure 4.5). A detailed portion of the trench region is shown in Figure 4.8. The red arrows are the locations of the CIG shown in Figure 4.10. This figure shows three locations for the gathers. The first is located near the trench before subduction and the remaining two near the trench after subduction. The reflection events on the first CIG are clearly visible but the flat events from the reflector are not easily detectable from the remaining two CIG. This is because the overlying velocity structure is very complex above the subducted sediments. The reflectors are mapped between the CIG locations with the help of arrows shown in the figure. The flatness of the events in a CIG suggests the velocity used for migration is near to true.

Figure 4.9 is the same image of line NIC-30 as in Figure 4.8 with my fault and reflector interpretation superimposed. The first three rotated fault blocks after subduction are well imaged, but after that the sediments become compacted enough to produce propagation velocities that exceed the seismic resolution limit at that depth. Still there is evidence of two contrasting dipping reflectors along the plate boundary. The shallower dipping reflector being the decollement and the steeper opposite dipping reflector being the rotated fault blocks preserved after subduction. The dip of the plate boundary from the image is also consistent with tectonic models..

Figure 4.11 is the pre-stack depth migrated image of the lower slope of line NIC-70 off southern Nicaragua using the velocity model derived after five iterations of RMVA. This image also shows subduction of rotated fault blocks as we observed in the image of the MCS line NIC-30. The extensional faults are more pronounced in the subducting plate for this line compared to that of NIC-30. We had shown in chapter 2 that the incoming plate is more intensely faulted off central Nicaragua then off southern Nicaragua. Therefore the lower slope area of line NIC-70 is structurally more complex then that of line NIC30. Thus applying imaging and velocity analysis is a more challenging job for this line. The detail of the trench region of Figure 4.11 is shown in Figure 4.12. Figure 4.13 is the same image as in Figure 4.12 with my interpretation included. There are clear indications of contrasting dips along the plate boundary. The shallower dipping reflector being the decollement and the steeper opposite dipping reflector being the rotated fault blocks preserved after subduction.

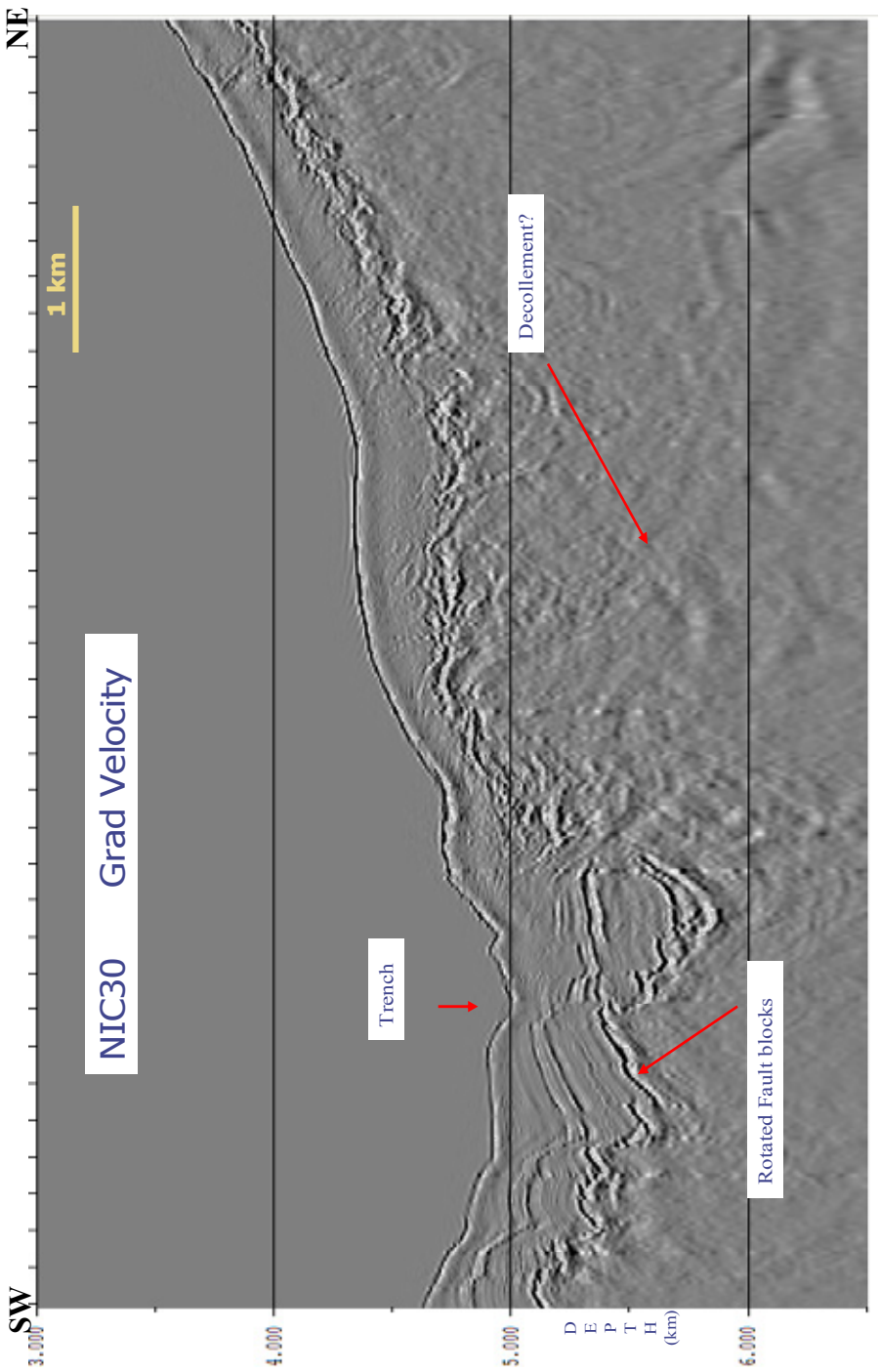

Figure 4.3. PSDM of line NIC-30 using 1D gradient velocity model in Figure 4.4.

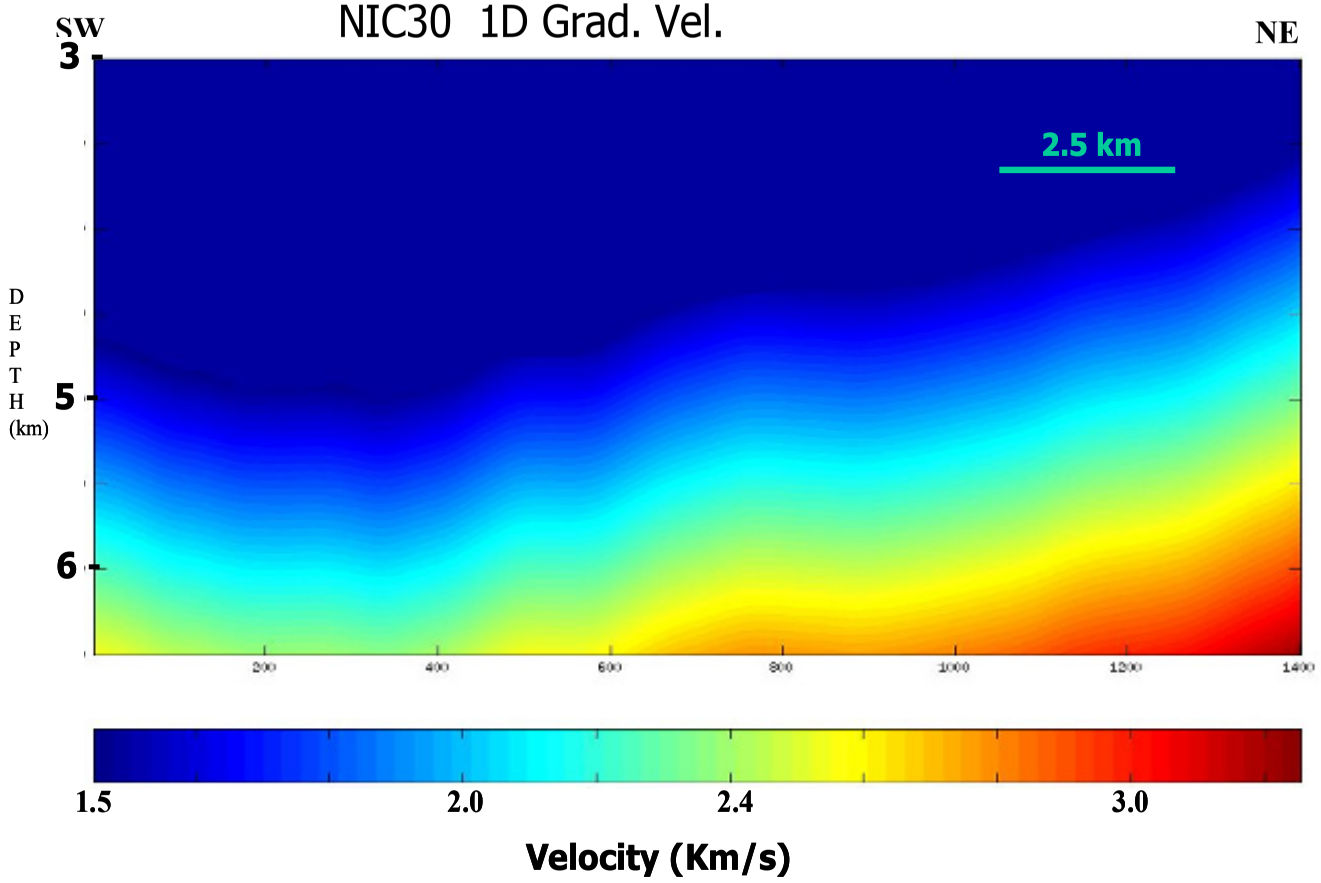

Figure 4.4. Starting 1D gradient velocity model for NIC-30.

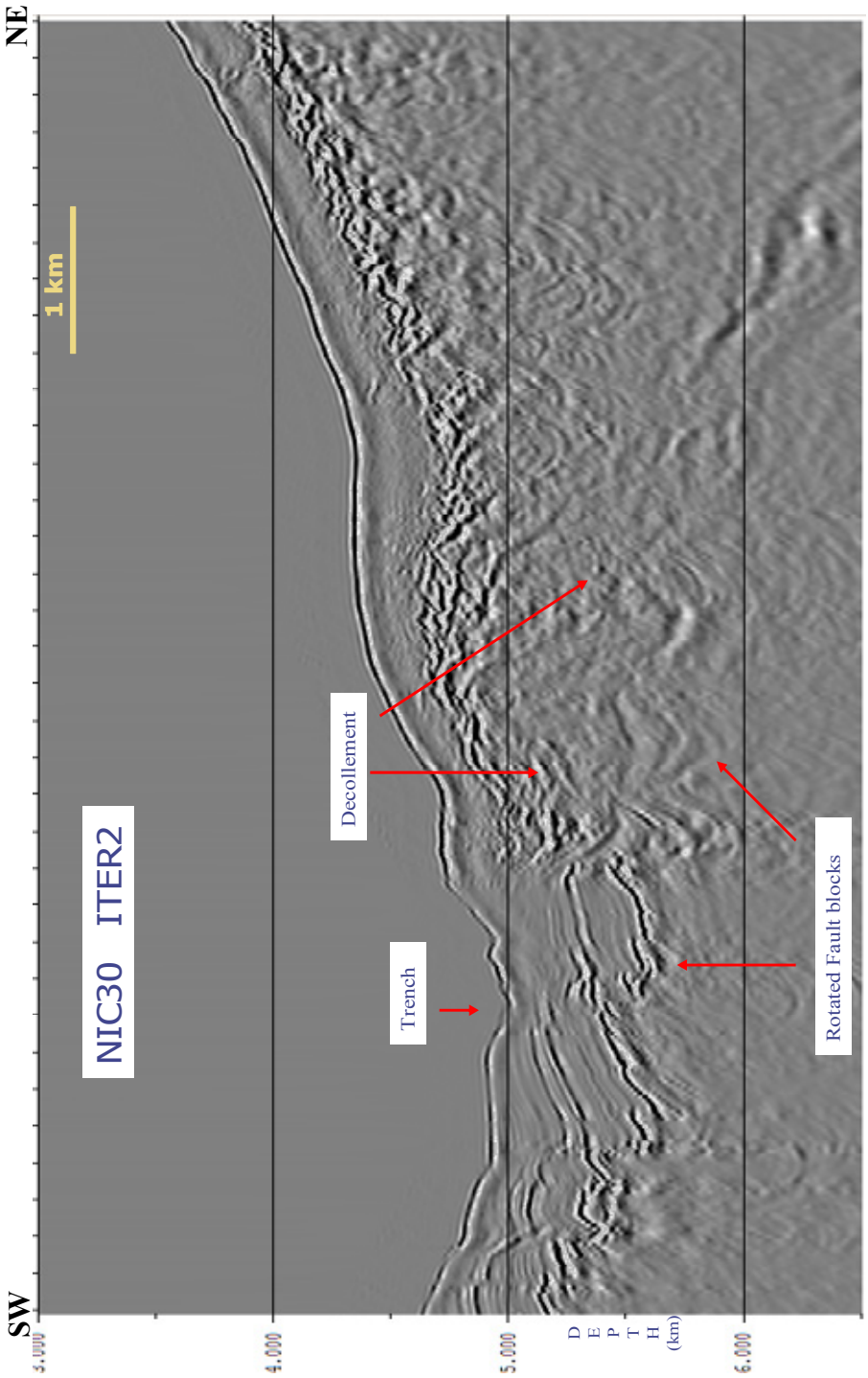

Figure 4.5. PSDM of line NIC-30 using the velocity model after two iterations of RMVA.

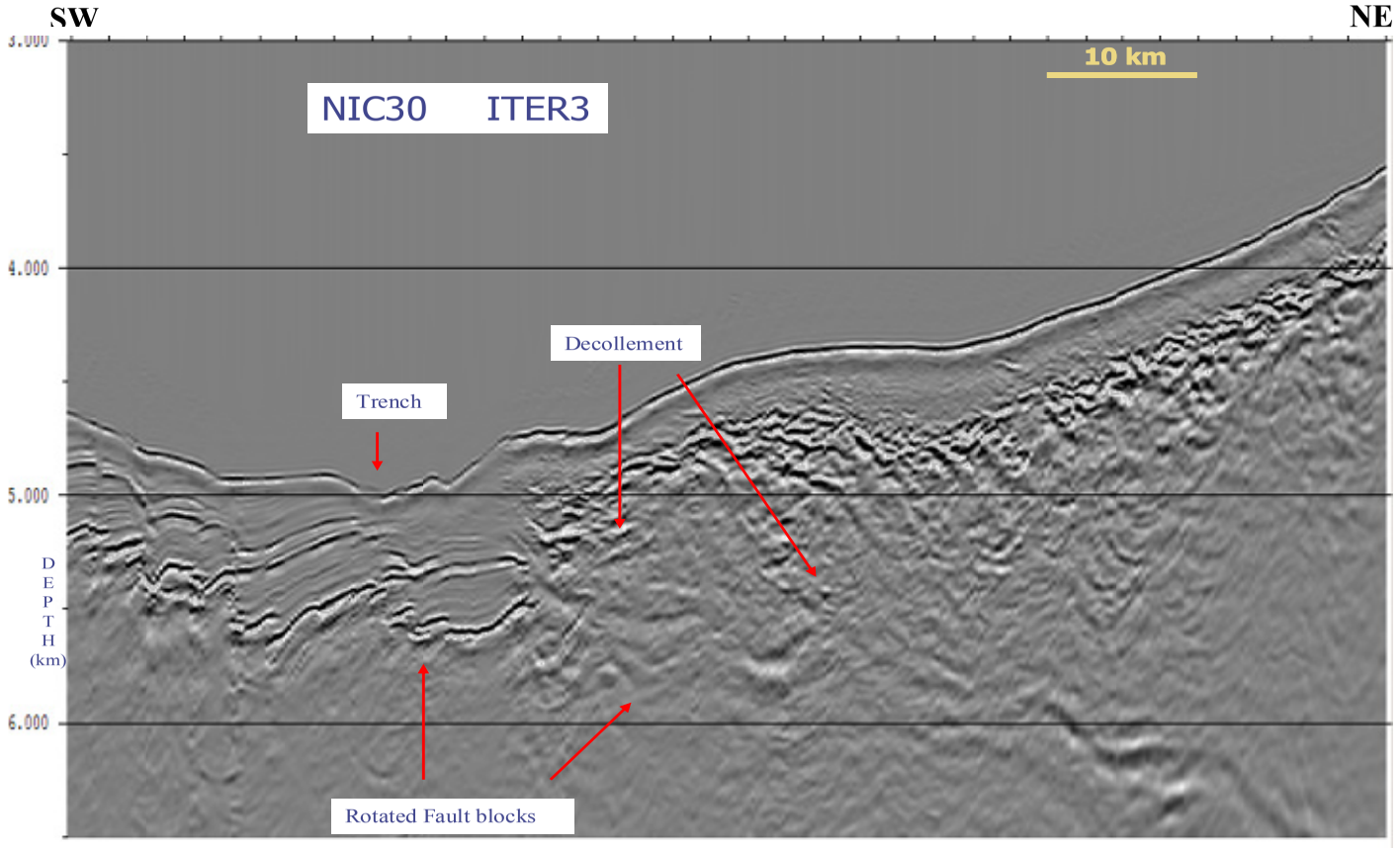

Figure 4.6. PSDM image of line NIC-30 using the velocity model after three iterations of RMVA (Figure 4.7).

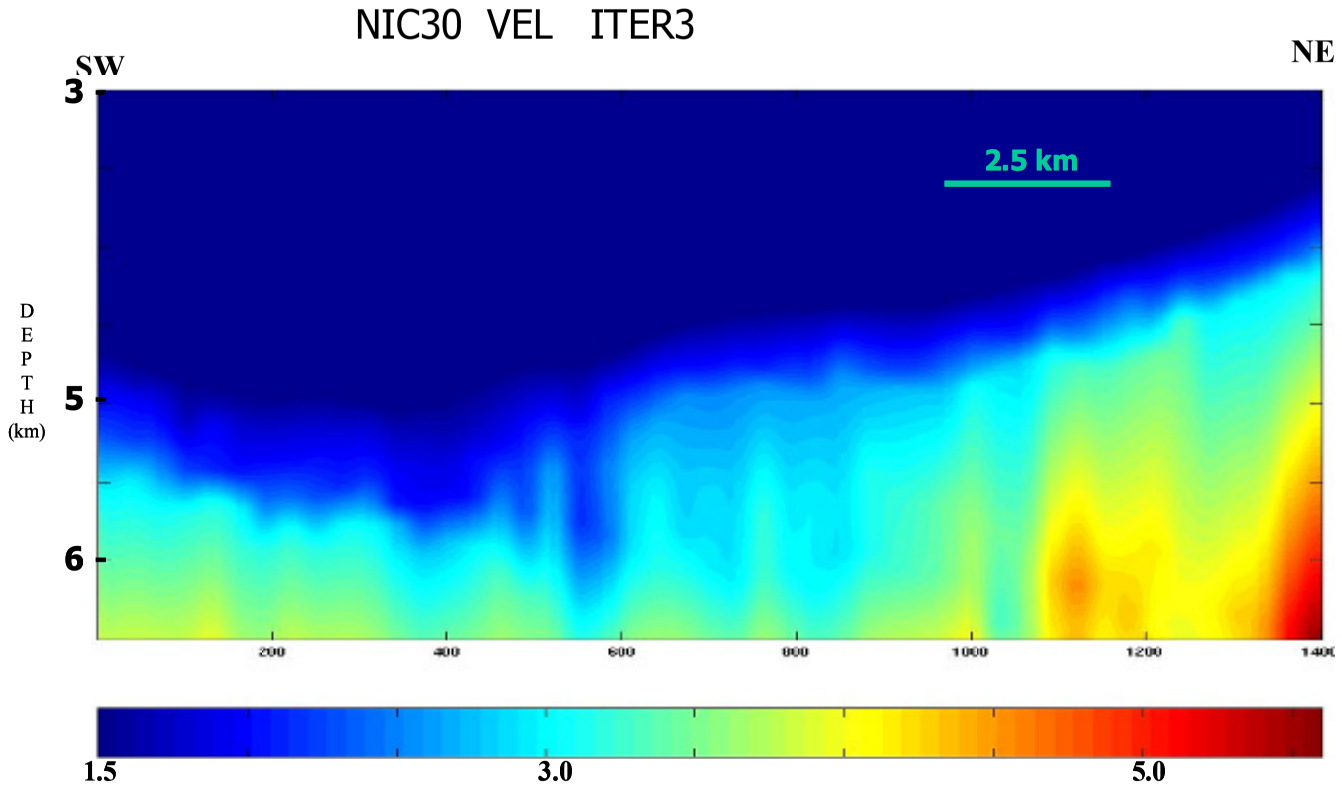

Figure 4.7. Velocity model of NIC-30 after three iterations of RMVA.

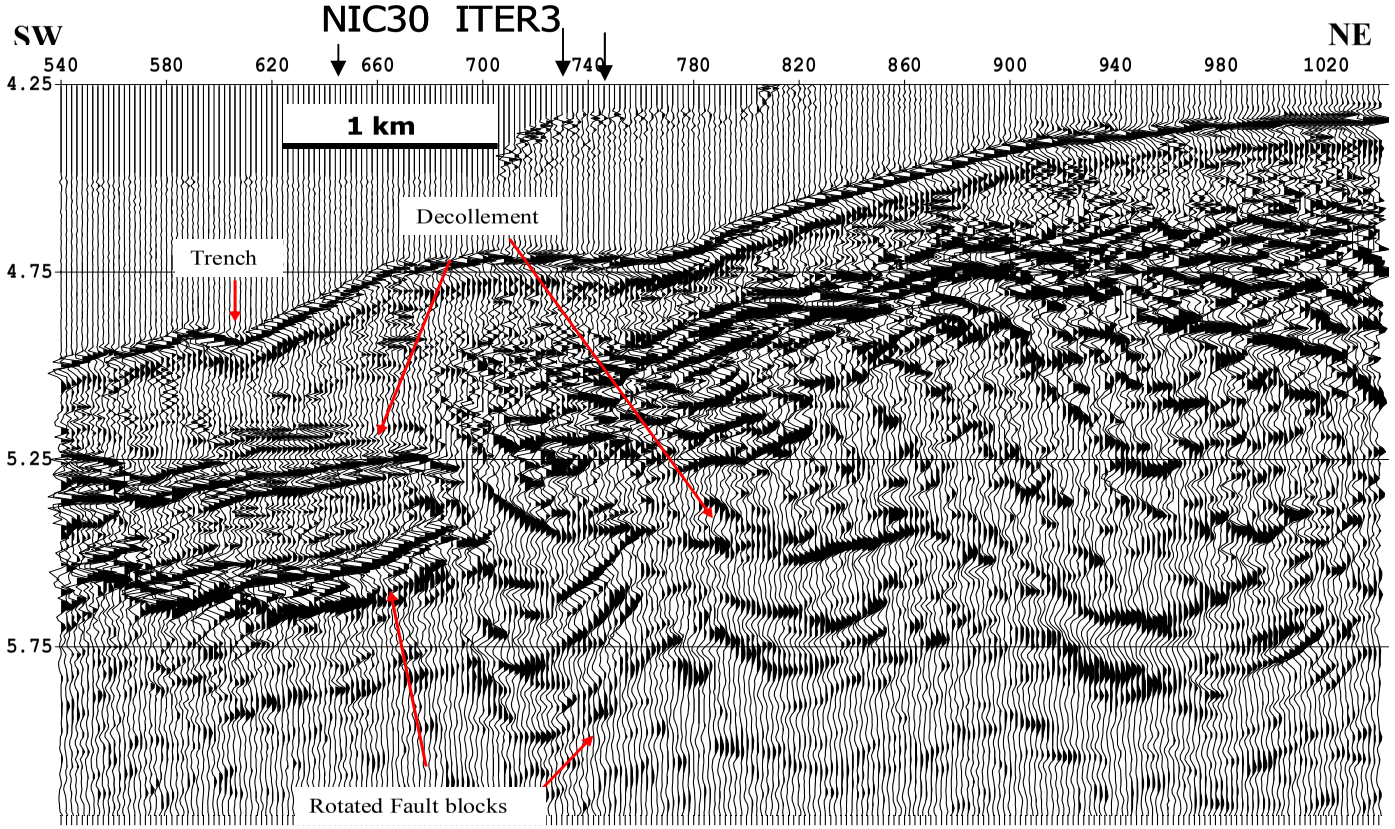

Figure 4.8. Detail of PSDM image of line NIC-30 using the velocity model after three iterations of RMVA. The black arrows are the positions of the CIGs shown in Figure 4.10.

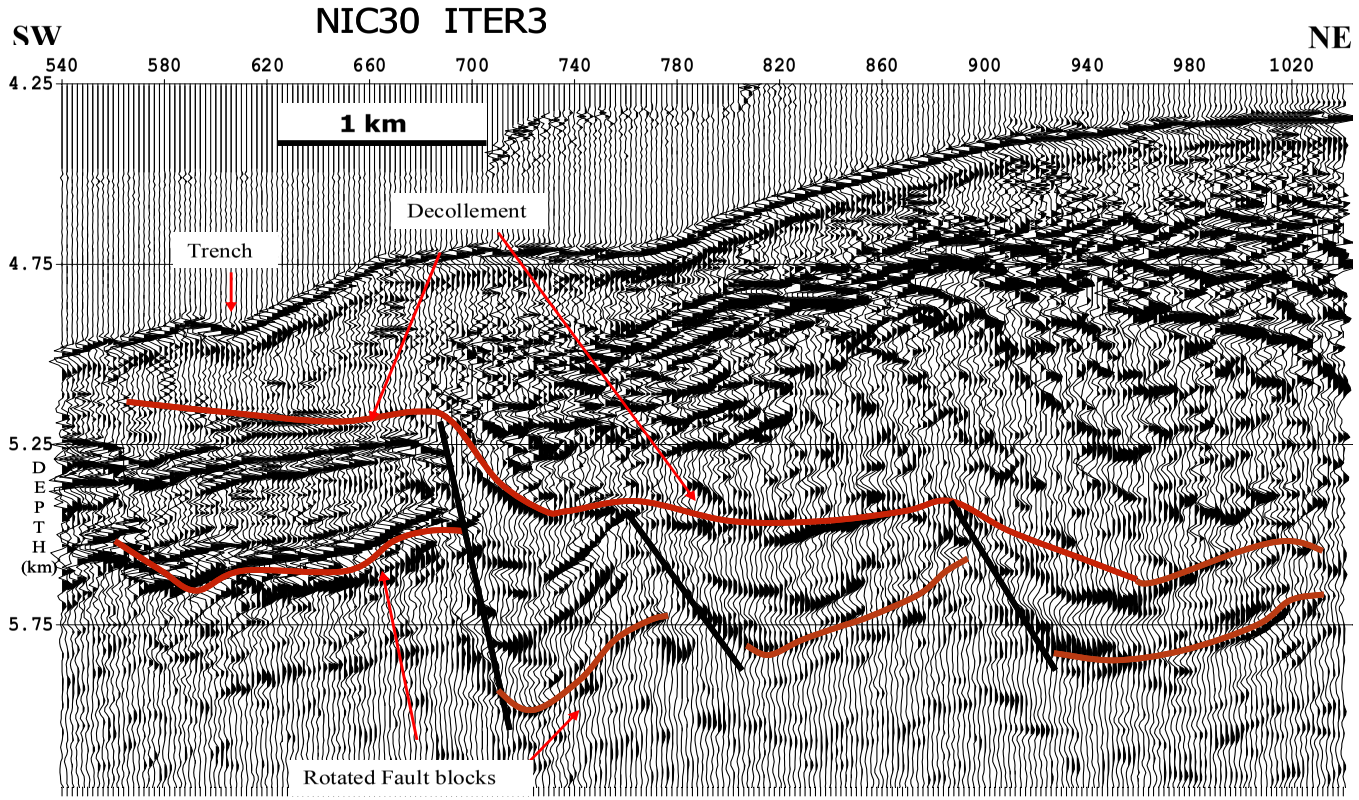

Figure 4.9. Detail of PSDM image of line NIC-30 using the velocity model after three iterations of RMVA with fault and correlative reflectors interpretation superimposed.

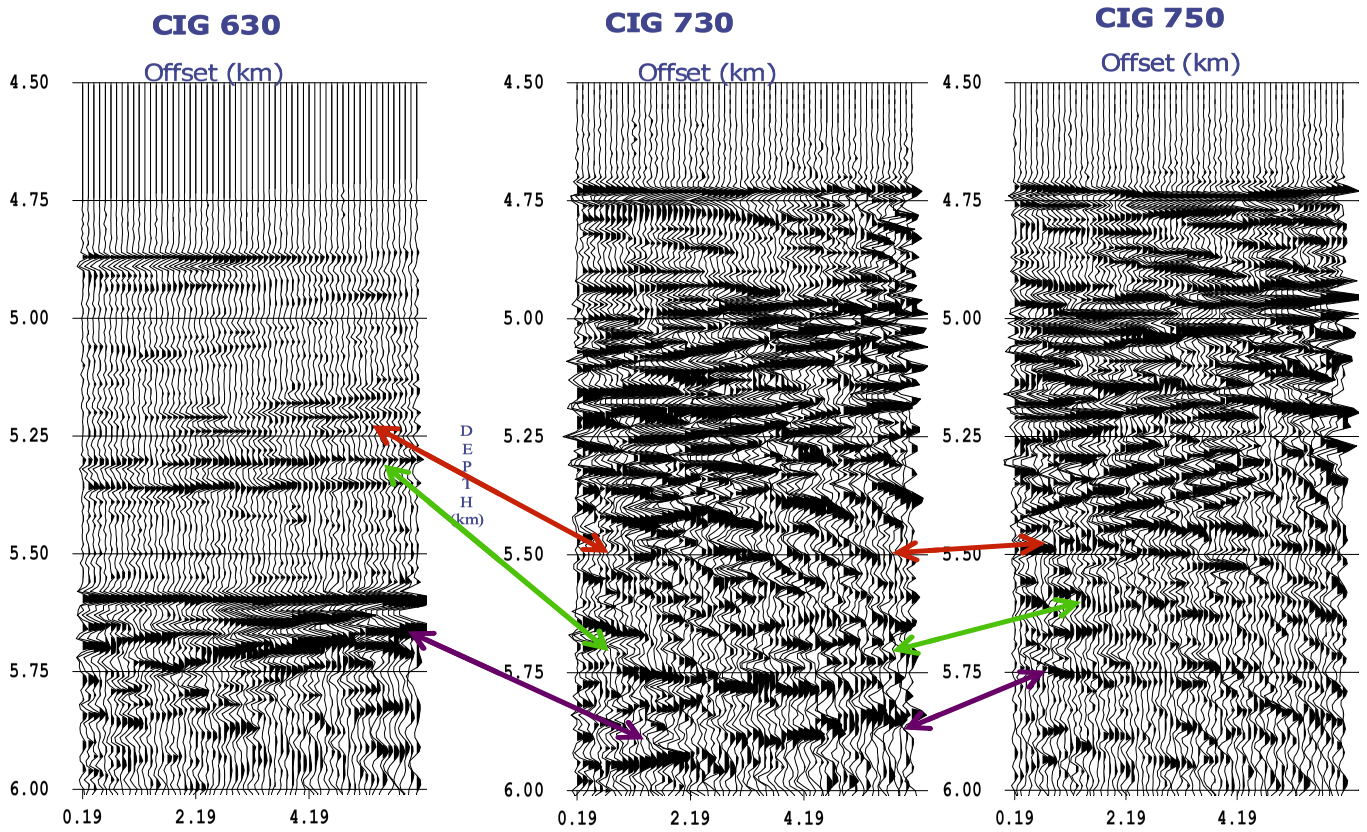

Figure 4.10. CIGS generated after performing PSDM of line NIC-30 using velocity model derived after three iterations of RMVA. The arrows map the events between the CIGs.

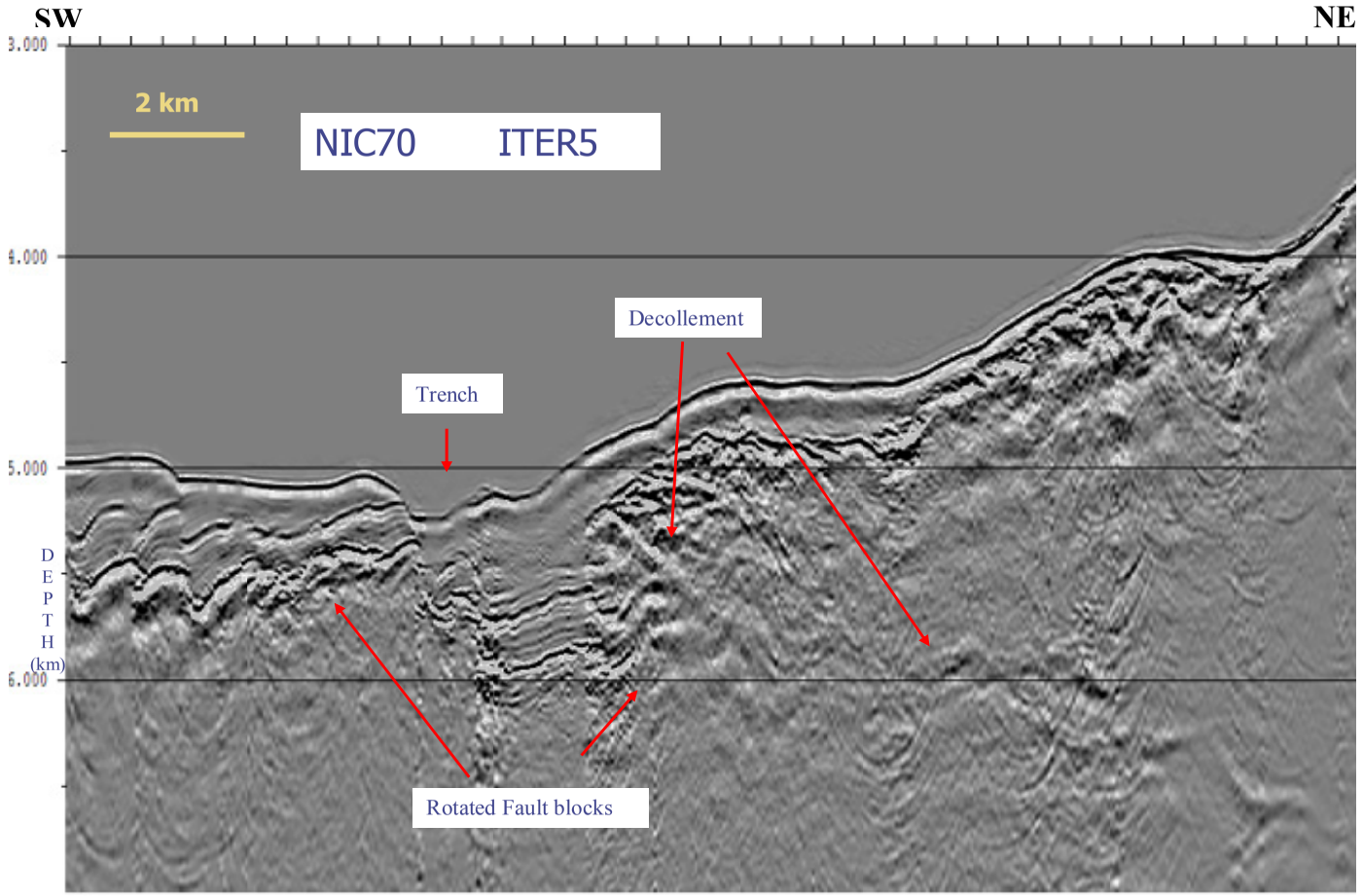

Figure 4.11. PSDM image of line NIC-70 using the velocity model after five iterations of RMVA.

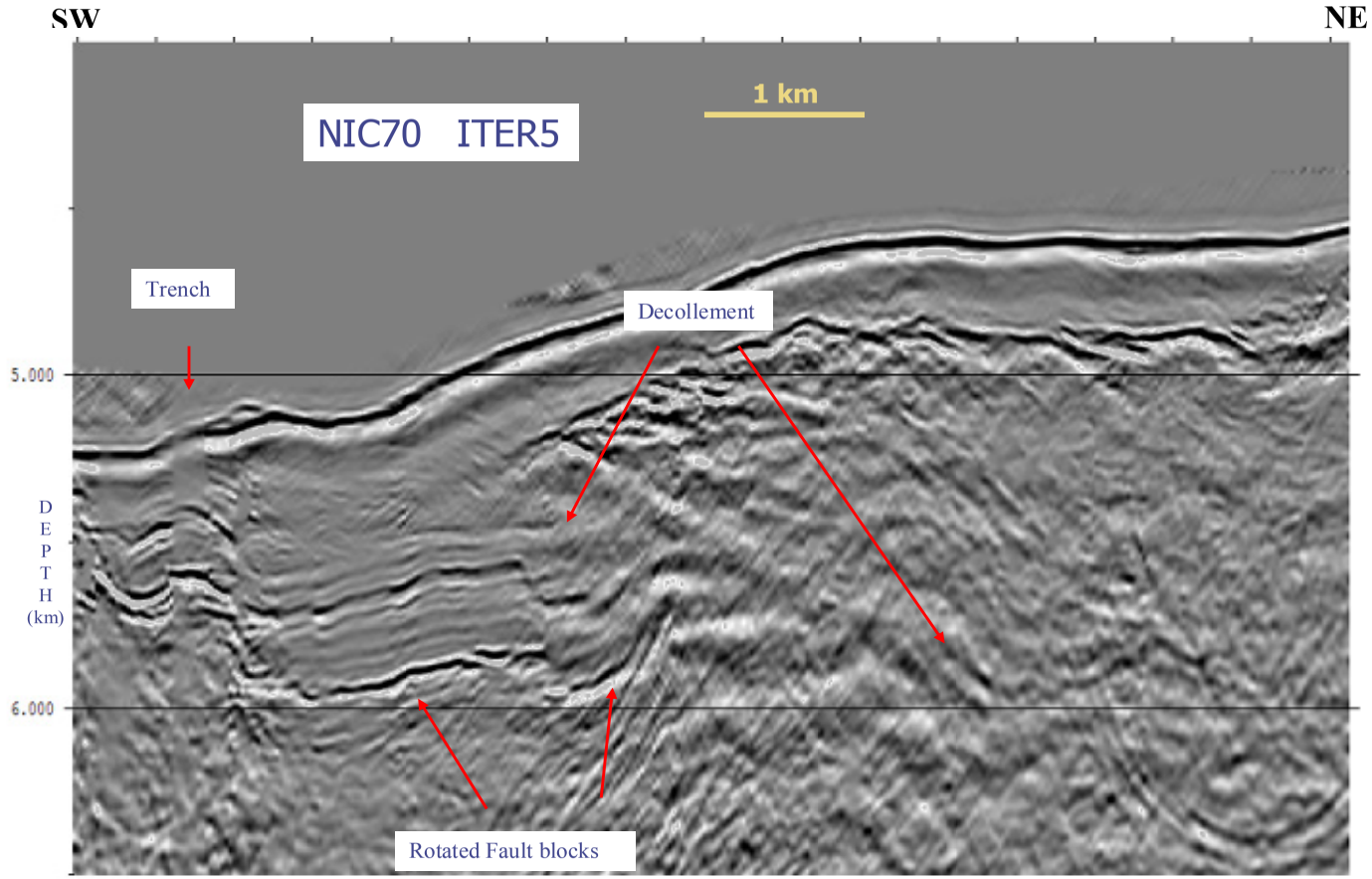

Figure 4.12. Detail of PSDM image of line NIC-70 using the velocity model after five iterations of RMVA.

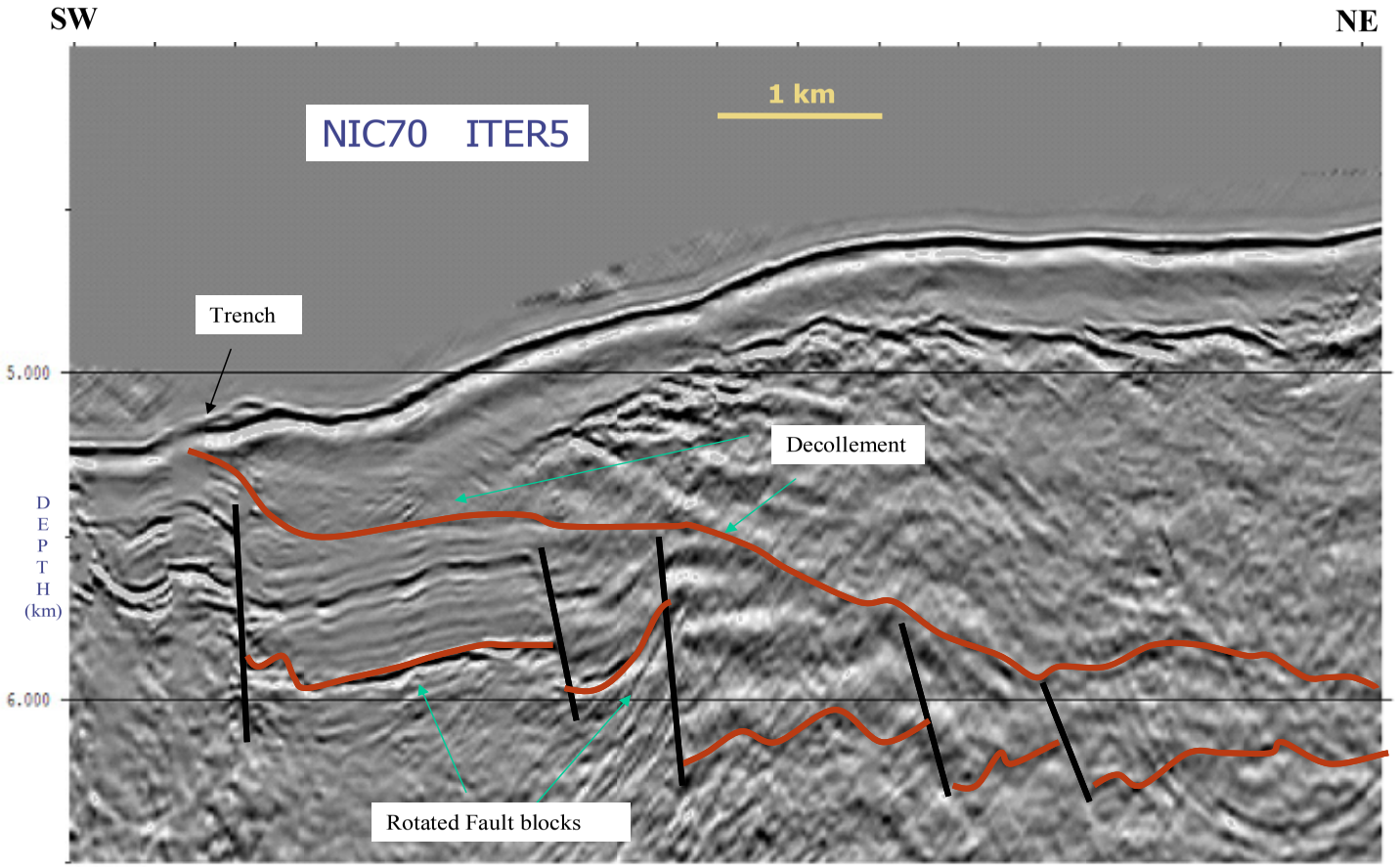

Figure 4.13. Detail of PSDM image of line NIC-70 using the velocity model after five iterations of RMVA with my interpretation included.

4.4.2 Images offshore Costa Rica

Figure 4.14 is the pre-stack depth migrated image of the lower slope of line CR-20 (off central Nicoya) using the velocity model (Figure 4.15) derived after five iterations of RMVA. The extensional faults on the subducting plate are not as pronounced in this MCS line offshore Costa Rica compared to that of MCS lines from Nicaragua. There is no development of half-graben like structures in the subducting plate. Repeated stratigraphic sections are present between the present decollement and the upper plate basement. The detailed portion of the trench region of Figure 4.14 is shown in Figure 4.16. The red arrows in Figure 4.16 are the locations of the CIG shown in Figure 4.18. The first of the three CIGs is located near the trench before subduction and the remaining two near the trench after subduction. The flatness of the events on the CIGs suggests that the velocity model used for migration is valid.

Figure 4.17 is the same image of the line CR-20 as in Figure 4.16, with my interpretation included. The entire sediment column is initially underthrust offshore the Nicoya Peninsula area of Costa Rica (e.g., Kimura et al., 1997), but the top unit or the younger sediments are considerably deformed 3-4 km from the trench. On the other hand the base units just undergo subduction without any noticeable deformation.

Figure 4.19 is the prestack depth migrated image of the lower slope of CR-60 (off central Nicoya) line using the velocity model derived after five iterations of RMVA. The extensional faults on the subducting plate are least pronounced in this MCS line offshore Costa Rica compared to the three MCS profiles discussed

in previous sections. There is also no obvious development of half-graben like structures in the subducting plate of this Costa Rica. Repeated stratigraphic sections are also present between the present decollement and the upper plate basement. A detail of the trench region of Figure 4.19 is shown in Figure 4.20.

Figure 4.21 is the same image as in Figure 4.20 with my interpretation superimposed. This image clearly shows initial subduction of the entire sediment column near the trench. Here also landward of the trench the subducted top unit gets initially thinner but at deeper positions is considerably thicker; even thicker then its original thickness before subduction. The upper unit is considerably deformed 5-6 km from the trench but the base units subduct without noticeable deformation.

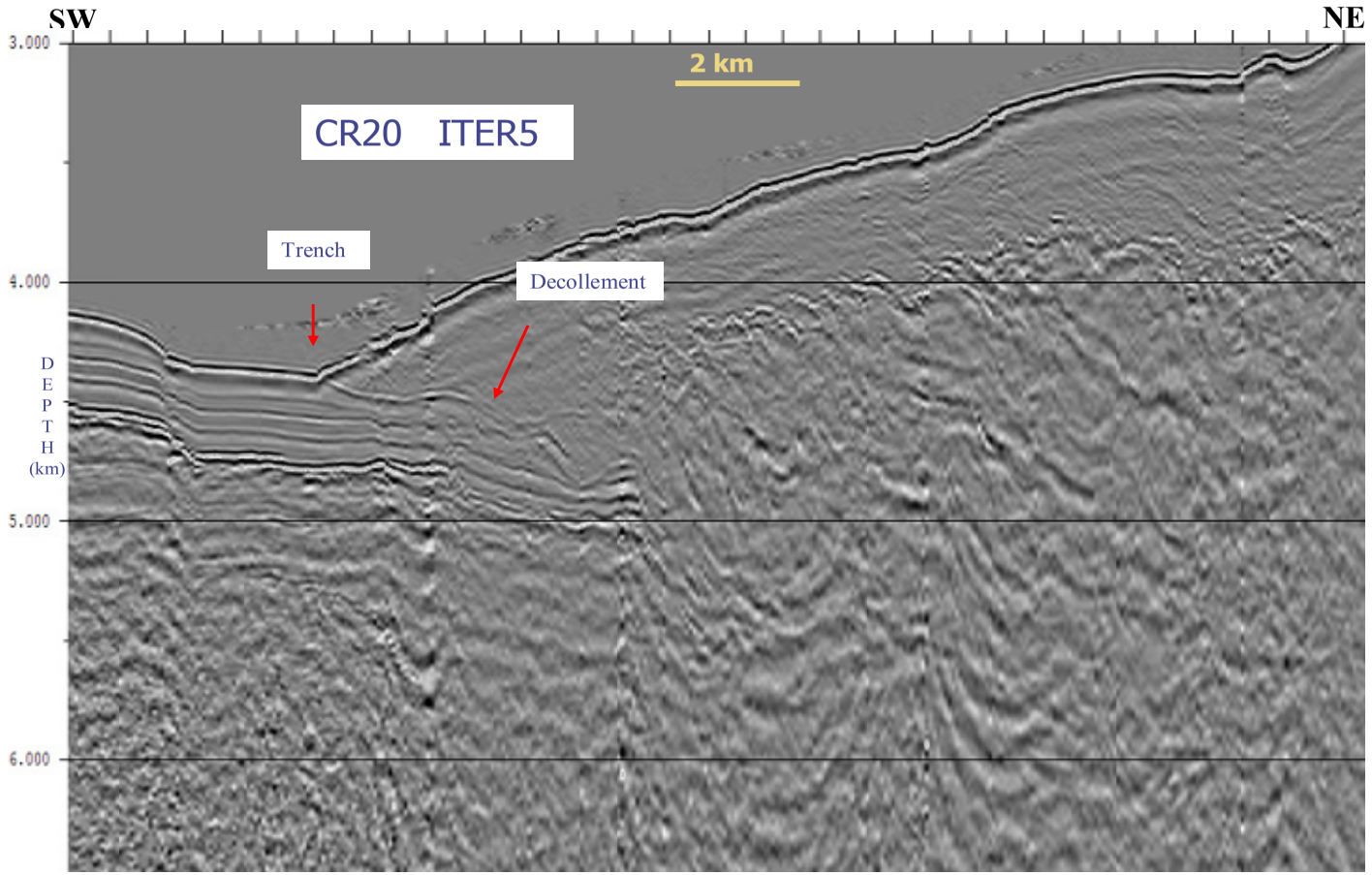

Figure 4.14. PSDM image of line CR-20 using the velocity model after five iterations of RMVA (Figure 4.15).

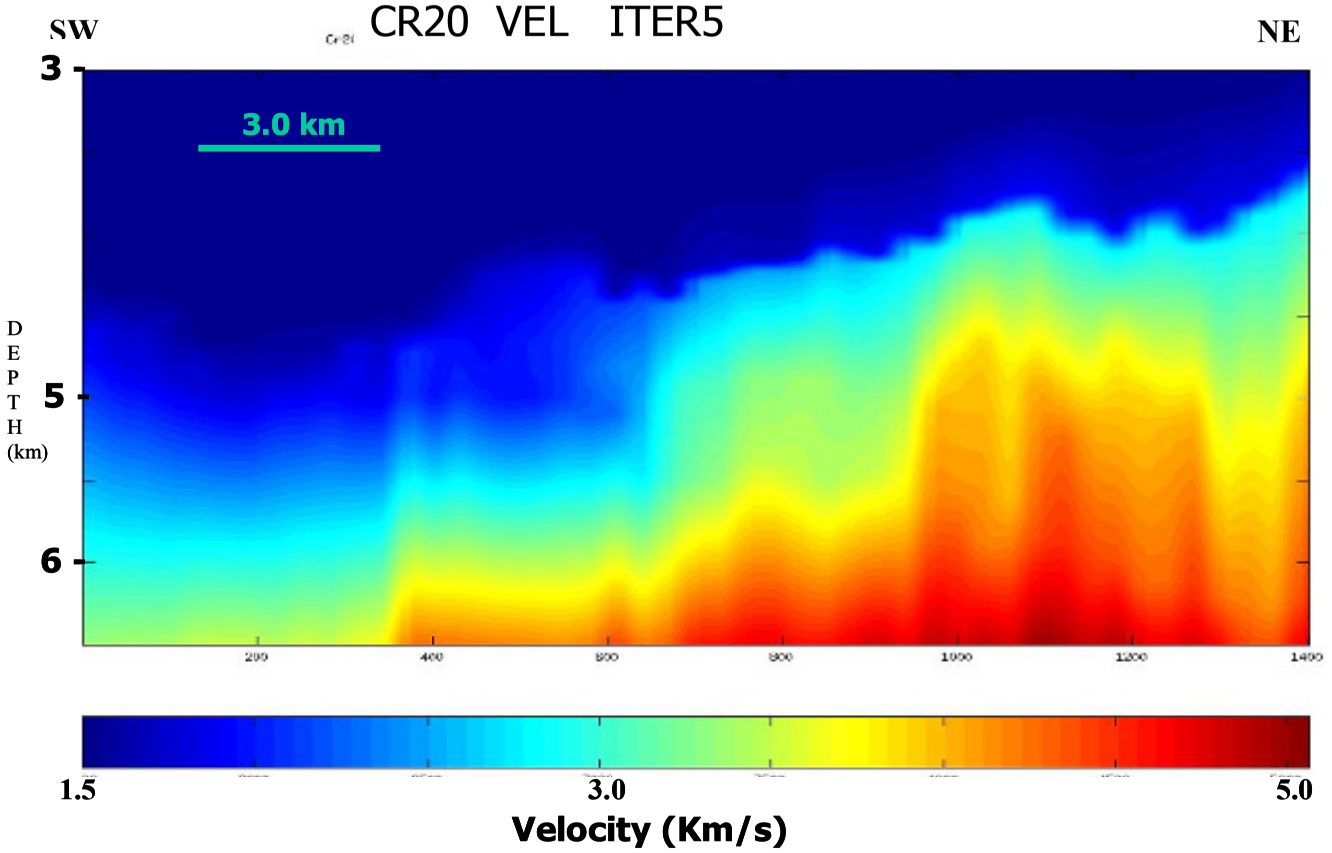

Figure 4.15. Velocity model of CR-20 after five iterations of RMVA.

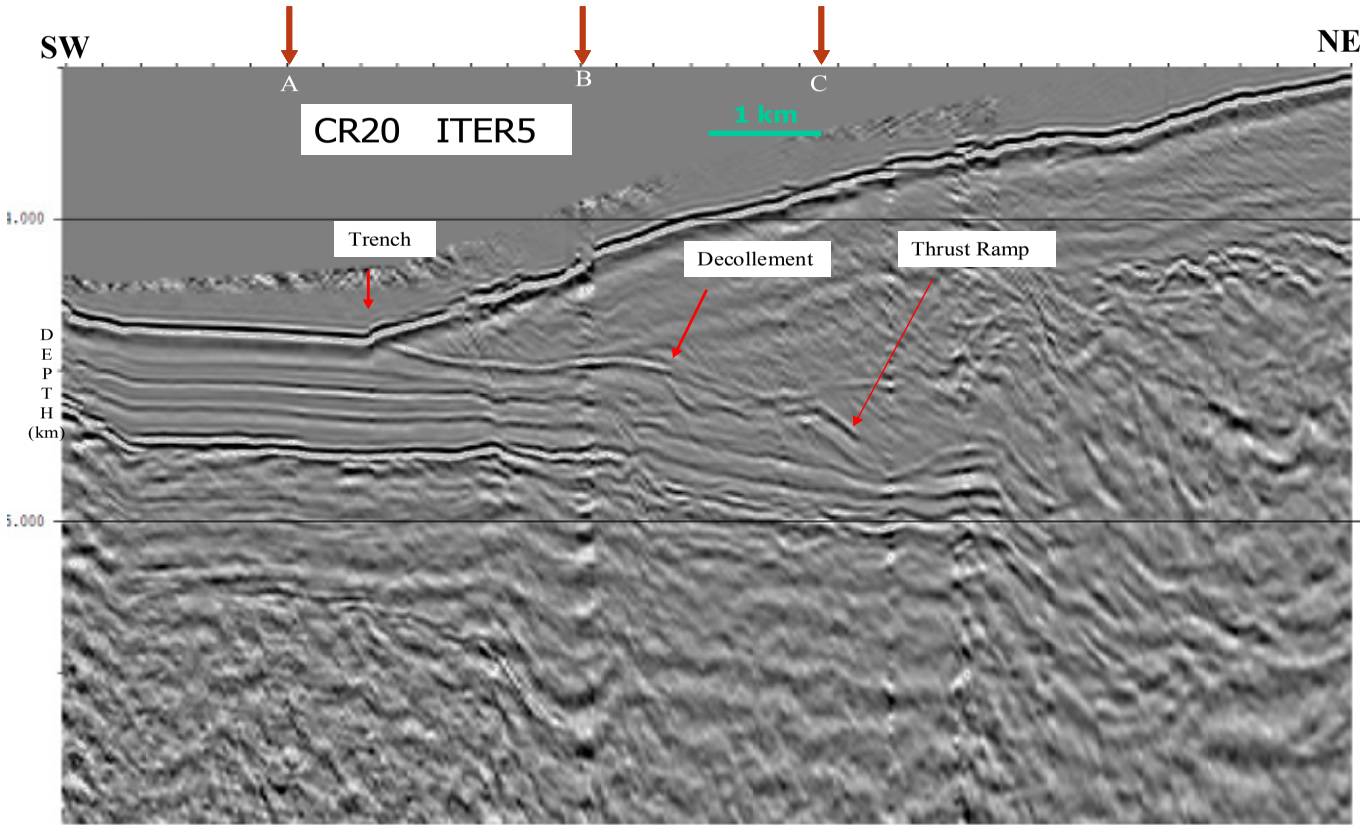

Figure 4.16. Detail of PSDM image of line CR-20 using the velocity model after five iterations of RMVA. The arrows mark the CIGs shown in Figure 4.18.

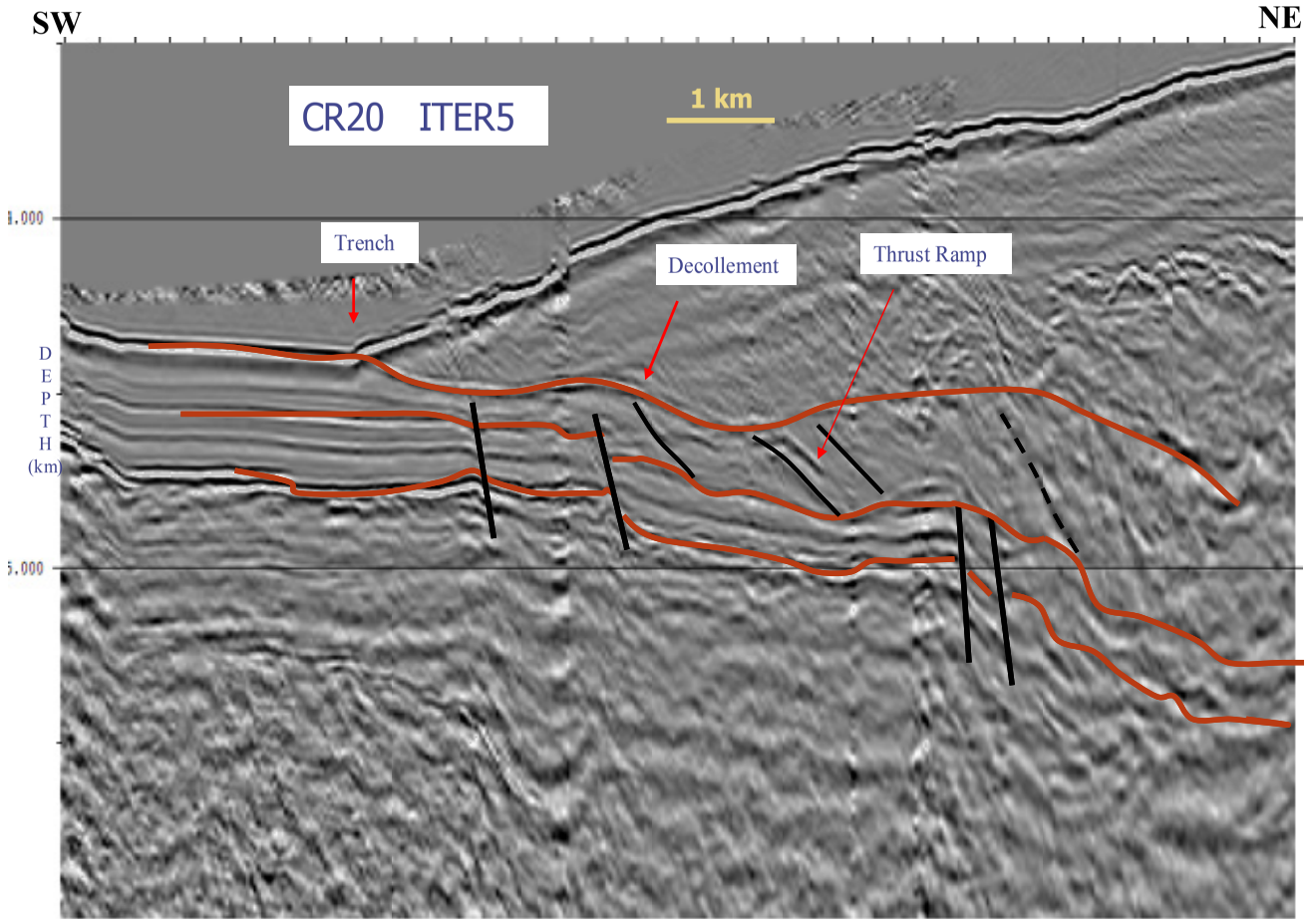

Figure 4.17. Detail of PSDM mage of line CR-20 using the velocity model after five iterations of RMVA with my interpretation superimposed.

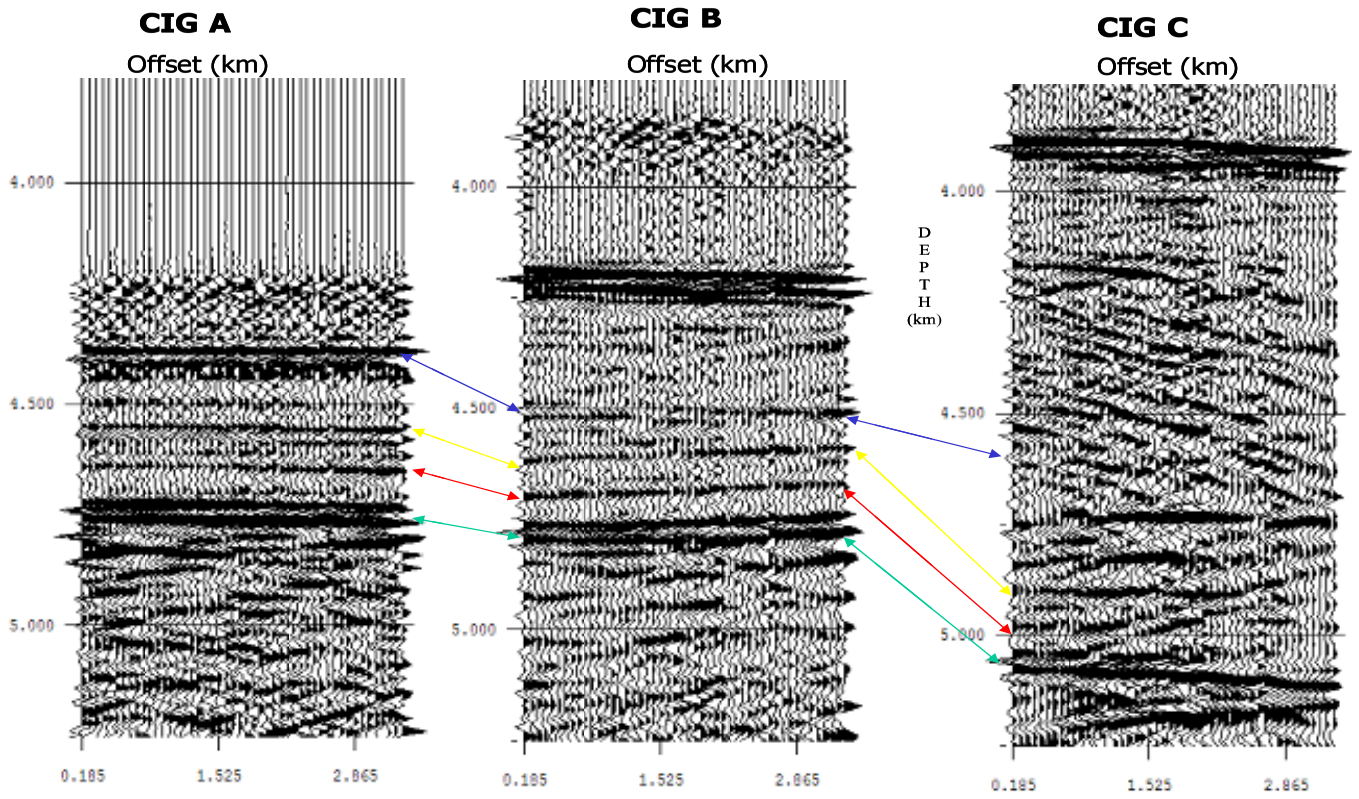

Figure 4.18. CIGS generated after performing PSDM of line CR-20 using velocity model derived after five iterations of RMVA. The arrows map the events between the CIGs.

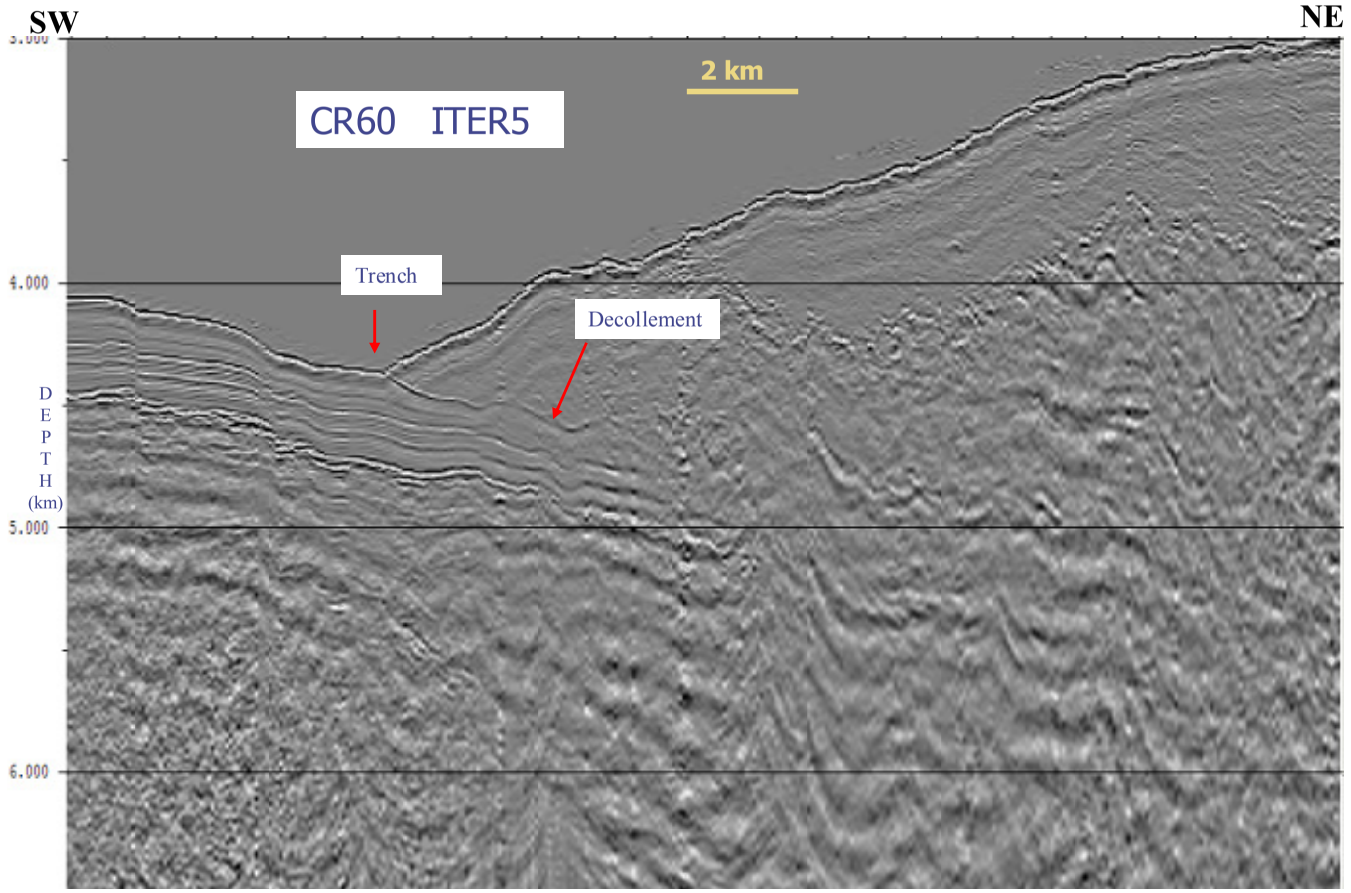

Figure 4.19. PSDM image of line CR-60 using the velocity model after five iterations of RMVA.

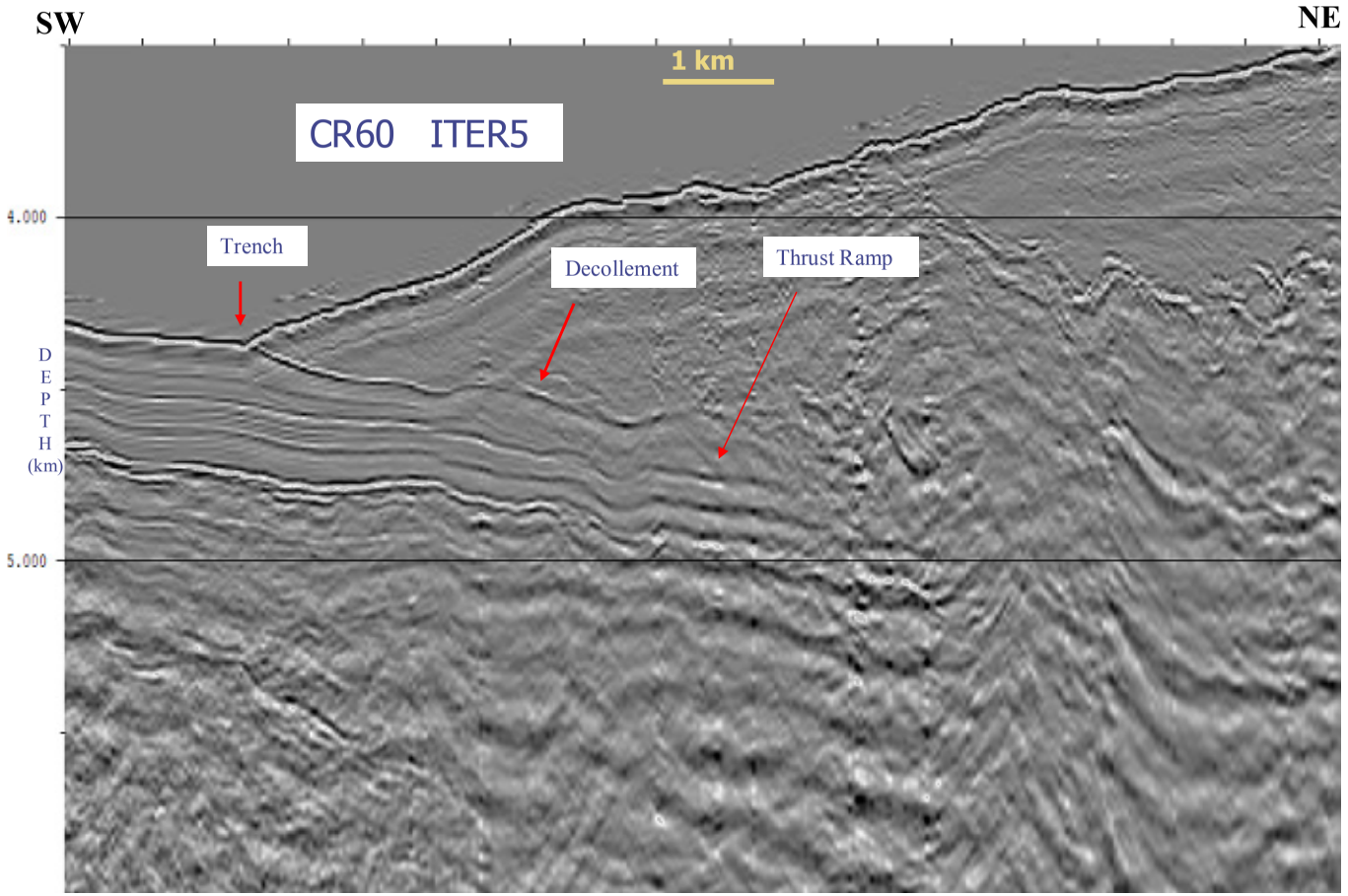

Figure 4.20. Detail of PSDM image of line CR-60 using the velocity model after five iterations of RMVA.

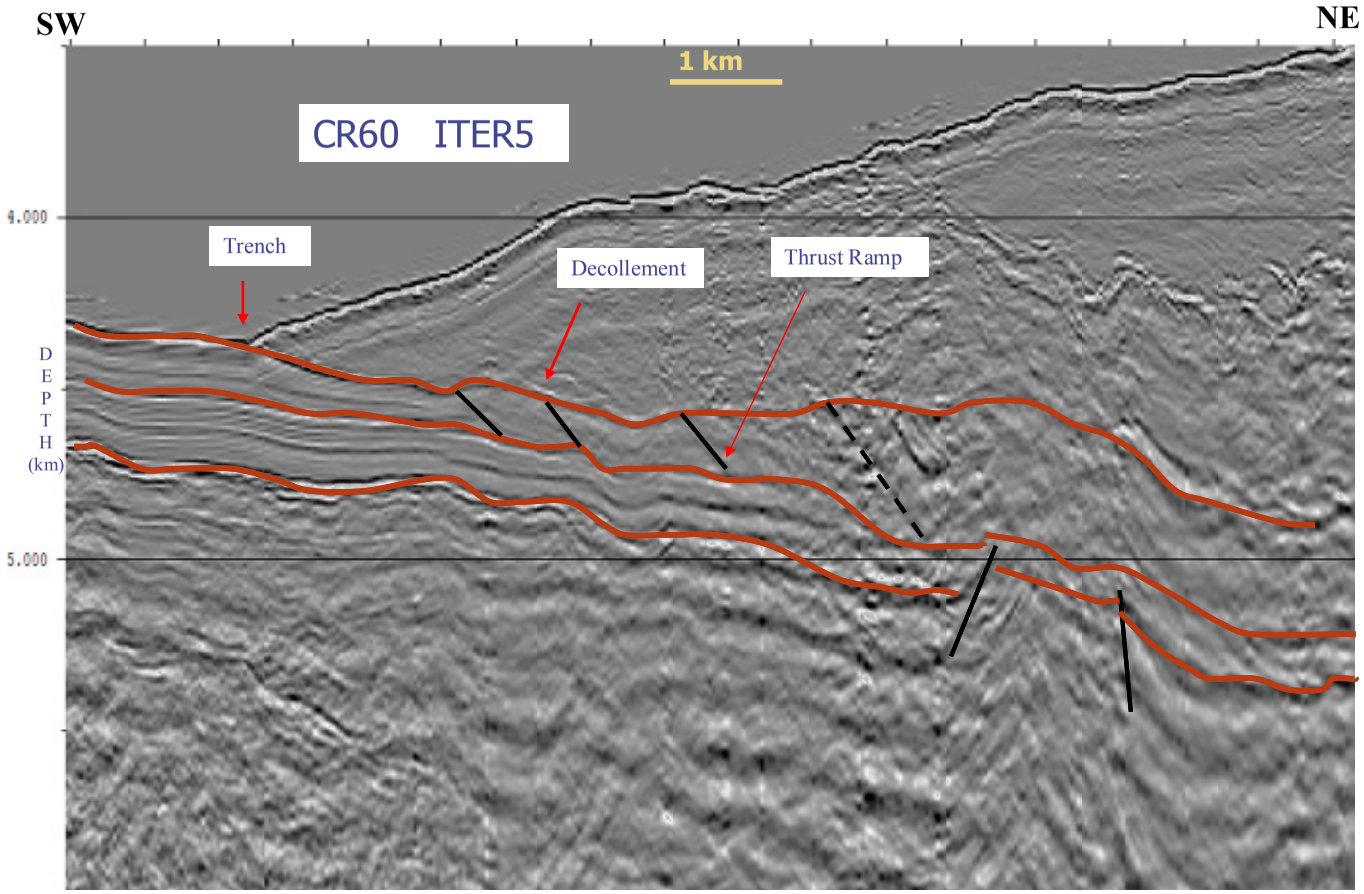

Figure 4.21. Detail of PSDM image of line CR-60 using the velocity model after five iterations of RMVA with my interpretations superimposed.

4.5 DISCUSSIONS

4.5.1 Nicaragua

The seismic images (Figure 4.9 & 4.13) clearly show the subduction of the entire sediment column near the trench. The shallowly dipping decollement clearly overrides the subducting rotated fault blocks. We can observe that all the sediment units are preserved in the subducted rotated fault block. Offshore Nicaragua, the large basement fault blocks would minimize or inhibit the development of a décollement within the subducting sediment package. Thus preventing subsequent frontal accretion and/or underplating and subducting almost the entire sediment column to the volcanic roots.

Ranero et al. (2000) suggests apparent lack of sedimentary accretion at the Nicaragua margin but also suggested decreased rates of subduction erosion offshore Nicaragua compared to that of Costa Rica as a probable explanation for ^{10}Be transition from northwest Nicaragua to southeast Costa Rica. As discussed before in chapter 2, we do observe deformation of the overriding plate in response to structure of the subducting plate offshore Nicaragua (Figure 2.9 and 2.10). Also some MCS lines (Figure 2.9) show considerable thinning of the overriding plate suggesting tectonic erosion. In seismic images we do see slumps of material on the surface of the overriding plate and normal fault dipping trenchward and cutting through the surface of the overriding plate suggesting that the top of the overriding plate is being eroded. Also we observe that the overriding plate has a steep slope with narrow lower slope and considerably thicker slope away from the trench, suggesting that there is frontal erosion of the overriding plate. There may

also be suggestions of basal erosion, particularly when a seamount gets subducted beneath the overriding plate.

Subduction erosion would cause retreat of Nicaragua volcanic arc front to migrate landward but studies onshore Nicaragua by Plank et al. (2002) and Ehrenborg (1996) suggests migration of the Nicaragua volcanic arc front trenchward since ~13 Ma. Also the sedimentary architecture of the Sandino basin (Figure 4.22) offshore Nicaragua suggests alternate progradation and retreat of the shelf edge and that the shelf edge has not had a sudden huge landward motion due to starvation of sediments because of large subsidence associated to large tectonic erosion.

Based on the above arguments I summarize that that tectonic erosion is limited to space (where) and time (when) seamount like structures are getting subducted and thus does not dominate the subduction on the recent time scale of ^{10}Be recycling for Central American island arc system. In the Nicaragua margin with high relief half-graben features (rotated fault blocks), the surficial sediment does not undergo much dilution from the upper plate and appears to be efficiently subducted and incorporated into the arc magmas, as illustrated by the high ^{10}Be signature of the Nicaraguan arc volcanoes.

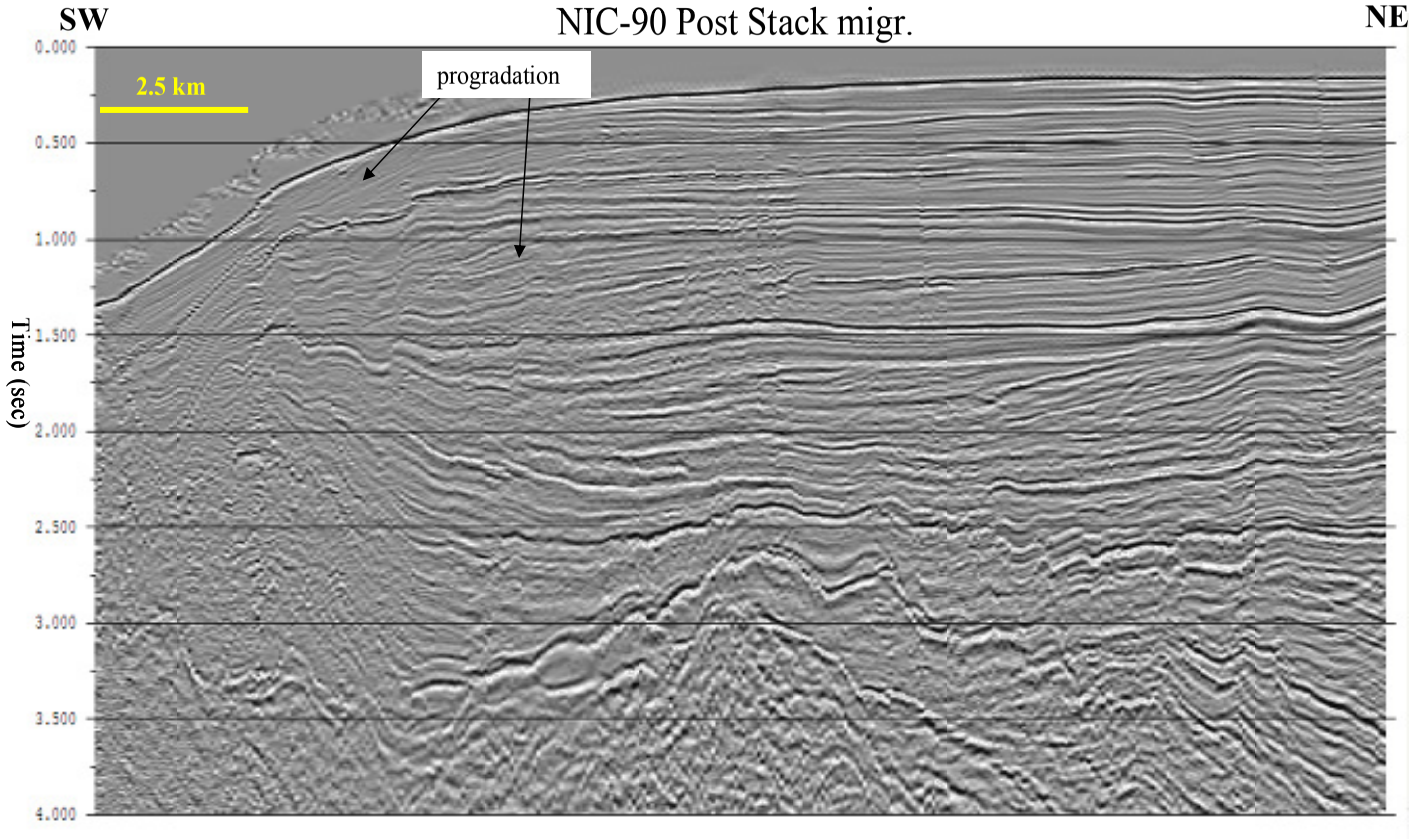

Figure 4.22. Post-stack time migrated image of the shelf and the upper slope area of line NIC-90. We can see sequences of progradation.

4.5.2 Costa Rica

The Seismic images (Figure 4.17 & 4.21) clearly document the thickening and the deformation of the uppermost sedimentary unit landward from the trench on subduction. We observe the presence of several thrust ramps in the top unit along which the slip has occurred to thicken and deform the top unit as shown by Shipley et al. (1992). The rapid dewatering of the uppermost sediments (Saffer et al., 1999) probably causes the initial decollement to gain strength, while the poorly drained middle and deep section becomes relatively weaker, thus allowing deeper detachments to form and possibly leading to modest amounts of underplating (McIntosh and Sen, 2000). We also observe repeated stratigraphic sections between the present decollement and the upper plate basement. Christeson et al. (1999) using seismic reflection and refraction data showed stacked velocity duplicates, interpreted as repeated stratigraphic sections because of underplating.

However, the ultimate fate of the deformed underthrust sediment is unclear from the images (Figure 4.17 & 4.21). Leg 170 Site 1042 penetrated the slope apron and the top of the wedge ~7 km landward from the trench and encountered Early to Middle Miocene rocks (Kimura et al., 1997). Refraction studies also indicated that high velocity rock extended to within 10-20 km landward of the trench (Christeson et al., 1999, Ye et al., 1996). Thus the upper plate apparently has had no significant net seaward growth since Middle Miocene times and the part of the wedge with refraction determined velocities appropriate for accreted sediments is limited to the seaward 10-20 km. Though based on

seismic images, McIntosh et al. (1993) suggested underplating at deeper depths from the trench below the middle and upper slope as one of the probable causes for forearc extension at the Costa Rica convergent margin.

There have also been studies citing subduction erosion being the dominant active process along the Middle American convergent margin and that the decrease in subduction erosion off Nicaragua gives rises to the geochemical disparity in ^{10}Be along this margin (Ranero et al., 1999, 2000; Vannucchi et al., 2001). The low ^{10}Be of the Costa Rican volcanoes could be produced by dilution of sedimentary ^{10}Be with very large amounts of such as 34-36 km^3 Myr^{-1} km^{-1} in the past 16 -17 Myr of forearc basement, being removed by subduction erosion (Vannucchi et al., 2001). Von Huene et al. (2000) based on a seismic reflection data study suggested that subducted seamounts causes thinning of the upper plate of the Costa Rica margin through basal erosion. Ranero et al. (2000) identified lenticular bodies along the interplate surface in seismic images, interpreting it as upper plate material being transported downdip by a process of subduction erosion. The primary evidence for the subduction erosion process is based on studies at the Deep Sea drilling project Leg 170 drillsite, approximately 7 km from the trench. Based on the evidence of vertical subsidence of the early Neogene breccia from a shallow to a deep water setting, Vannucchi et al. (2001) suggested that there has been substantial subsidence of the outer forearc due to subduction erosion.

Subduction erosion will cause a general landward migration of the arc. Marshall et al. (2003) documented the migration of volcanic arc landward in

central Costa Rica in late Neogene due to shallow subduction of buoyant, hot spot thickened ocean crust and not due to subduction erosion. In northern Costa Rica much smoother, thinner and steeper oceanic crust subducts because the oceanic crust here has a minimal influence of the buoyant Cocos Ridge and the Galapagos hot spot. Consistent with this, there is no significant landward retreat of volcanic arc in northern Costa Rica (Marshall et al., 2003). In fact, Gans (2002) documented a general trenchward migration of volcanic arc front of Costa Rica. He suggested 30^{o} counterclockwise rotation of the arc from its middle Miocene position to the present volcanic front, with a pole of rotation centered on southern Costa Rica.

Also arguing against subduction erosion, Marshall et al. (1995) documented Quaternary uplift of the Nicoya Peninsula. As the uplift in onshore central and southern Costa Rica can be attributed to the subduction of the buoyant Cocos Ridge and Galapagos hot spot generated seamounts, Marshal et al. (1995) suggested underplating as one of the probable causes for uplift onshore northern Costa Rica where smooth, less buoyant oceanic crust subducts.

The abrupt change in the observed ^{10}Be pattern in the Central American Volcanic Arc between SE Nicaragua and NW Costa Rica is not well explained by the other elements used to constrain geochemical recycling of slab constituents (e.g., Patino et al., 2000). Costa Rica lavas from volcanic arcs have a much lower but variable amount of sediment tracers, having little contribution from the uppermost hemipelagics of the incoming plate, and a proportionally larger contribution from the basal carbonate section (Tera et al., 1986, Morris et al.,

1990). Significant dilution of sedimentary ^{10}Be by adding a large amount of mass with no ^{10}Be from the forearc basements through subduction erosion is a possible explanation for reducing the ^{10}Be signal in Costa Rica volcanics (Ranero et al., 2000, Vannucchi et al., 2001). This would, however, also reduce signals from other geochemical tracers due to addition of large amount of forearc basement material. Between SE Nicaragua and NW Costa Rica the Ba/La ratio (Figure 4.23) remains relatively constant (Carr et al., 2003), whereas the ^{10}Be enrichment significantly decreases across this boundary.

In the above paragraphs we have discussed two contradicting theories, one supporting sediment accretion and the other supporting subduction erosion as the most likely processes to reduce the ^{10}Be signal in the Costa Rica volcanics. The subduction erosion theory is primarily based on evidence of subsidence at the site Leg 170. However, the Arc movement record does not support subduction erosion process. The PSDM images from the two Costa Rica lines CR-20 and CR-60 suggests likely sediment accretion off Nicoya. This accretion process provides a more straight forward explanation for the ^{10}Be signal reduction in the Costa Rica volcanics.

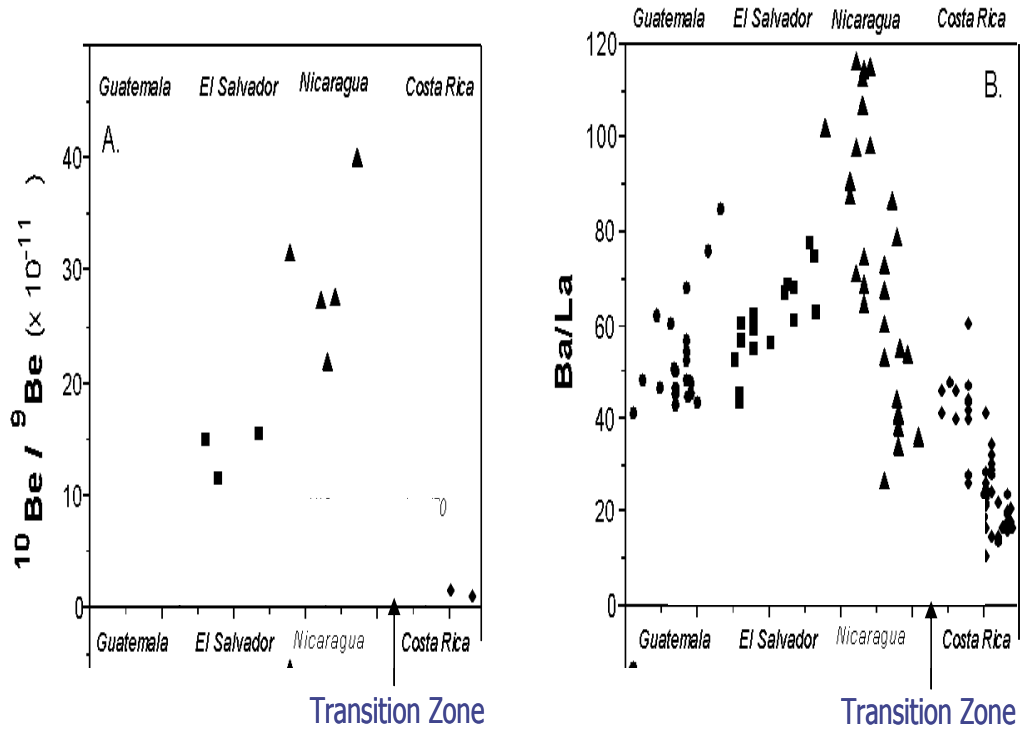

Figure 4.23. Regional variations in the (A) $^{10}Be/^{9}Be$ and (B) Ba/La isotope ratio of Central American arc volcanics. The transition zone here is the location along the margin where there is an abrupt change in $^{10}Be/^{9}Be$. We don't observe such dramatic variation in Ba/La isotope ratio across this transition zone.

4.6 CONCLUSIONS

Based on the discussions in the previous sections I make the following conclusions:

(1) The PSDM images from the two Nicaragua seismic profiles NIC-30 and NIC-70 show complete sediment subduction off Nicaragua due to rotated fault block structures in the downgoing plate.

(2) The PSDM images from the two Costa Rica seismic profiles CR-20 and CR-60 suggests likely sediment accretion off Nicoya.

(3) The most straight forward explanation for the ^{10}Be anomaly is the variation in sediment dynamics noted in the above conclusions (1 & 2).

(4) Previous studies have suggested subduction erosion as an explanation for the observed ^{10}Be concentrations. However, the Arc movement record does not support erosion.

(5) Erosion is limited both in space and time off Nicaragua. It depends on when and where seamounts like structures are subducted.

Chapter 5: Summary and Future work

5.1 SUMMARY

In this dissertation I have worked on a NSF funded project, which is investigating the disparities in arc geochemistry and seismogenic characteristics along the margin off Costa Rica and Nicaragua. My goal was to provide the geophysical framework that allows investigation into how the processes of mass transfer (sediment subduction, accretion, and erosion) and deformation may relate to geochemical properties observed in volcanic lavas. I have seismically imaged the lower slope offshore Nicaragua and Costa Rica using a new residual migration velocity analysis technique and tried to answer this question through detailed analysis of these improved seismic reflection images.

The trench and its surrounding area of a Subduction zone are structurally very complex, with significant lateral changes in seismic propagation velocity and velocity inversions. Imaging an area of this complexity is a very challenging problem. In order to produce a seismic image capable of providing the detailed structure of this area we need an accurate interval velocity model. Thus, seismic velocity analysis is a very important step for prestack depth migration.

In this dissertation I have derived and developed a new residual migration velocity analysis in the depth-offset domain by the analysis of residual depth correction in the depth-plane wave domain. Using an interactive velocity analysis method, I successfully applied these equations to both 2D synthetic data and 2D field data to build velocity depth models. The main advantage of the new method

is that it gives interval velocities directly and it's computationally very efficient because only a top down residual migration is needed for velocity analysis after application of the prestack depth migration. I used this method to derive a velocity depth model of lower slopes offshore Nicaragua and Costa Rica. These velocities produce good interpretable depth images.

In Chapter 1, I introduced my dissertation topic, describing the motivation for my work and giving a brief description of my geographic study area. There is a large disparity in arc geochemistry associated with the subduction system offshore Nicaragua and Costa Rica. Presence of high concentrations of ^{10}Be in the arc volcanics of Nicaragua requires that the youngest sediments be subducted to the arc volcanic root. On the other hand presence of low concentration of ^{10}Be in the arc volcanics in the neighboring country of Costa Rica requires underplating of younger sediments or significant subduction erosion. In order to provide geophysical evidence for these suggestions we need to image the underthrust plate at the toe of the trench and see if we observe subduction, underplating or erosion. Imaging the toe of a subduction margin is very difficult, because the structure and seismic velocity model of this region is very complex. Velocity model determination for complex structures has attracted much attention in the last decade. In this dissertation I have developed a new residual migration velocity analysis technique in the depth-offset domain, which extends some of the developments of RMVA in plane wave domain developed by Jiao, 2002.

In Chapter 2, I described the basics of seismic data processing in the x-t domain and discussed the requirement for applying migration after stack. Here I

present a brief description of post-stack migration. Then I analyzed several post-stack time migrated stack sections from Nicaragua and Costa Rica. Based on these preliminary post-stack migrated images I propose geophysical models for the subduction system offshore Nicaragua and Costa Rica. The models proposed are structurally very complex and have significant laterally velocity changes. Thus to obtain an interpretable image I propose to apply prestack depth migration. Prestack depth migration uses the available seismic shot records and the velocity model to image the subsurface structures. At one point in the image domain, diffraction energy is collapsed from different shot records and the migrated results of a common offset are stacked. Therefore, at the common point, we obtain migrated results from the recorded different offsets which are called a Common Image gather (CIG). The CIG are stacked to give the final prestack migrated image. I conclude this chapter with images of a seismic line offshore Nicaragua. There is a significant improvement in the quality of the images from post-stack time to prestack time to prestack depth.

In chapter 3, I developed, explained and tested my new residual migration velocity analysis technique in the depth-offset domain. If the correct velocity depth model is used for prestack depth migration, events on the CIG are horizontally aligned since they represent the image of the same subsurface scatterer, obtained from different angles. Otherwise, if an incorrect velocity-depth model is used in migration, the events on the CIG exhibit migration errors or residuals. The residual migration contains information about how close the

velocity used for migration was to the correct velocity model. This is the foundation for migration velocity analysis.

In chapter 3, I first discussed the basics of seismic waves in the plane wave domain. From there onward I explained the mathematical development of RMVA in the plane wave domain, and then extended this development to the depth-offset domain. I also designed a procedure to perform the RMVA and developed an interactive software package to implement the velocity analysis. The residual migration equations were tested successfully on a half space model and on a relatively complicated 2D model. The synthetic shot gathers for these models were generated by using the finite difference solution of the wave equation. Compared to the other methods (Yahya, 1989, Liu & Bleistein, 1992 and 1995, and Meng & Bleistein, 1999 and 2001) which require top-down layer stripping pre-stack depth migration to obtain interval velocities, the two main advantages of the new method are that it derives interval velocities directly and is computationally very efficient. This method only requires top down residual migration for velocity analysis after one prestack depth migration for all depths. I successfully tested the new method on both 2D synthetic SEG/EAEG salt data and field data from offshore Nicaragua. The number of iterations of RMVA performed to get an accurate model depends on the initial model used for migration and the precision desired.

In chapter 4, I applied the new RMVA technique to derive improved velocity models for the lower slope offshore Nicaragua and Costa Rica. I started with a 1D gradient velocity as an initial velocity model. The quality of the images

obtained after a few iterations of RMVA improved significantly. The events on the CIG are much flatter. The images from the lower slope offshore Nicaragua clearly shows subduction of the entire sediment column. The images from the lower slope offshore Costa Rica shows deformation of younger sediments on subduction, and subsequently undergoing possible accretion. Figure 5.1 and 5.2 compares the hypothetical models with the images I obtained after prestack depth migration. The images therefore satisfactorily substantiate the hypothesized models. Thus through this dissertation we have been able to provide convincing geophysical evidence for the geochemical disparities in the arc volcanics off Nicaragua and Costa Rica.

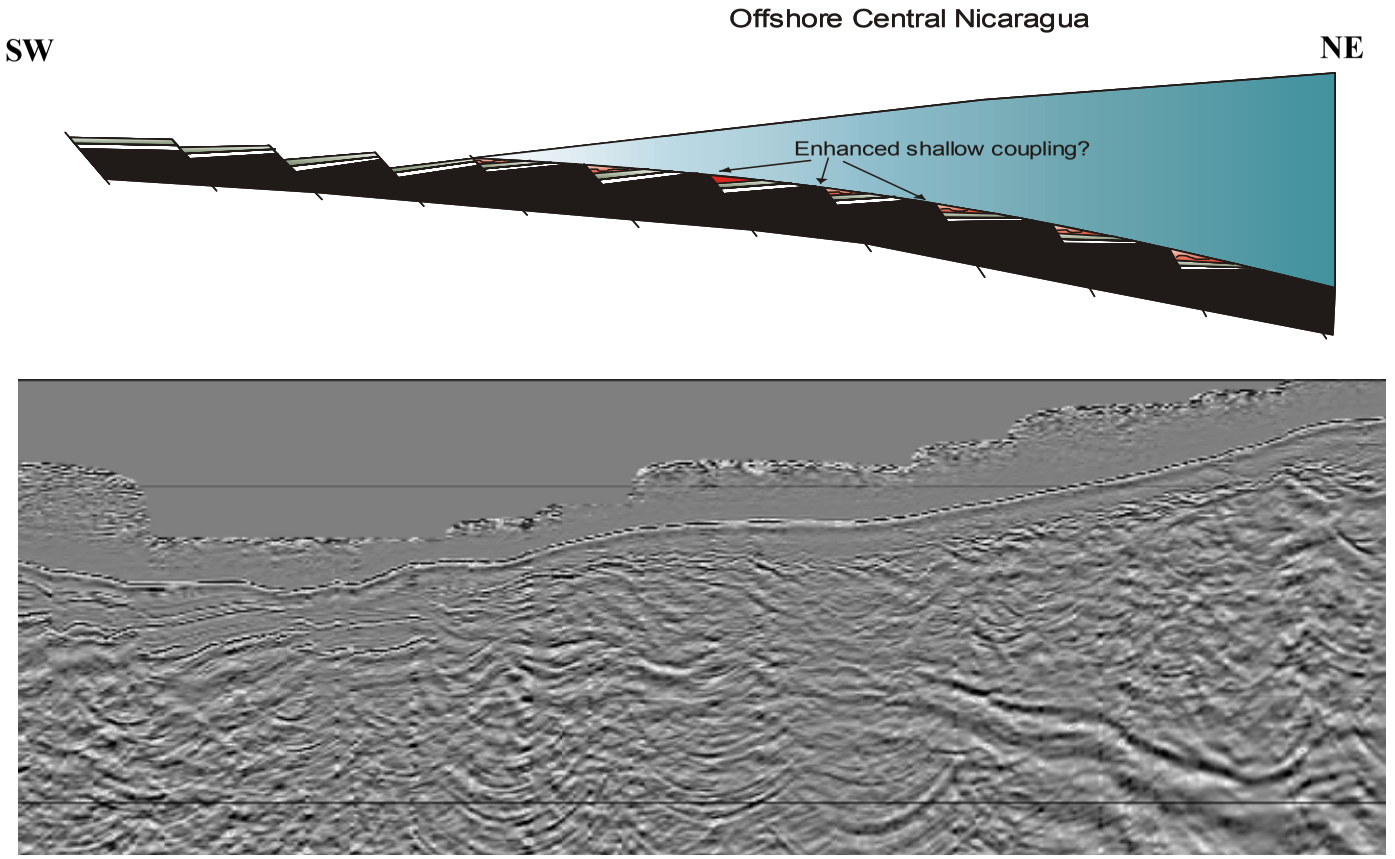

Figure 5.1. Comparison of the hypothetical model and the prestack depth image offshore Nicaragua. The subducted rotated fault blocks are quite well imaged.

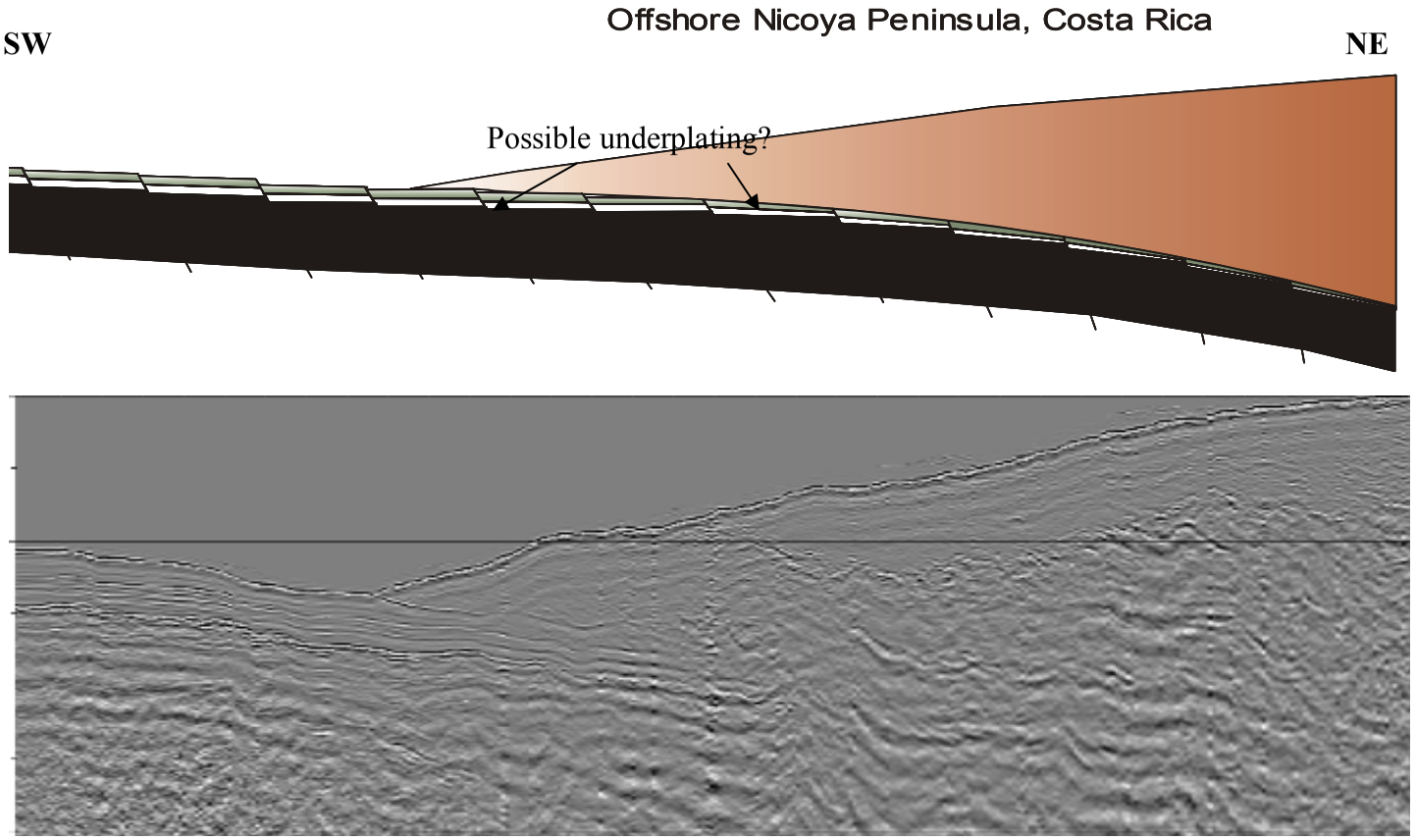

Figure 5.2. Comparison of the hypothetical model and the prestack depth image offshore Costa Rica. The upper sediment column is deformed on subduction and undergoes possible accretion.

5.2 FUTURE WORK

There are many seismic imaging applications that can be investigated to exploit the advantages of this new RMVA method. They can be divided into two categories: extensions of the new method and combining the new method with other velocity building methods to improve the computational efficiency of the process of velocity depth modeling.

It is possible to extend this RMVA technique to a transversely isotropic medium with a vertical axis of symmetry (VTI medium). For VTI media, Thomsen's (1986) notation is very popular in the seismology community. Thomsen (1986) used five parameters, namely α_0 (the vertical compressional wave velocity), β_0 (vertical shearwave velocity), ε, δ and γ, which are related to the components of the reduced expression of the elastic coefficient matrix *Cij*. The equation for NMO (normal move out) in a weak VTI medium for seismic data in the plane-wave domain was derived by Sen & Mukherjee (2003):

$$\tau(p) = 2\sum_{j=1}^{n} \tau_{0_j} (1 - p^2 \alpha_{el\,j}^2)^{1/2} \left[1 - \frac{2p^4 \alpha_{el\,j}^4 \kappa_j}{(1 - p^2 \alpha_{el\,j}^2)} \right]^{1/2}, \tag{5.1}$$

where, τ_0 is the two way normal time, and α_{el} and κ are related to the Thomsen parameters as

$$\alpha_{el}^2 = \alpha_0^2 (1 - 2\delta), \tag{5.2}$$

$$\kappa = \frac{(\varepsilon - \delta)}{(1 + 2\delta)^2}. \tag{5.3}$$

Equation (5.1) can be rewritten to obtain the equation for the two way normal time of an n layer 1D model in the τ_0-p domain as

$$\tau_0(p) = \sum_{j=1}^{n} \Delta\tau_{0_j}(p) = \sum_{j=1}^{n} \frac{\Delta\tau_j(p)}{2} (1 - p^2\alpha_{el\,j}^2)^{-1/2} \left[1 - \frac{2p^4\alpha_{el\,j}^4 \kappa_j}{(1 - p^2\alpha_{el\,j}^2)} \right]^{-1/2}, \qquad (5.4)$$

The apparent two way normal time, τ_0^{m} (the superscript m stands for trial velocity cases) at a given CIG, using trial vertical velocity α_{el}^m and trial κ^{m} is given by

$$\tau_0^m(p) = \sum_{j=1}^{n} \Delta\tau_{0_j}^m(p) = \sum_{j=1}^{n} \frac{\Delta\tau_j(p)}{2} (1 - p^2\alpha_{el_j}^{m^2})^{-1/2} \left[1 - \frac{2p^4\alpha_{el_j}^{m^4} \kappa_j^m}{(1 - p^2\alpha_{el_j}^{m^2})} \right]^{-1/2}. \qquad (5.5)$$

The difference between the true elliptical velocity, κ and the trial velocity, κ will cause a misfit between the true two way normal time τ_0 and the migrated two way normal time τ_0^{m}. This misfit is given by

$$\tau_{0RMIG}(p) = \tau_0(p) - \tau_0^m(p)$$

$$\tau_{0RMIG}(p) == \sum_{j=1}^{n} \Delta\tau_{0_j}^m(p) \left[\frac{A_j}{A_j^m} - 1 \right], \qquad (5.6)$$

where,

$$A_j = (1 - p^2\alpha_{el\,j}^2)^{-1/2} \left[1 - \frac{2p^4\alpha_{el\,j}^4 \kappa_j}{(1 - p^2\alpha_{el\,j}^2)} \right]^{-1/2}, \qquad (5.7)$$

$$A_j^m = (1 - p^2\alpha_{el_j}^{m^2})^{-1/2} \left[1 - \frac{2p^4\alpha_{el_j}^{m^4} \kappa_j^m}{(1 - p^2\alpha_{el_j}^{m^2})} \right]^{-1/2}. \qquad (5.8)$$

We can use equation (5.6) to do RMVA in weak VTI media in the plane wave domain. We can generate a p table in offset-time (x-t) domain in VTI medium, by using the same methods demonstrated in chapter 3. We can use this table to map the above corrections in the plane wave domain given by equation 5.6 to the offset-time domain. As demonstrated in Chapter 3, this can be developed into an interactive RMVA technique in a weak VTI medium in the offset-time domain.

The new RMVA method for isotropic media can also be extended to velocity analysis for converted waves by using different velocities for the up-coming and the down-going waves. For example, if we generate P waves at the source point and record S wave at the geophones, we should use the P wave velocity for the down- going waves and the S wave velocity for the up-coming waves. This can be accomplished with a small change to the method developed here.

We can use the velocity depth model from the new method as the input to a global tomographic inversion. This will help in significantly improving the computation of the velocity depth model building process as the new model would be closer to the true model than the initial model. This will cause the tomographic inversion to converge rapidly.

No matter how good the velocity model and how robust and accurate our migration algorithm is, we will not be able to generate good images from 2D prestack depth migration if we have very complicated 3D structures and consequently out of plane energies. We require 3D datasets and 3D prestack depth images for such areas. The lower slope of offshore Nicaragua and Costa Rica

convergent margin is such a complex area. So in order to realize good seismic images we need to ultimately acquire and analyze 3D dataset. We have 3D data offshore Costa Rica (Shipley et al., 1992) but not offshore Nicaragua. It is very encouraging to see the quality of the images generated from 2D data offshore Nicaragua. I am sure if we had 3D data from offshore Nicaragua we will be able to image the lower slope much better, which will help us answer questions related to subduction in a convergent margin. For example, what is the explanation for the difference in seismogenic characteristics offshore Nicaragua and Costa Rica?

Deep sea drilling will help investigate better the processes of mass transfer (sediment subduction, accretion, and erosion) in this area and how these relate to the arc geochemical variations. Previous drilling (ODP Leg 170) near the trench offshore Costa Rica could not penetrate to the depth of possible underplated sediments (Kimura et al., 1997). Deeper drilling will help us to test the different hypothesis and provide us with the most likely solution.

References

Akbar, F. E., 1997, Three-dimensional prestack plane-wave Kirchhoff depth migration in laterally varying media: *Ph.D. Dissertation*, The University of Texas at Austin.

Aki, K., and Richards, P., 1980, Quantitative Seismology – Theory and methods: W.H. Freeman and Company.

Ambraseys, N. N., and Adams, R. D., 1996, Large-magnitude Central American earthquakes, 1898-1994, *Geophys. J. Int.*, *127*, 665-692.

Aminzadeh, F., Brac, J., and Kunz, T., 1997, 3-D salt and overthrust models, SEG/EAGE 3-D Modeling Series, No. 1, Soc. Expl. Geophys. Tulsa, OK.

Arnold, J. R., 1956, *Science*, 124, 584-585.

Barckhausen, U., Ranero, C. R., von Huene, R., Cande, S. C., and Roeser, H. A., 2001, Revised tectonic boundaries in the Cocos Plate off Costa Rica, Implications for the segmentation of the convergent margin and for plate tectonic models, *J. Geophys. Res.*, 106, 19,207-19,220.

Carr, M. J., 1984, Symmetrical and segmented variation of physical and geochemical characteristics of the Central America volcanic front, *J. Volcan. Geotherm. Res.*, , 20, 231–252.

Carr, M. J., Feigenson, M. D., and Bennet, E. A., 1990, Incompatible element and isotopic evidence for tectonic control of souce mixing and melt extraction along the Central American arc, *Contrib. Mineral. Petrol., 105*, 369-380.

Carr, M. J., Feigenson, M. D., Patino, L. C., and Walker, J. A., 2003, Volcanism and geochemistry in Central America, Progress and problems, in The Subduction Factory, J.M. Eiler and G.Abers (eds.), *AGU Monog. Ser.*, Washington, D.C., in press.

Červený, V., 2001, Seismic ray theory: 1st ed., Cambridge University Press.

Christeson, G. L., McIntosh, K. D., Shipley, T. H., Flueh, E., and Goedde, H., 1999, Structure of the Costa Rica convergent margin, offshore Nicoya Peninsula, *J. Geophys. Res.*,104,B11, 25443-25468.

Claerbout, J. F., 1985, Imaging the Earth's Interior: Blackwell Science Publishers, Oxford, England.

DeMets, C., 2001, A new estimate for present-day Cocos-Caribbean plate motion: Implications for slip along the Central American volcanic arc: Geophys. Res. Lett., v. 28, p. 4043-4046.

DeMets, C., Gordon, R. G., Argus, D. F., and Stein, S., 1994, Effect of recent revisions to the geomagnetic reversal time scale on estimates of current plate motions, *Geophys. Res. Lett., 21*, 2191-2194.

Diebold, J., and Stoffa, P. L., 1981, The traveltime Equation Tau-p Mapping and Inversion of Common Midpoint Data, *Geophysics*, 46, 238-254.

Ehrenborg, J., 1996, A new stratigraphy for the Tertiary volcanic rocks of the Nicaragua Highland, *GSA Bulletin*, 108, 830-842.

Gans, P. B., Alvarado-Induni, G., Perez, W., Macmillan, I., and Calvert, A., 2003, Neogene evolution of the Costa Rican arc and development of the Cordillera Central, *GSA – 99th Annual meeting*, paper no. 33-4.

Gazdag, J., 1978, Wave-equation migration by phase shift method, *Geophysics*, 43, 1342-1351.

Gazdag, J., and Sguazzero, P., 1984, Migration of seismic data by phase shift plus interpolation, *Geophysics*, 49, 124-131.

Hey, K., 1977, Tectonic evolution of the Cocos-Nazca spreading center, *Geol. Soc. Am. Bull.*, 88, 1404-1420.

Hilde, T. W. C., 1983, Sediment subduction versus accretion around the Pacific, *Tectonophysics*, 99, 381–397.

Jiao, J., Stoffa, P. L., Sen, M. K., and Seifoullaev, R. K., 2002, Residual migration velocity analysis in the plane-wave domain, *Geophysics*, 67, 1258-1269.

Judson, D. R., Lin, J., Schultz, P. S., and Sherwood, J. W. C., 1980, Depth migration after stack, *Geophysics*, 45, 361-375.

Kanamori, H., and Kikuchi, M., 1993, The 1992 Nicaragua earthquake: a slow tsunami earthquake associated with subducted sediments, *Nature*, 361, 714-716.

Kelly, R. K., 2003, Subduction Dynamics at the Middle America Trench: New Constraints from Swath Bathymetry, Multichannel Seismic Data, and 10Be, Ph.D. Thesis, Woods Hole Oceanographic Institution, Woods Hole MA, 341 pp.

Kimura, G., Silver, E. A., Blum, P., et al., 1997, *Proc. ODP, Init. Repts., 170*, Ocean Drilling Program, College Station, TX.

Larner, K. L., Hatton, L. and Gibson, B., 1981, Depth migration of imaged time sections, *Geophysics*, 46, 734-750.

Liu, Z., and Bleistein, N., 1992, Velocity analysis by residual moveout, 62th Ann. Internat. Mtg., Soc. Expl. Geophys., Expanded Abstracts, 1024–1037.

Liu, Z., and Bleistein, N., 1995, Migration velocity analysis, Theory and an iterative algorithm: *Geophysics*, 60, 142–153.

Loewenthal, D., Lu, L., Robertson, R., and Sherwood, J., 1976, The wave equation applied to migration, *Geophysical Prospecting*, 24, 380-399.

Marshall, S. J., and Anderson, R. S., 1995, Quaternary uplift and seismic cycle deformation, Peninsula de Nicoya, Costa Rica, *GSA Bulletin*, 107, 463-473.

Marshall, S. J., Idleman, B. D., Gardner, T. W., and Fisher, D. M., 2003, Landscape evolution within a retreating volcanic arc, Costa Rica, Central America, *Geology*, 31, 419-422.

McIntosh, K. D., 1999, Proposal to the National Science Foundation: Structure of the Nicaragua/ Costa Rica Subduction Zone, A framework for the Subduction Factory and Seismogenic Zone Initiatives, submitted to *NSF*.

McIntosh, K. D., and Sen, M. K., 2000, Geophysical evidence for dewatering and deformation processes in the ODP Leg 170 area offshore Costa Rica, *EPSL 178*, 125-138.

McIntosh, K. D., Silver, E. A., and Shipley, T. H., 1993, Evidence and mechanisms for forearc extension at the accretionary Costa Rica convergent margin, *Tectonics*, *12*, 1380-1392.

McMechan, G. A., 1983, Migration by extrapolation of time-dependent boundary values: *Geophysical Prospecting*, 31, 413-420.

Meng, Z., Bleistein, N., and Wyatt, K. D., 1999, 3-D analytical migration velocity analysis I: Two-step velocity estimation by reflectornormal update, 69th Ann. Internat. Mtg., Soc. Expl. Geophys., Expanded Abstracts, 1727–1730.

Morris, J. D., Lehman, W. P., and Tera, F., 1990, The subducted component in island arc lavas: constraints from Be isotopes and B-Be systematics, *Nature*, 334, 31-36.

Morris, J. D., Valentine, R., and Harrison, T., 2002, ^{10}Be imaging of sediment accretion and subduction along the northeast Japan and Costa Rica convergent margins, *Geology*, 30, 59-62.

O'Brien, M., and Gray, S., 1996, Can we image beneath salt?, *The Leading Edge*, 15, 17-24

Patino, L. C., Carr, M. J., and Feigenson, M. D., 2000, Local and regional variations in Central American arc lavas controlled by variations in subducted sediment input, *Contrib. Mineral. Petrol*., 138, 265–283.

Plank, T., Balzer, V., and Carr, M., 2002, Nicaragua volcanoes record paleoceanographic changes accompanying closure of the Panama Gateway, *Geology*, 30, 1087-1090.

Protti, M., Guendel, F., and McNally, K., 1994, The geometry of the Wadati-Benioff zone under southern Central America and its tectonic significance: results from a high-resolution local seismographic network, *Phys. of the Earth and Planet. Inter., 84*, 271-287.

Protti, M., Guendel, F., and McNally, K., 1995, Correlation between the age of the subducting Cocos Plate and the geometry of the Wadati-Benioff zone under Nicaragua and Costa Rica: Geologic and tectonic development of the Caribbean Plate boundary in southern Central America *(GSA Special Paper), 295*, 309-326.

Ranero, C. R., and von Huene, R, 2000, Subduction erosion along the Middle America convergent margin, *Nature*, 404, 748-752.

Ranero, C. R., von Huene, R., Flueh, E. R., Duarte, M., Baca, D. and McIntosh, K. D., 2000, A cross section of the convergent Pacific margin of Nicaragua, *Tectonics*, 19, 2, 335-357.

Saffer, D. M., Silver, E. A., Fisher, A. T., Tobin, H., and Moran, K., 2000, Inferred pore pressures at the Costa Rica subduction zone: implications for dewatering processes, *Earth and Planet. Sci. Lett.,* v. 177, p. 193-207.

Schneider, W. A. J., Ranzinger, K., Balch, A., and Kruse, C., 1992, A dynamic programming approach to first arrival travel time computation in media with arbitrarily distributed velocities, *Geophysics*, 57, 39-50.

Schneider, W. A., 1978, Integral formulation for migration in two and three dimensions, *Geophysics*, 43, 49-76.

Sen, M. K., and Mukherjee, A., 2003, τ-p analysis in transversely isotropic media, *Geophys. J. Int.*, 154, 647-658.

Shipley, T. H., and Moore, G. F., 1986, Sediment accretion, subduction, and dewatering at the base of the trench slope off Costa Rica: A seismic reflection view of the decollement, *J. Geophys. Res.*, *91*, 2019-2028.

Shipley, T. H., McIntosh, K. D., Silver, E. A., and Stoffa, P. L., 1992, Three-dimensional seismic imaging of the Costa Rica accretionary prism: Structural diversity in a small volume of the lower slope, *J. Geophys. Res.*, *97*, 4439-4459.

Stoffa, P. L., Buhl, P., Diebold, J. B., and Wenzel, F., 1981, Direct mapping of seismic data to the domain of intercept time and ray parameter—A plane-wave decomposition: *Geophysics*, 46, 410–421.

Stoffa, P. L., Diebold, J. B., and Buhl, P., 1982, Velocity analysis for wide aperture seismic data, *Geophys. Prosp*., 30, 25–57.

Stoffa, P. L., Fokkema, J., de Luna Freire, R., Kessinger, W., 1990, Split-step fourier migration, *Geophysics, 55*, 410-421.

Stolt, R. H., 1978, Migration by Fourier transform, *Geophysics*, 43, 23-48.

Stork, C., and Clayton, R. W., 1991, Linear aspects of tomographic velocity analysis: *Geophysics*, 56, 483–495.

Taner, M. T., and Koehler, F., 1977, Wave-equation migration, Technical brochure, Seiscom-Delta, Inc.

Tera, F., Brown, L., Morris, J., Selwyn Sacks, I., Klein, J., and Middleton, R., 1986, Sediment incorporation in island–arc magmas: Inferences from 10Be, *Geochim. Cosmochim. Acta*, 50, 535–550.

Thomsen, L., 1986, Weak elastic anisotropy, *Geophysics*, 51, 1954-1966.

Tieman, H. J., 1995, Migration velocity analysis: Accounting for effects of lateral velocity variations, *Geophysics*, 60, 164–175.

Trorey, A. W., 1970, A simple theory for Seismic Diffraction, *Geophysics*, 35, 762-784.

Valentine, R. B., Morris, J. D., and Duncan, D. Jr., 1997, Sediment subduction, accretion, underplating, and arc volcanism along the margin of Costa Rica: constraints from Ba, Zn, Ni, and 10Be concentrations, *EOS, Trans., AGU*, 78, 673.

Vannucchi, P., Scholl, D. W., Meschede, M., and McDougall-Reid, K., 2001, Tectonic erosion and consequent collapse of the Pacific margin of Costa Rica: Combined implications from ODP Leg 170, seismic offshore data, and regional geology of the Nicoya Peninsula, *Tectonics*, 20, 649-668.

Versteeg, R. J., 1993, Sensitivity of prestack depth migration to the velocity model, *Geophysics*, 58, 873-882.

von Huene, R., and Scholl, D. W., 1991, Observations at convergent margins concerning sediment subduction, subduction erosion, and the growth of continental crust, *Reviews of Geophysics*, 29,279-316.

von Huene, R., Bialas, J., Flueh, E., Cropp, B., Csernok, T., Fabel, E., Hoffmann, J., Emeis, K., Holler, P., Jeschke, G., Leandro, M., C., Perez, F., I., Chavarria, S. J., Florez, H. A., Escobedo, Z., Leon, R., and Barrios, L. O., 1995, Morphotectonics of the Pacific convergent margin of Costa Rica, *in* Mann, P., ed., Geologic and tectonic development of the Caribbean Plate boundary in southern Central America, *Special Paper - Geological Society of America, 295*, Boulder, CO, Geological Society of America (GSA), 291-307.

von Huene, R., Ranero, C. R., and Weinrebe, W., 2000, Quaternary convergent margin tectonics of Costa Rica, segmentation of the Cocos Plate, and Central American volcanism, *Tectonics,* 19, 2, 314-334.

Walther, C., Flueh, E. R., Ranero, C. R., von Huene, R., and Strauch, W., 2000, Crustal structure across the Pacific margin of Nicaragua: evidence for ophiolitic basement and a shallow mantle sliver, *Geophys. J. Int.,* 141, 759-77.

Yahya, K. A., 1989, Velocity analysis by iterative profile migration, *Geophysics*, 54, 718–729.

Ye, S., Flueh, E. R., Klaeschen, and von Huene, R., 1997, Crustal structure along the EDGE transect beneath the Kodiak shelf off Alaska derived from OBH seismic refraction data, *Geophys. J. Int*., 130, 283-302.

Yilmaz, O., 1987, Seismic Data Processing: SEG, Tulsa, Oklahoma.

Yilmaz, O., and Chambers, R., 1984, Migration velocity analysis by wavefield extrapolation, *Geophysics*, 49, 1664–1674.

Vita

Imtiaz Ahmed was born in Calcutta, India, on January 30, 1974, to Ainul Haque and Saleha Bano. He completed his high school from Maulana Azad College, Calcutta, India in 1993. He qualified in the IIT joint entrance examination in 1994 and entered the Department of Geology and Geophysics at the Indian Institute of Technology, Kharagpur, India. He graduated with the Master of Science degree in Exploration Geophysics in 1999. In August 1999, he enrolled in the PhD program in the Department of Geological Sciences, The University of Texas at Austin. He spent the summer of 2002 in BP, Houston as an intern in the Geophysical Imaging group. Upon Graduation he will join BP, Houston in its Exploration and Production Technology (EPTG) group.

Permanent address: 21 Chandni Chowk St, Calcutta, West Bengal 700072, India.

This dissertation was typed by the author.